Plasmon Enhanced Hybrid Photovoltaics

Swayandipta Dey

Abstract Plasmonics is an emerging area concerning in the fields of optics, telecommunications, optoelectronics and photovoltaics. Plasmonic nanostructures in general possess the capability to effectively concentrate and trap the electromagnetic field into the active region of the device covering different spectral regions of the entire solar spectrum. This could be finely tuned by optimizing several parameters such as the type of material, its shape, size and the local dielectric medium surrounding the particles. Excitonics, on the other hand is another independent branch of study primarily involving with the manipulation in generation and recombination of electron-hole pairs in inorganic and organic semiconductors, dyes and polymers. There is a subtle, yet a strong complementarity that exists between Plasmonics and Excitonics which could be exploited to generate several hybrid functional materials and devices to potentially enhance/boost the performance and efficiency of the devices. In this book chapter, I will start by discussing with the background on Plasmonics and Excitonics and how we can combine materials from these individual fields to develop hybrid heterostructures and fabricate all next generation photovoltaic devices. Next, I will give a detailed survey on how these materials could be synthesized using several substrate and solution based wet-chemistry, solvothermal, continuous flow and hot-injection methods. Several surface, optical and electrical characterization techniques will be thoroughly discussed concerning the plasmonic and excitonic nanostructures. The latter half of the chapter will be followed by discussing the underlying design principles and the device physics involving the interfacial exciton generation, recombination and charge carrier extraction processes when these plasmonic and excitonic materials are incorporated/embedded in between other transport layers. Finally, in conclusion, I will briefly discuss certain future prospects and perspectives involving these materials that could potentially open up new opportunities in the fabrication strategies of several high performance hybrid photovoltaic devices.

Keywords Plasmonics · Excitonics · Plasmon-exciton coupling · Metal nanoparticle-quantum dot hybrid nanoheterostructures · Hybrid photovoltaics

S. Dey (✉)
Weizmann Institute of Science, Rehovot, Israel
e-mail: swayandipta.dey@weizmann.ac.il

F. A. La Porta and C. A. Taft (eds.), *Emerging Research in Science and Engineering Based on Advanced Experimental and Computational Strategies*, Engineering Materials, https://doi.org/10.1007/978-3-030-31403-3_1

1 Metal Nanoparticles and Localized Surface Plasmons

Nanoparticles are microscopic particulates which could be in the form of nanopowder, nanocrystal or nanocluster and typically of dimension in the order from a few to >100 nm. With its wide variety of shapes, sizes and the type of materials (metals, semiconductors) that can be now synthesized, nanoparticles have gained a significant research attention over the last few decades. Historically, the existence and usage of nanoparticles date back to appearance of metallic luster decorations of glazed ceramics as early as in Mesopotamia during the 9th century [1–3]. Another finest example of artwork rediscovered in Europe was the Lycurgus cup manufactured by the Romans as early as 5th century A.D. where noble metal nanoparticles such as Ag, Au, Cu was dispersed in ruby glass matrix (Fig. 1a shows the original Lycurgus cup displayed in the British museum). Although, from a scientific standpoint, the next big leap in nanoparticle research was initially taken by Michael Faraday approximately 150 years ago (Fig. 1b shows the first original bottles of MNP samples as prepared by Faraday) [4].

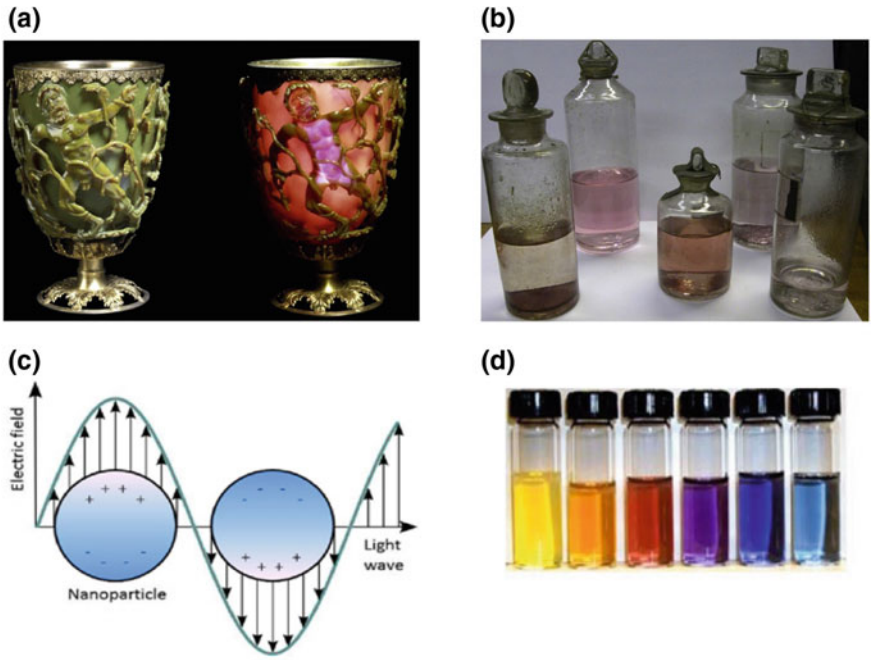

Fig. 1 **a** The Lycurgus Cup in reflected (left) and in transmitted (right) light. © Trustees of the British Museum. **b** Five original bottled samples prepared by Michael Faraday. *Source* http://aveburybooks.com/faraday/catalog.html. **c** Coherent oscillation of electrons in the form of localized surface plasmon resonance in metal nanoparticles and its interaction with EM light field. **d** Colored colloidal suspensions of gold nanoparticles. *Source* http://esciencenews.com/articles/2010/03/12/a.golden.bullet.cancer. Reproduced with permission from Heiligtag et al., 2013

As a result of his systematic study on the interaction of light with MNPs, it gave birth to a new era of modern colloidal chemistry with the emergence of Nanoscience and Nanotechnology. Some of these man-made works of extraordinaire obviously indicate that nanoparticles are not necessarily synthesized in modern scientific laboratories, but have obviously existed in nature for a significantly long period and their usage can be even traced back to ancient times.

Noble metal nanoparticles (MNPs) like Ag, Cu, Au, Fe etc. have long fascinated scientists due to their unique optical properties including large optical field enhancement resulting in the form of strong scattering and absorption of light [5–7]. Due to their intrinsic property of possessing a negative real and small positive imaginary dielectric constant over a range of wavelengths, they are capable of supporting what is known as surface plasmon resonance (SPR) when these MNPs interact with electromagnetic light. SPR in MNPs arise as a result of coherent and collective oscillation of free electrons interacting with the oscillating electromagnetic (EM) light as can be seen from Fig. 1c [6, 8]. This process is resonant at a particular frequency of light and it could be visualized as a coherent motion of conduction band electrons of the metal. The SPR can be either propagating or localized. Propagating surface plasmons are frequent in thin metallic films whereas the localized surface plasmons (LSPR) are observed in metallic nanostructures. Typically, when the dimension of the metallic nanoparticles smaller than the wavelength of interacting electromagnetic radiation field, the plasmons are confined (localized, and therefore the term LSPR).

The classical model states that the electric field component of the incoming light wave induces a polarization of conduction band free electrons with respect to the heavier ionic core in MNP. This in turn acts as a restoring force which initiates a coherent dipolar oscillation (as represented in Fig. 1c). When the frequency of the incoming light matches with the frequency of this electron motion, it creates a resonance condition which is manifested as the strong absorption and the physical origin of the color observed in noble MNPs (as seen in Fig. 1d from the colored colloidal suspensions of Au NPs).

The physical origin of linear optical properties such as extinction and scattering of a spherical MNP was first explained theoretically in the groundbreaking work by Mie in 1908 [9]. By solving the Maxwell's equations, he was able to explain the theory of scattering of an electromagnetic wave induced by a spherical particle. The extinction (absorption plus scattering) of a sphere of radius a with dimensions smaller than the wavelength of light can be expressed as:

$$E(\lambda) = \frac{(1+\chi)^2 8\pi^2 N a^3 \varepsilon_{out}^{3/2}}{3\lambda ln10} \left\{ \frac{\mathcal{E}_i(\lambda)}{(\mathcal{E}_r(\lambda) + \chi\mathcal{E}_{out})2 + \mathcal{E}_i(\lambda)^2} \right\}$$

with ε_r and ε_i being the real and imaginary parts of the metal dielectric function, respectively, and χ a shape factor whose value is 2. Later on, it was Gans who extended this theoretical model to other Au and Ag spheroidal particles [10, 11]. Apart from the geometry and dimension of the MNPs itself, other significant factors

that influence the frequency and width of LSPR peak are the dielectric constant of the MNPs itself and the local dielectric environment $\mathcal{E}_{out}$ (or refractive index, η of the medium that includes solvent and the surroundings in which the MNPs are dispersed or adsorbed in). For the noble metals like Cu, Ag, Au, the plasmon resonance is strongest in the visible part of the electromagnetic spectrum; whereas for other transition metals, the LSPR absorption peak is broad and only poorly resolved in the ultraviolet region. This difference in optical response could be attributed to the different dielectric constants of the metals as explained adequately in Drude's free-electron model and to the effects of interband excitation of plasmon transition [12, 13].

Elementary excitations such as plasmon when interact with the photon can result in a coupled excited state such as Polaritons. When surface plasmon in MNPs interact with the incoming photon of the electromagnetic wave, it forms surface plasmon polariton (SPP). These SPPs are essentially two-dimensional EM wave which are observed to be propagating at the interfaces between the conductor surface and dielectric [14–16].

In regard to this context, it is worth mentioning that some of the recent advancement in optical technology and the emerging various photonic applications rely vastly on the unique optical properties possessed by the MNPs such as the localized and propagating surface plasmon polaritons. To name a few, where this optical behavior of MNPs are widely exploited are development of near-field optical probes and enhanced optical detection techniques such as Tip-Enhanced Raman Spectroscopy, Surface-Enhanced Raman Spectroscopy and plasmon-based nanophotonic waveguide devices. Some of these techniques will be discussed later on under the topic of characterization tools and techniques of nanoparticles.

2 Excitons in Semiconductor Nanocrystals

With the emergence and improvement of several epitaxial growth techniques like Molecular Beam Epitaxy (MBE), Metal-Organic Chemical-Vapor Deposition (MOVCD) and microscopy based characterization methods like Scanning Electron Microscopy (SEM), Transmission Electron Microscopy (TEM) in the early 1970 s and 80 s, solid state physicists initiated the early investigations of so-called "quantum structures". The introduction of these early one dimensional spatially confined quantum-well structures had a profound impact on the later development of compound semiconductors in terms varied dimensions and extending the spatial quantum confinement into two dimensions (quantum wires, QWs) and in all three dimensions (quantum dots, QDs) [17, 18]. Under optical or electrical excitation, when a semiconductor absorbs a photon, it promotes an electron to the conduction band leaving behind a positively charged state 'hole' in the valence band thereby generating a bound electron-hole pair (known as "*exciton*") as can be seen from Fig. 2a. When the size of the semiconductor nanocrystallite is of the same order as the electrostatically bound characteristic length scale of electron-hole pair ("*exciton*

Bohr radius", describes the order of spatial extension of excitons and typically denoted in terms of length scale nm or angstrom, Å), the electron and hole are "quantum confined" by the crystallite boundary. In simpler terms, a quantum dot (QD) is a nanometer-sized crystallite composed of several thousand of atoms and usually of the size 1–10 nm. These QDs, often called "artificial atoms" exhibit discrete energy levels and electronic excitations with electron and hole wavefunctions delocalized within and confined by the dot boundary. Due to this particular discretization of density of states (DOS) and spatial confinement of electron and hole wavefunction, unlike the bulk material, these nanocrystals display strong dependence of their optoelectronic properties to their size and shape (Fig. 2b shows the energy band gap and dependence of emission properties on the size of NCs and degree of quantum confinement of excitons).

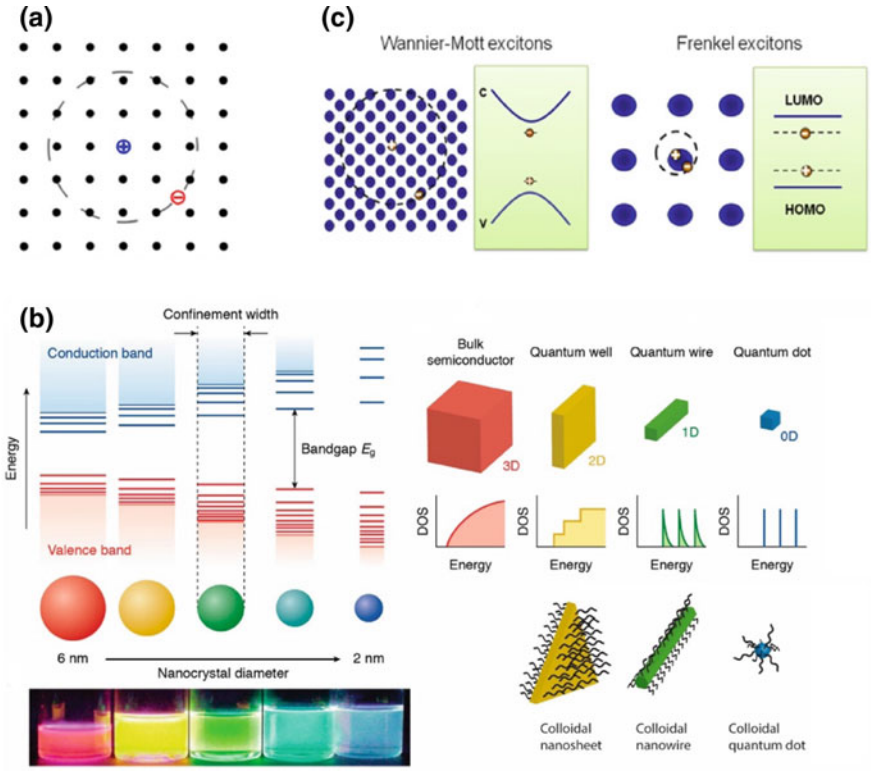

Fig. 2 **a** Cartoon shows the creation of electron-hole pairs ("exciton") within the crystal lattice. *Source* https://en.wikipedia.org/wiki/Exciton. **b** Schematic shows the quantum confinement of excitons in quantum dots and their continuous tuning of energy band-gap levels (emission color) as a function of their size. It also exhibits how the density of states (DOS) gradually change from continuous (bulk semiconductors) to discrete function (quantum confined semiconductors) Reproduced with permission from Donega et al., 2010. **c** Comparison of Wannier-Mott and Frenkel excitons

Louis Brus, who pioneered the field of "colloidal quantum dots" chemistry and photophysics offered a convenient description for these systems by treating them as particle in a sphere [19–23]. Using an effective mass approximation model, the Hamiltonian of the system could be described as:

$$\widehat{H} = -\frac{\hbar}{2m_h}\nabla_h^2 - \frac{\hbar}{2m_e}\nabla_e^2 - \frac{e^2}{\epsilon|r_e - r_h|} + polarization\ terms$$

where m_e is the effective mass of the electron, m_h is the effective mass of the hole and $\in$ is the bulk dielectric constant of the semiconducting material. This expression comprises of the kinetic energy terms of the confined charge carriers (hole and electron), and a Coulomb interaction. Finally, the polarization terms correct for the form of Coulomb interaction to consider the surface properties. From this Hamiltonian, the approximated energy expression of the lowest electronically excited state can be further derived as:

$$E(r) = E_g + \frac{\hbar^2\pi^2}{2R^2}\left(\frac{1}{m_e} + \frac{1}{m_h}\right)^2 - \frac{1.8e^2}{\in R} + smaller\ terms$$

Here, two main contributions are added to the bulk band gap energy (Eg). The first term represents the quantum localization of the electron and hole and scales as $1/R^2$. The second term represents the Coulomb interaction between the electron and the hole, and scales as $-1/R$. Since the Coulomb interaction is not strong, the confinement potential can be treated separately for electrons and holes. From this expression, we can see that for small enough particles the apparent band gap will increase when reducing the QD diameter. This is manifested as a blue-shift of the absorption band that correlates to the lowest-energy excitonic transition, as well as a blue shift of the emission band that correlates to the band-edge transition. Furthermore, the photoluminescence (PL) band in QDs is usually red-shifted compared to the wavelength of the absorption of the first exciton.This red-shift is terms *Stokes shift* [24], and is the result of coupling of the exciton to phonons which allows non-radiative relaxation of the excited charge carriers to the band edges prior to their radiative recombination. This relaxation typically occurs at a time scale of several tens to hundreds of fs (10^{-15} s).

Both electrons and holes can mutually coexist within the nanocrystal provided they are far apart from each other and therefore their mutual interaction could be neglected. In this case, each quasiparticle whether its an electron or hole behaves as an independently existing particle. However, if an electron and hole are located relatively close to each other, then it constitutes an electrically neutral formation. This kind of behavior is typically observed in *Mott exciton*, which although may move within the crystal lattice but doesn't necessarily contribute to charge transport. The *Wannier-Mott* type excitons exist as a result of reduced Coulomb interaction (screened electrostatic interaction) and they typically have radii larger than the lattice spacing [25]. Consequently, this type of excitons possesses much lower binding energy, of the order of 0.01 eV. On the other hand, in materials with a

relatively small dielectric constant, the Coulomb interaction between an electron and a hole may be strong enough such that the exciton radii is of the same order as the size of a unit cell. This type of molecular excitons with a much higher binding energy, of the order 0.1–1 eV is known as *Frenkel exciton*, named after Frenkel [26]. This type of excitons are typically found in alkali halide crystals and in organic molecular crystals composed of aromatic molecules, such as anthracene and tetracene. Besides these, an intermediate type between Frenkel and Wannier excitons, *Charge-transfer (CT) excitons* has been observed when the electron and the hole occupy adjacent molecules [27]. They are primarily observed in ionic crystals. Unlike Frenkel and Wannier excitons (displayed in Fig. 2c) they display a static electric dipole moment. Irrespective of the kind, an exciton in a semiconductor nanocrystal is not infinitely long-lived, instead they possess some finite lifetime (referred to as photoluminescence decay lifetime) and sooner or later they disappear. This typically happens in two ways: either by annihilation (recombination) of electron and hole constituting the exciton or by the dissociative process where an exciton breaks up into a free electron and a free hole.

It has been well recognized at this point that the key to most device development lies in the quality and the properties of the material from which the device is fabricated. As a part of semiconductor device development process and in the interest of performance characteristics, it is therefore essential to have a thorough understanding of the structure-property relationships, including the effect of impurities (intrinsic or extrinsic), nature of defects as well as uniformity of incorporation and position in the host lattice. These are some of the factors that most often determine the efficiency and performance of devices. Intense photoluminescence can be experimentally observed in many semiconductors utilizing most of the standard optical spectroscopy setups. The photoluminescence spectra provides an extensive source on identification of different electronically excited states and the spectral transitions arising either from different impurities, defects, surface or trap state related emission. The peaks and sharp lines appearing in the absorbance and photoluminescence spectra help us identify the bound excitonic states that act as a fingerprint of band-edge emission or bound-to-bound transitions. So, this makes exciton an important probe as far as the photophysical investigation of semiconductors are concerned.

3 Fabrication Techniques of Metal NPs, Semiconductor NCs and Metal-Semiconductor Hybrids

3.1 Synthesis of Metal NPs

The development of novel materials with varied functionality is the primary aim for the scientific community involved in materials chemistry research. After several decades of intense research effort and subsequent evolution of modern fabrication

techniques that has now made us possible to synthesize a wide variety of metal nanoparticles. Any researcher entering the nanoscience arena should definitely read Feynman's 1959 "There's Plenty of Room at the Bottom" speech, if only for its historical relevance. Besides just exploring the interesting optical properties of metal nanoparticles (MNPs), in recent times there has been a huge demand in the mass production of these MNPs due to its diverse applications in the field of catalysis, electronics, nanophotonics, photovoltaics (energy production and storage), health monitoring, environmental, biotechnology and so on. Noble MNPs such as Ag, Au and Cu usually exhibit increased photochemical activity because of their high surface/volume ratio and unusual electronic properties. Hollow nanostructures using these metals are a particularly interesting class of materials with unusual chemical and physical properties often determined by their shape and composition holds immense potential in the development of novel bio-sensing and drug-delivery applications [28–33]. Until now, several hollow nanospheres, cubes, rods, tubes, and triangles have been successfully synthesized using the colloidal bottom-up synthetic methods. Furthermore, recent usage of core/shell, alloyed, bi-/tri-metallic nanoparticles have attracted a significant amount of interest since they exhibit improved catalytic performance as compared to monometallic catalysts [34, 35].

Nanoparticles, in general can be broadly prepared by either physical (top down) or chemical (bottom up) methods (Fig. 3a shows the schematic of these fabrication approaches on how metal NPs can be derived from its bulk form). The physical methods which frequently involve vapor deposition of various reaction precursors depend on the principle of subdividing these bulk precursors into the form of nanoparticles. Several other physical methods such as ion-implantation [36–39], RF sputtering [40–42], pulsed laser ablation [43–46], proton beam irradiation, spray pyrolysis [47–49], atom beam co-sputtering, microwave irradiation [50, 51] and electrochemical based multi-pulsed techniques has emerged over the last few decades. These methods provide the possibility of controlling the nanoparticle size by adjusting several reaction parameters such as temperature, pressure, power density, gas flow rate etc. Figure 3b show the experimental schematics of vapor phase and laser assisted method of synthesizing metal NPs.

On the other hand, chemical approaches including solution based liquid phase routes are based on primarily reducing the metal ions to metal atoms in the presence of different colloidal stabilizers or surfactants, followed by controlled growth process and aggregation of atoms. Besides the early developed method of chemical reduction, electrochemical and photochemical reduction are widely used as well to fabricate metal nanoparticles. Wet-chemistry solution based techniques are frequently preferred because they are not only economical/inexpensive with advantages of low reaction temperatures and flexibility, but also they are highly effective in good size and morphology control with near uniform homogeneity of the as prepared nanocrystal samples.

Many of the earliest syntheses of nanoparticles were achieved via co-precipitation technique of sparingly soluble products from aqueous solutions followed by thermal decomposition of those products to oxides. Due to the

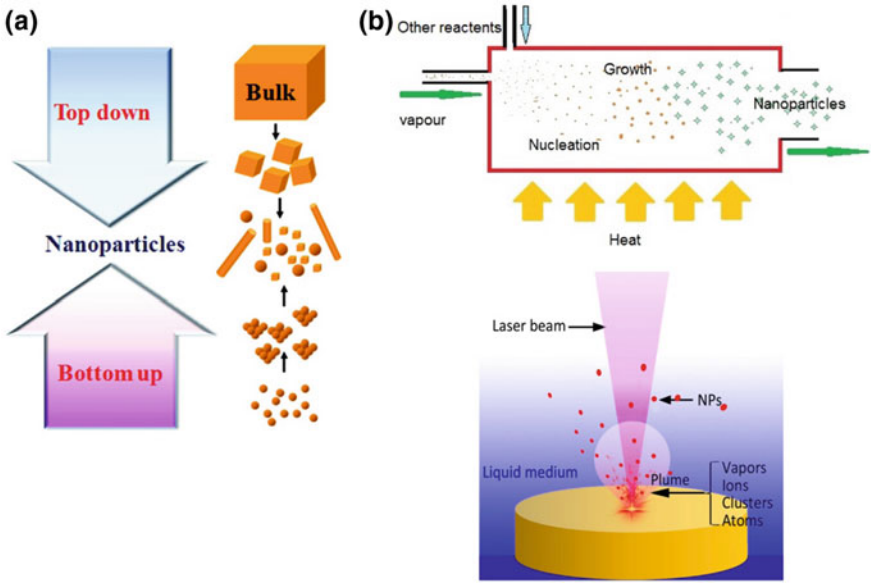

Fig. 3 **a** Schematic illustration of fabrication techniques of nanoparticles. **b** Cartoon shows chemical vapor phase (top) and pulsed laser beam-assisted (bottom) modes of syntheses. *Source* https://ninithi.wordpress.com/gas-phase-synthesis/. Reproduced with permission from Zhang et al., 2017

simultaneous processes of nucleation, crystal growth, coarsening and agglomeration, it is often challenging to isolate these individual stages of reaction which makes even difficult to control the size of the particles. It has still not been very clear on the fundamental growth mechanisms of this co-precipitation technique.

Enormous progress has been made in developing the general architecture method of fabricating multicomponent and multi shaped MNPs using template based methods such as: (a) *hard template* such as anodic alumina oxide (AAO) (b) *soft template* such as cationic surfactant CTAB, CTAC and (c) *sacrificial templates*. Hard templates provide a facile route to grow one-dimensional nanowires. In this method, the template acts as the scaffold where the wire-like nanostructure grow in the voids of the scaffold. Several other porous inorganic scaffold such as polymer membranes carbon nanotubes have been used too.

Using electrochemical deposition of the precursors into porous membrane of the scaffolds, freely standing one dimensional nanowires of different materials could be synthesized using this technique. Nanowires of magnetic materials involving transition metals (Fe, Co, Ni and alloyed forms like Fe–Pt, Co–Pt and others) have been prepared by several research groups using porous AAO templates. These materials are potentially useful in ultra-high density magnetic data storage devices. On the other hand, soft matter templates involve use of surfactant assemblies such as liquid crystals, micelles, vesicles, organic and organometallic ligands, polymers,

and hydrogels to grow metal nanostructures of varied morphologies. In the case of syntheses of Au and Ag nanorods with well controlled diameters and aspect ratios, this has been achieved from the self-assemblies of soft templates like cetyltrimethylammonium bromide (CTAB) or liquid crystalline phases made of sodium bis(2- ethylhexyl) sulfosuccinate (AOT), p-xylene, and water [50–60] (Fig. 4a, b shows the general see-mediated synthetic approach of fabricating Au nanorods of various aspect ratios).

Silver nanodisks have also been synthesized by sonicating $AgNO_3$ and hydrazine (N_2H_4) in the presence of reverse micelles self-assembled from an AOT/isooctane/water system. Polyol synthesis has proven to be a simple and versatile route to fabricating colloidal particles made of metals and alloys with typical examples including Ag, Au, Cu, Co, Ir, Ni, Pd, Pt, Ru, CoNi, and FeN. Among a few others, Xia's group demonstrated a polyol synthesis method to control silver nanostructures by reduction of silver salt ($AgNO_3$) with ethylene glycol in the presence of poly-vinylpyrrolidone (PVP) [61–70]. This process involves the reduction of an inorganic salt (silver nitrate) by polyol at an elevated temperature with PVP as the surface stabilizers (also prevent in agglomeration) of as prepared colloidal Ag NPs. The rate of nucleation and growth processes can be ideally controlled with careful monitoring of temperature. It is believed that PVP kinetically control the growth rates of various faces of silver by adsorption and desorption effects, suggesting that there seems to exist a selectivity capping of specific facets for the functional group. Consequently, the growth rates of some surfaces would be greatly decreased, leading to a highly anisotropic growth of these nanostructures. Figure 5 shows the schematic of Ag NP synthesis with various morphologies from nanocubes to nanowires with different edge lengths and aspect ratios.

When it comes to the synthesis of gold nanoparticles, probably the most convenient and widely used synthesis technique so far is the so-called "citrate route" (now more widely known as "Turkevich method") originally developed by Turkevich et al. more than 60 years ago. The chemistry of this reaction process is very simple which involves reduction of Au^{III} salt (used in the form of $HAuCl_4{\cdot}3H_2O$) to Au NPs in the presence of sodium citrate (reducing agent) and water as the reaction medium (solvent) [71–76]. The obtained gold nanoparticles using this rather simple method exhibit a spherical morphology with a relatively narrow size distribution (20 ± 1.5 nm). Although the citrate route is still very popular for the preparation of aqueous gold nanoparticle sols, many other approaches have been developed, performed in specific organic solvents or in the presence of different types of surfactants like long chain alkylamine or alkyl acids and reducing agents to fine-tune the morphology and develop fascinating architectures from nanocubes to hexagonal shapes, nanorods, nanoprisms, nanoflowers and nanostars [77–79]. Brust et al., however, reported the synthesis of alkanethiol stabilized colloidal Au nanoparticles that are stable almost indefinitely in nonpolar solvents [77–79]. Using the similar reaction, Ag NPs have been prepared by reduction of $AgNO_3$ or $AgClO_4$ by N,N-dimethylformamide (DMF), where APTES (3-(aminopropyl)trimethoxysilane) served as the stabilizing agent. With the variation of different synthetic parameters like reaction precursor concentration, type of

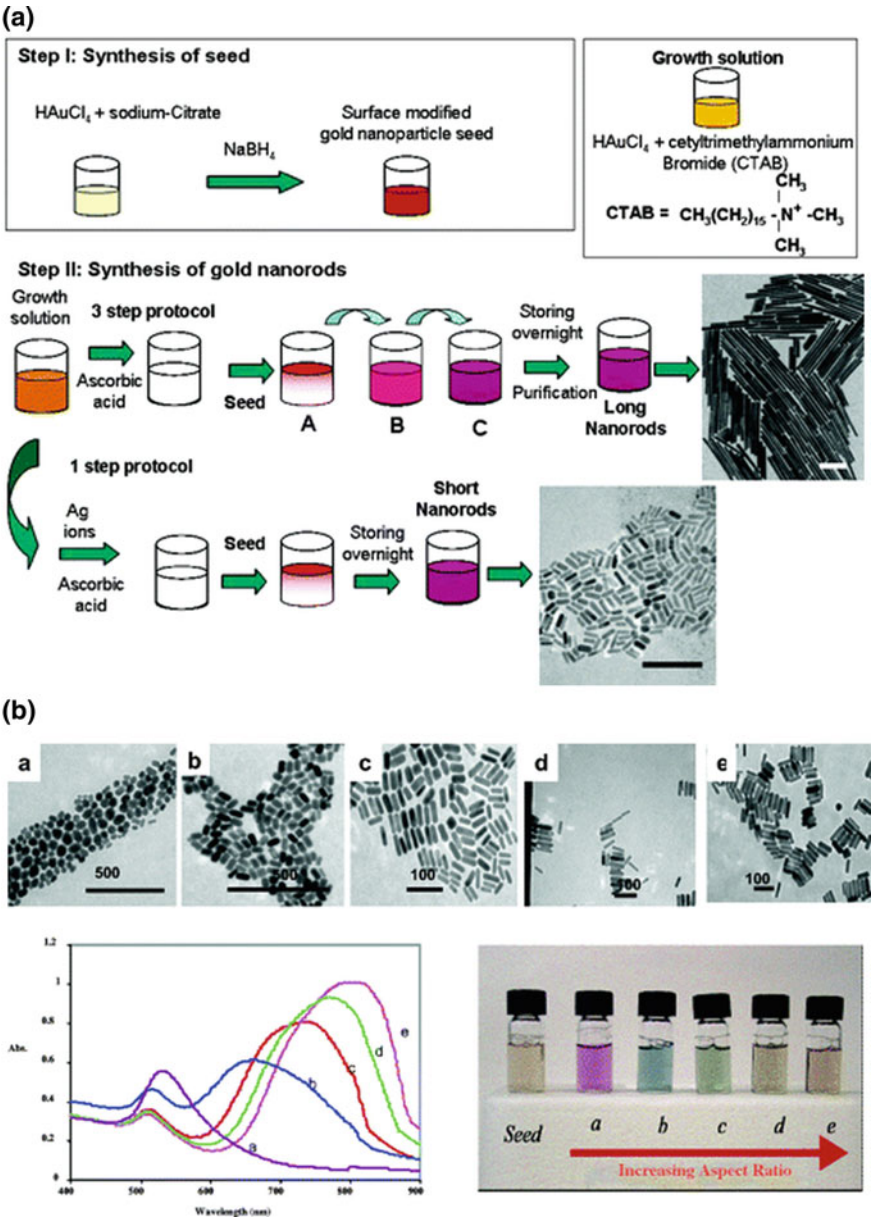

Fig. 4 **a** Schematic of the seed-mediated synthesis of gold nanorods The seed is modified with citrate (that acts as the reducing agent); ascorbic acid here acts as weak reducing agent A−C are each growth solutions; the seed is added to A, and then after the color changes, an aliquot of solution A is added to B, etc. For short gold nanorods, silver nitrate and ascorbic acid are added to the growth solution, followed by the seed solution. Shown at the right are TEM micrographs of the final purified (centrifuged and washed) gold nanorod products. Scale bars represent 200 nm. Reproduced with permission from Murphy et al., 2006. **b** Transmission electron microscopic images (top), optical extinction spectra (left), and photographs of (right) aqueous solutions of gold nanorods of various aspect ratios prepared via seed-mediated approach. Reproduced with permission from Murphy et al., 2005

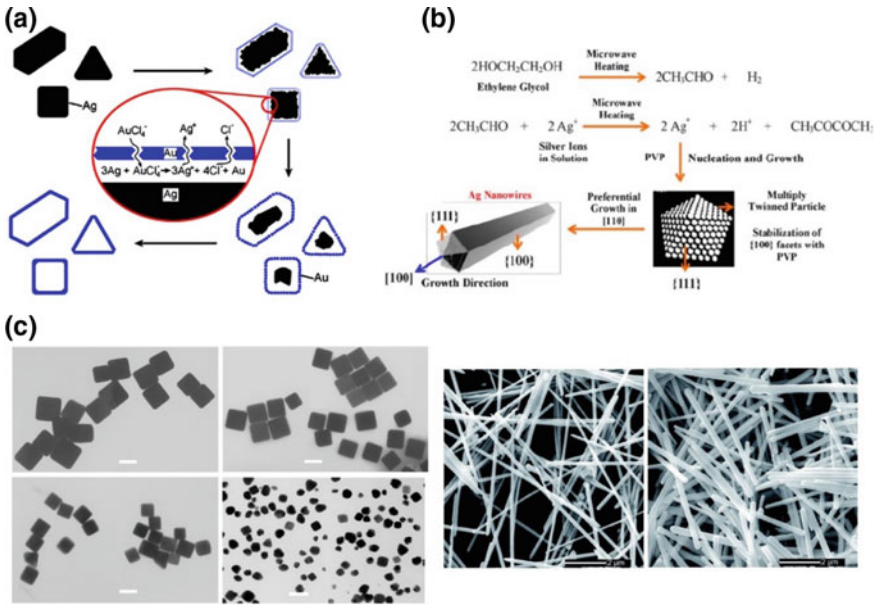

Fig. 5 **a** Schematic illustration of the experimental procedure that generates nanoscale shells of gold from silver templates with various morphologies. Note that the shape of each silver nanoparticle is essentially preserved in this template-engaged reaction. Reproduced with permission from Sun et al., 2002. **b** Schematic shows the microwave-assisted synthetic methodology of polyvinyl pyrrolidine (PVP) capped anisotropic silver nanowires Reproduced with permission from Melendrez et al., 2015. **c** TEM images of silver nanocubes (left) with different edge lengths; Reproduced with permission from Sun et al., 2002 and silver nanowires (right); Reproduced with permission from Ma et al., 2014

surfactants or co-surfactants temperature and growth time, these solution phase methods can facilitate in fine tuning and shifting the major plasmon resonance peaks of the MNPs as experimentally observed from their optical absorption spectra.

Growth of metal nanostructures with a hollow interior by utilizing the outer shell or surface as the template is the heart of the sacrificial template method. In regard to this, a number of different approaches has been recently developed involving the *Ostwald ripening* and *Kirkendall effect* to synthesize various hollow core-solid/porous shell metal nanostructures [80–84].

The *Kirkendall effect* (as can be seen from Fig. 6a which shows the schematic with its general mechanism which is explained by the difference in diffusion rates of two or more different solids, its origin lies at the field of general metallurgy. Due to the differential rate in the diffusive migration of solids (or reactants), the resultant product often exhibit some alloyed form and a certain degree of porosity. It was later experimentally proven that atomic diffusion occurs between cation exchange vacancies and not by actual interchange of atoms. The sacrificial template has

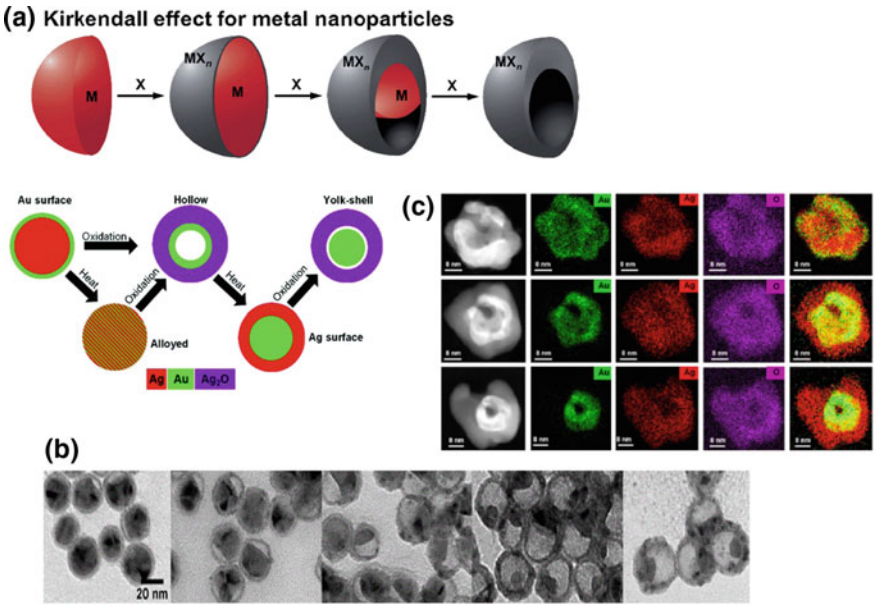

Fig. 6 **a** Graphical depictions of examples of NP conversion chemistry via- Kirkendall effect: during the reaction of the metal (M) with reactive species X to form MX_n, void formation occurs resulting in alloyed, hollow and yolk-shell like structures Reproduced with permission from Tracy et al., 2014. **b** TEM images of single Au NPs and gradual incorporation of Ag resulting in formation of Ag–Au hollow NPs. **c** Real-time imaging and HAADF STEM elemental mapped images showing the transformation of a single nanoparticle, from an Au surface segregated Ag–Au structure to a hollow Au-core Ag_2O-shell structure. Reproduced with permission from Lewis et al., 2014

proven to be an effective method for fabrication of hollow metal nanostructures by consuming the more reactive component (template) exploiting the process of galvanic replacement occurring between the template and the reactant. This process of controlled synthetic methodology using *Galvanic replacement* reaction allows us to design varied structures of hollow (Fig. 6b) and bi, trimetallic MNPs that are extensively desirable towards photocatalytic and electrocatalytic applications. Transforming metal nanostructures into hollow structures improves their performance because doing so reduces their densities with increment in their surface areas above those of their solid counterparts [84–91].

3.2 Synthesis of Semiconductor NCs

Semiconducting nanocrystals (NCs), especially the class of inorganic semiconducting fluorophores which are more popularly known as quantum dots (QDs) have

long proven an excellent track record in the field of electronics, photovoltaics and optoelectronics. In addition to broad range light absorption capability with sharp, spectrally pure tunable emission these materials also possess superior charge carrier mobilities with high thermal and photo stability. Due to their interesting opto-electronic properties and their ever-increasing demand in applications ranging from electronics, biosensing, bioimaging, catalysis to renewable energy, it is becoming more necessary now than ever to fabricate these functional nanostructures in a more inexpensive and versatile fashion [92–104]. Therefore, solution processed colloidal fabrication of these inorganic semiconducting nanostructures is itself developing into a whole new branch of synthetic chemistry. Starting with preparation of simple objects like monodispersed spherical inorganic core particles, over the last few decades the field has evolved into fabricating more sophisticated and complex nano architectures like core/shell, core/(multi) shell, quantum rods, quantum wires, dumbells, tetrapods, quantum dots in rods, nanoplatelets and so on [105–113]. Figure 7a shows the architecture of semiconducting NCs with various morphologies that can be fabricated using wet-chemistry colloidal method.

These colloidal hetero nanocrystals can be regarded as solution grown hybrid nanoparticles since most frequently it possesses an inorganic component that are overcoated with a layer of organic component. These organic components usually composed of either ligand of different functional groups, polymers or molecular linkers that act as some sort of surfactant or surface stabilizers for the inner inorganic component (Fig. 7b). The interaction between the inorganic component and the outer organic surfactant layer allows us to tune the size and shape of the heteronanocrystals that are manifested by novel optoelectronic properties of these materials [114]. One of the important manifestations of quantum confinement in these semiconducting nanocrystals is the correlation between the particle size and their electronic structure. The degree of discrete spatial delocalization between electron and hole states can be precisely tuned by varying the particle size. In addition to this, the organic layer allows the synthetic chemists another degree of freedom to tailor the material's properties by manipulating its surface chemistry. Typically, these colloidal semiconducting nanocrystals are chemically synthesized using appropriate molecular compounds such as inorganic salts or organometallic precursors. Early attempts based on the wet chemical solvothermal syntheses were successful in fabrication of several type II-VI, III-V classes of chalcogenides like CdSe, CdS, CdTe, PbSe, PbS, InS, ZnTe, InP, InAs and so on. Later on, with further synthetic efforts, compound heterointerface based semiconducting nanocrystals with designs including core/shell, core/multishell, alloyed core/shell etc. by combining different types of materials were also obtained. The most popular method of preparing these nanocrystals in a rather flexible and inexpensive fashion is the *hot-injection method*, which was introduced in a seminal paper published by Murray, Norris and Bawendi in early 90s, which skillfully applied a principle of 'separation of nucleation and growth' to prepare high quality monodispersed quantum dots [115, 116]. In this method, the precursors are rapidly injected into the hot solvent followed by subsequent quenching (cooling down) of the reaction. This method, in general involves several consecutive stages of crystal formation starting

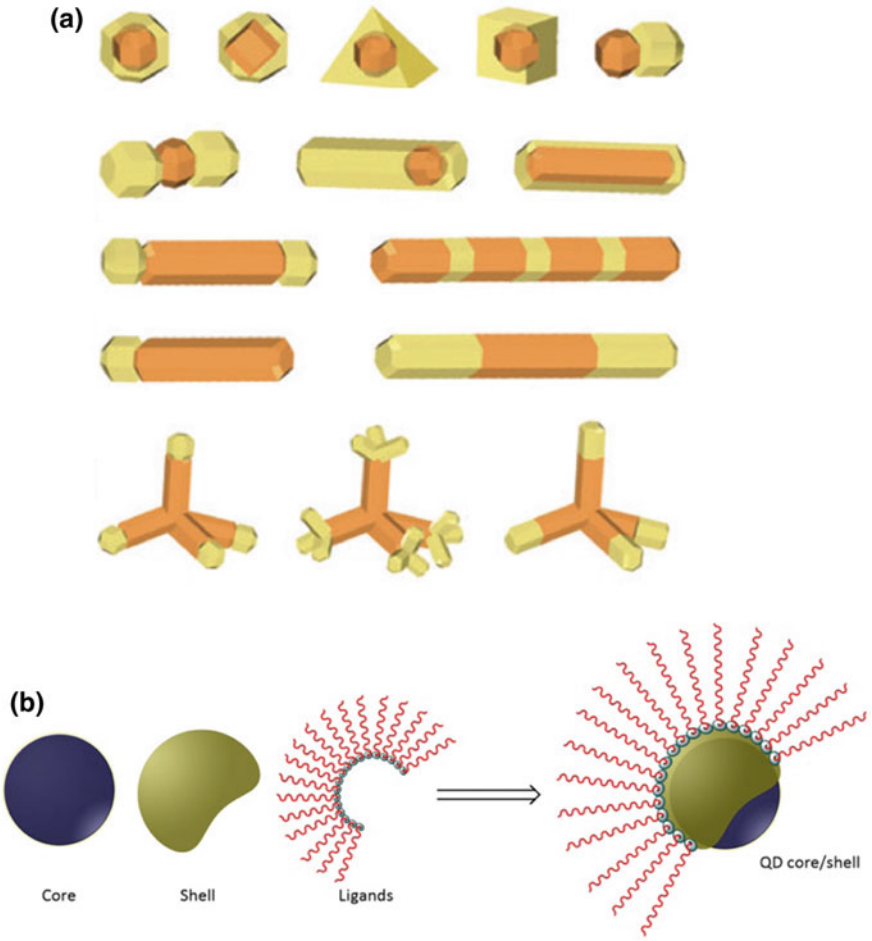

Fig. 7 **a** Schematic survey of colloidal HNC architectures (for clarity the surfactant layer is not represented). The diversity of possible material combinations for each category can be illustrated by a few examples with morphologies ranging widely from core/shell, dot-in-rod, dumbbell, core/shell nanorod, tetrapod and so on. Reproduced with permission from Donega et al., 2011. **b** Cartoon shows the transformative process of core to core/shell overcoated with organic ligands. *Source* https://www.intechopen.com/books/green-nanotechnology-overview-and-further-prospects/-green-quantum-dots-basics-green-synthesis-and-nanotechnological-applications

with nucleation from homogenous solution mixture of molecular salts (precursors), growth of preformed nuclei followed by arresting the growth process and further isolation of the nanocrystals of desired size from the reaction mixture and other post-preparative processing or treatments. Using this method, most often the size and the optoelectronic properties (as a result of quantum confinement of excitons) of the nanocrystals can be finely tuned by variation of precursor and surfactant

concentration, injection and reaction growth temperature, reaction growth time and cooling process. In a colloidal synthesis, the semiconducting nanocrystals grow through a process known as *Ostwald ripening* mechanism wherein the largest particles grow at the expense of dissolving smaller nuclei in the solution. As a result, the average particle size increases with time and the monomer (precursor) concentration decreases. In order to understand the growth mechanism process and the particle size distribution, Peng et al identified two separate regimes involving the growth process that were referred to as "focusing" and "defocusing" [117–123]. *Nano-Ostwald ripening* model was further proposed to describe the evolution of an ensemble of particles in nanoscale form. The nucleation and growth process occurs in the presence of different organic surfactant molecules like long chain carboxylic acids (Oleic acid), phosphonic acids (Tetradecylphosphonic acid, TDPA; Octadecylphosphonic acid, ODPA), amines (Oleylamine, Hexadecylamine), alkanethiols (Dodecanethiol, DDT), alkyl phosphines (Tributylphosphine, TBP; Trioctylphosphine, TOP) or alkyl phosphine oxides (Trioctylphosphine oxide, TOPO) used either as coordinating solvents such as (also acts as ligands) or non-coordinating solvents like 1-octadecene, ODE (act as reaction medium). With a judicious control and manipulation of surface chemistry utilizing these ligands, one can eliminate the mid-gap, shallow or surface trap states that are associated with surface dangling bonds resulting in highly photostable and with better luminescence quantum efficiency of the nanocrystals. Discussion of solution phase semiconducting nanocrystals will be left incomplete without mentioning other methodologies like low temperature aqueous phase or sol-gel synthetic techniques. In comparison to high temperature synthesis taking place in non-polar organic solvents, the aqueous phase follow milder and greener conditions using low temperature and utilizing thiol molecules with polar groups (thioglycolic acid, cysteamine) or amino acids (L-cysteine, Glycine) or even silica or polymer (polyethylene glycol, PEG) capped nanocrystals. Generally, the NCs made in aqueous medium are not as monodisperse or as high quality as those prepared typically in organic solvents, but in other aspects, such as luminescence efficiency, colloidal stability, and, especially, cost per gram, they can be very competitive. The other prominent methodology is the *sol-gel* route which has been widely used for synthesis of oxide based materials. Typically, it involves hydrolysis or polycondensation of metal alkoxides or metal chloride precursors to form a colloid. Traditional sol-gel technique involves a series of hydrolysis and condensation in pH controlled acidic or basic aqueous or alcoholic media resulting in formation of colloidal (sol) which controllably aggregate to form a wet network of agglomerates or nanocomposites (gel). Depending on how the wet gel has been dried, the density and porosity of the extended network can be modified. Post-synthetic treatments including thermal annealing, drying and supercritical extraction of solvent from the gel often results in aerogels and xerogels. Analogous to bulk crystals, the nanoparticles are terminated by crystal facets of different surface energies that expose various crystallographic planes. Site selective attachment of surfactant molecules (ligands) to certain crystal facets and preferential growth along a specific plane or crystalline axis allow us to tune the growth kinetics and morphology of nanocrystals, often resulting in highly

anisotropic materials like dumbbell, arrow shaped, tetrapods, teardrop like architectures. Other growth mechanism techniques like the oriented attachment and solid-liquid-solid are often applied to engineer the shape of the nanocrystals resulting in the formation of nanowires or oriented branched chains [117–123].

Besides the conventional type II–VI, compound semiconducting nanocrystals belonging to category II–V have attracted much attention since they exhibit strong size- and composition—dependent optical and electrical properties capable to incorporating in large-gain low-threshold quantum cascade lasers, light emitting diodes, single electron transistors, avalanche photon detectors and so on. GaAs and InGaAs are one of the most important semiconducting materials with potential applications in developing integrated circuit technology, infrared photodetectors, quantum well lasers, solar cells etc. So far, electrochemical based and laser ablation techniques have been widely used to fabricate GaAs nanocrystals with various sizes and densities. In addition, laser-induced etching method using a Nd:YAG (1060 nm laser) has been also used to synthesize GaAs nanocrystals with high purity. Most importantly, one of the prevalently used top-down fabrication method of *molecular beam epitaxy (MBE)* has been acting as the primary synthetic workhorse in semiconductor based microfabrication industries to prepare InAs and GaAs based devices. *Metal-organic vapor-phase epitaxy (MOVPE)* has also been used earlier to prepare these classes of semiconducting nanocrystals.

The toolbox of wide variety of synthetic techniques is rapidly expanding with many novel structures of wide functionality are getting reported every year. No doubt, the synthetic efforts among the material scientists will further continue, providing both scientists and engineers with potential functional building blocks to design and progress the field of nanoelectronics and nanophotonics.

3.3 Synthesis of Metal-Semiconductor Hybrid Nanostructures

With an advancement in nanoscale optics that led to a major progress in the development of nanoelectronic and nanophotonic devices over the last few decades, it is becoming more obvious to us the necessity of designing novel multifunctional hybrid nanostructures involving disparate building blocks like metal nanoparticles (MNPs) and semiconducting nanocrystals (SNCs). Hybrid nanoassemblies and nanostructures fabricated from plasmonic MNPs and excitonic SNCs often exhibit unconventional optoelectronic properties arising from the mutual synergistic interaction between these individual components. As a result of plasmon-exciton interaction occurring in most of the metal-semiconductor hybrid nanoparticles, it often alters their optical properties like plasmon resonance (spectral linewidth, line shift), scattering, exciton generation and exciton recombination dynamics which lead to particles with entirely new properties that are different from either of the

nanocomponents. This opens up new doors of applications in the fields of optical communication, lasing, biosensing and photovoltaics.

Over the past decade, numerous synthetic strategies have been developed as a result of improving the synthetic efforts involved in nanoscale systems. Until now, several multicomponent hybrid nanostructures utilizing MNPs and SNCs have been fabricated with well controlled morphology and composition both via colloidal bottom-up and top-down methods. Synthetic methods can be broadly categorized as such in two parts: solution-based approaches and substrate-based techniques [124] (Fig. 8 shows the diagrammatic representation of solution and substrate based bottom up strategies to fabricate colloidal quantum dots).

In order to obtain such hybrid heterostructures with desired optoelectronic properties, several factors like shape, size, composition, relative concentration, spatial orientation, geometry & inter-particle distance between the individual nanoconstituents need to be considered while designing them. While perhaps the simplest means of achieving MNP-SNC hybrid assemblies rely on solution based technique, it comes with its own set of limitations, namely, precise control and arrangement of different nanoconstituents is hard to control. This often results in

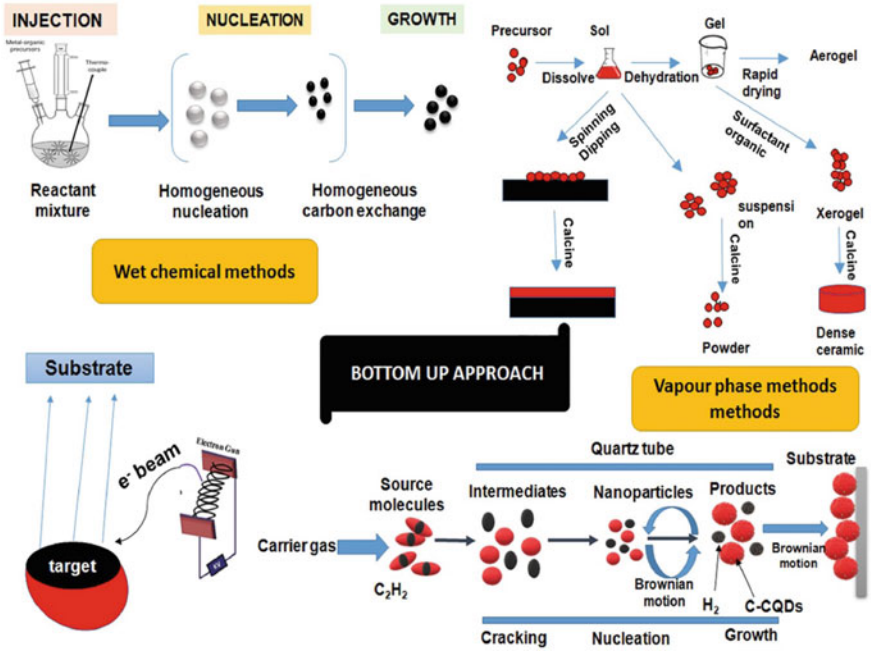

Fig. 8 A diagrammatic representation of different bottom–up approaches for quantum dots synthesis. Bottom–up approaches involves the rearrangement and assembling of small atoms and molecules to achieve large nanostructures which could involve techniques ranging from wet-chemical based to vapor-phase methods (sputtering, substrate based physical and chemical vapor deposition), Reproduced with permission from Singh et al., 2018

low reproducibility and low yield. Nevertheless, a wide variety of other techniques have been introduced and utilized by several research groups to fabricate such hybrid assemblies in solution, including covalent linkage of small molecules, biomolecules, DNA hybridization and self-assembly to build superlattices. Generally speaking, the solution based synthetic methods can be broadly categorized into two categories. The first method involves growing metal (or semiconductor) components onto pre-synthesized semiconductor (or metal) nanocrystals, either growing them at the tips or terminal ends of the nanocrystals. The second approach relies on combining pre-fabricated metal and semiconducting nanoconstituents by means of either wet-chemistry methods or by physical adhesion or adsorption. Some of the solution based approaches on developing these multicomponent heterostructures was initiated earlier by Banin's group [107, 112, 125, 126] which involved site-selective deposition of noble metals (Au, Ag) onto the tips of pre-synthesized semiconductor nanocrystals resulting in metal-semiconductor heterointerfaces or segmented heterojunctions (Au-tipped CdS, CdSe nanorods) [127–129] as can be seen from Fig. 9.

This site-selective deposition [130] has been further applied to fabricate other structural variations such as Au, Pt, Pd tipped CdS, Ag_2S and so on as displayed in Fig. 10.

Combining two or more metals on the same semiconductor-metal hybrid system through core/shell structures or by creating interfacial alloys can often lead to enhanced physicochemical properties including electric field enhancement,

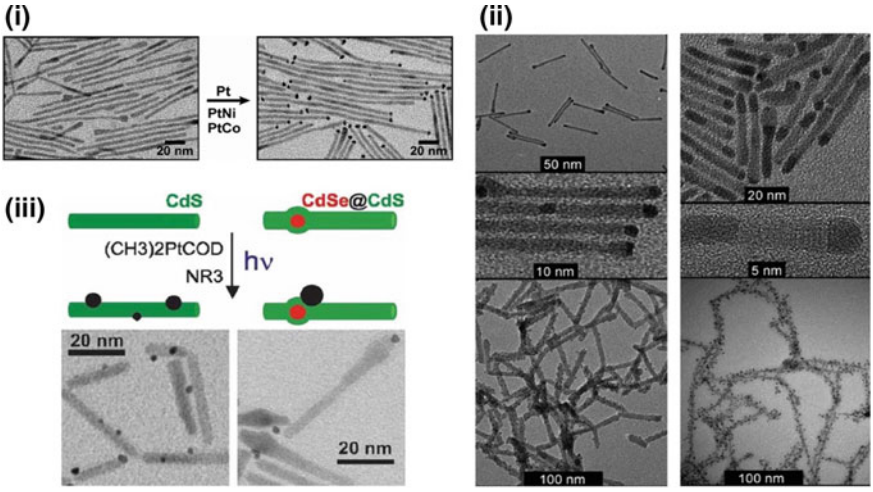

Fig. 9 (**i**) TEM images showing selective growth of Pt, PtNi and PtCo on the tips of CdS nanorods, Reproduced with permission from Habas et al., 2008 (**ii**) TEM images showing family of hybrid CdS-PdX (X = O, S) nanoparticles, Reproduced with permission from Shemesh et al., 2010 (**iii**) Diagrammatic representation and resultant TEM images of preferential photochemical deposition of Pt on CdS nanorods and CdSe@CdS core@shell heteronanorods, Reproduced with permission from Dukovic et al., 2008

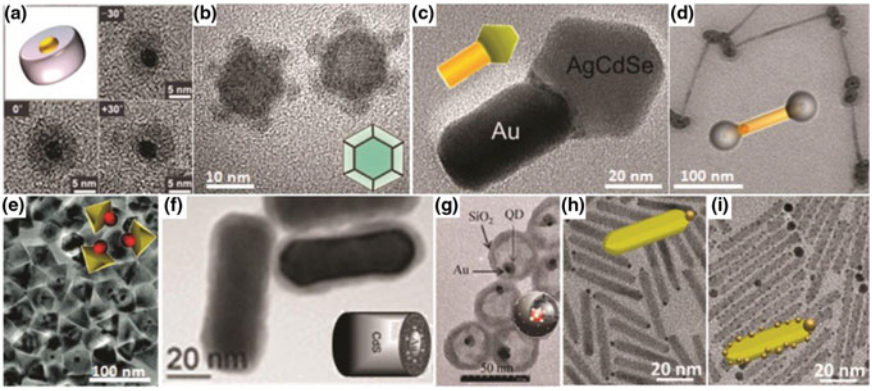

Fig. 10 Various hybrid nanoparticles with their corresponding schematic architectures and TEM images ranging from **a** Cu_2S-Au **b** Ru nanocaged Cu_2S **c** AgCdSe-Au nanorods **d** CoO-tipped CdSe/CdS nanorods **e** ZnO-Au nanohexagonal pyramid **f** CdS-Au core/shell nanorod **g** CdSe/CdS/ZnS- Au @ hollow SiO_2 yolk/shell nanospheres **h** Au-tipped CdS nanorod **i** CdS-Au body decorated nanorod, Reproduced with permission from Banin et al., 2014

surface plasmon modification. Due to efficient charge separation at the metal-semiconductor interface, these hybrid nanostructures also exhibited enhanced photocatalytic activity upon optical excitation. Another method is seed-mediated growth approach where metal nanocrystals act as seed and help initiate one dimensional growth of different metal chalcogenides (CdS, MnS, ZnS, CdSe) onto specific crystal facets. Other solution based methods via photoinduced heteroepitaxial nucleation, hydrothermal growth and aqueous phase oxidation resulted in different forms of hybrid materials such as metal/semiconductor core@shell heterostructures.

For strategies relying on covalent linkage, the MNPs and SNCs are most often coated with ligands with different reactive functional groups which upon mixing forms a covalent bond such as amide, imine or disulfide linkage between the metal and semiconductor nanocomponents [131–134]. Usage of small molecules (cross-linkers) and activators like EDC (dimethylaminopropyl) carbodiimide and N-hydroxysuccimide (NHS) via EDC-NHS coupling has been a facile route to link quantum dots (QDs) and small metal NPs through formation of an amide linkage between them. The QDs are initially made water soluble through surface functionalization with certain polymers like polyethylene glycol (PEG) ligand terminated with either carboxylated (-COOH) or carboxy-thiol groups e.g. 3-mercaptopropionic acid (-COOH-SH) so as to bind both the QDs and the MNPs. To this end, EDC-NHS coupling has been successfully used to couple Au, Ag NPs and CdSe/CdS, CdSe/ZnS QDs via a peptide linker (Fig. 11a). Equally as effective was an azo linkage wherein the QDs are functionalized with 4-aminothiophenol and further converting into diazonium group (Fig. 11b). In both these cases of covalent linkage strategy, it was possible to bind two to four MNPs surrounding the QDs

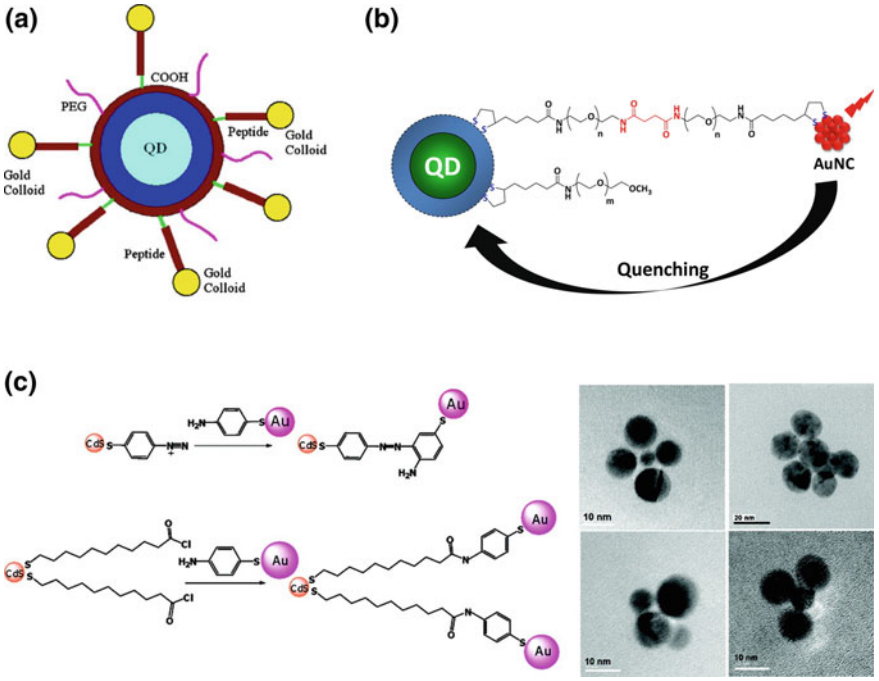

Fig. 11 **a** Schematic shows Au NP linkage to quantum dots (QD) via peptide-bond, Reproduced with permission from Chang et al., 2005. **b** Schematic representation of the QD-PEG-AuNC conjugates; one cluster per conjugate is shown, Reproduced with permission from Aldeek et al., 2013. **c** Schematic shows the amido- and azo-linkage chemistry of nanoparticles alongside with the TEM images of typical assembly of nanoparticles with amido- linkages with dimer, trimer and tetramers of Au dots surrounding the CdS QD, Reproduced with permission from Maneeprakorn et al., 2010

based on the relative concentration of individual constituents or one in excess of other (Fig. 11c).

Compared to linking via small molecules, linking with biomolecules especially DNA offers several advantages. With DNA being such a versatile molecule where the specific lengths can be varied using number of base pairs. In addition, its double helix structure is fairly rigid which allows precise control of inter-particle spacing between the nanoparticles. Until now, DNA hybridization has been used by several researchers to link MNPs to QDs ranging from different inter-particle distance to different conformations forming superlattice self-assembled MNP-QD nanostructures [135–138]. Usually, in order to link the nanoparticles through DNA hybridization, a single-stranded DNA (ssDNA) has been utilized so far to functionalize both the MNPs and QDs. Since linkage of Au NPs is usually strong and stable with thiol- (-SH) group, direct addition of thiol-terminated ssDNA has been used to accomplish successful binding of DNA to Au NPs. On the other hand, in order to link DNA with QDs, they first need to be aqueous soluble which

is done through ligand exchange using carboxylate molecules such as DHLA, 3-mercaptopropionic acid (MPA) or even pre-coating the QDs with water soluble polymers like PEG which can then be further coupled with DNA. The techniques of using DNA origami has been extensively used by Liedl group [135, 137] to achieve better control over the coupling process. Using DNA origami scaffolding methodology, the general shape of the obtained structures varied in different topological forms from triangle, square to even arms with satellites. By altering the DNA origami structure by varying the length and number of arms or even the arrangement of satellites per arm, a remarkable precision could be obtained between the nanoparticles in terms of their relative location, orientation and spatial arrangement as can be observed from Fig. 12.

Similarly, using biomolecules like proteins with affinity for each other have been exploited so far for coupling of MNPs and QDs. The most commonly used is the biotin/streptavidin complex due to its well-known affinity between these two partners as well as easy commercial availability of core/shell QDs functionalized with streptavidin which could be linked to biotin functionalized MNPs. To this end, Kotov's lab has performed extensive work using biotin-streptavidin complex binding to attach MNPs on the surface of QDs and nanowires [139–141]. Bovine serum albumin (BSA) is another functional protein that has also been used to fabricate self-assemblies between MNPs and QDs. This could be done via EDC coupling by attaching MPA-capped QDs to BSA-stabilized MNPs. BSA can also interact with the nanoparticles through charge or electrostatic interactions with the ligands attached to nanoparticles. Self-assembly of similar and disparate nanoparticles occur through electrostatic attraction, ligand exchange or hydrophobic interactions. With no additional chemistry being involved, self-assembly techniques are the most straightforward tools when it comes to fabricating nanoassemblies with usually large area network of interconnected particles. While relying on electrostatic

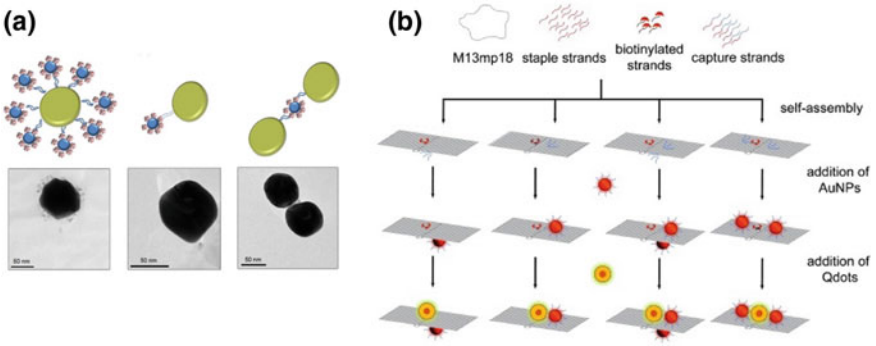

Fig. 12 **a** QD-Au NP hetero-complexes where QDs are surrounded by streptavidin which are intermediately connected to biotin-dsDNA-thiol molecule attached to Au NPs, Reproduced with permission from Cohen-Hoshen et al., 2012. **b** Engineering of QD-Au NP conjugates and their self-assembly using DNA origami constructs, Reproduced with permission from Hyeon Ko et al., 2012

self-assembly, the MNPs and QDs must be functionalized with oppositely charged ligands. With varying molar ratio of individual components, the architecture and particle size distribution could be more or less controlled, though not to a very high degree of precision. A more complex self-assembled organization was previously undertaken by Kotov's group where the positively charged CTAB-stabilized Au nanorods and negatively charged cysteine capped CdTe QDs were mixed resulting in monomeric subunits of Au nanorods surrounded by QDs. Self-assembly can be also achieved by relying on surface manipulation of via ligand exchange which provides a more rugged connection than electrostatic self-assembly and also leading to a better control over the spacing and structure of the assembly. Besides short chain organic molecular linkers, block copolymers such as poly(isoprene)-b-PEG have been also utilized as ligands to facilitate thiol-based self-assembly. In order to control particle spacing between the assembled nanoconstituents, polymer, siloxane and silane shells have been also exploited to instead of using longer linkers like DNA or protein. Using such shells added extra advantage providing rigidity and even preventing such nanoassemblies from aggregation. MNPs coated with silane shells via amine group ligand exchange and then controlling the thickness with addition of tetramethoxysilane (TMOS) have been used earlier to attach QDs pre-functionalized with mercaptopropyltrimethyl- (MPTS) or trimethoxysilane (MPTMS). Specifically, the surface of the MNPs was modified with a layer of dielectric silica spacer via a Stober's reverse microemulsion method followed by specific adsorption of QDs onto these amino functionalized shells. This method resulted in one to two monolayers of QDs surrounding the MNPs. Another similar study was conducted by growing silane shells around Ag nanowires and then attaching CdSe/ZnS QDs. Here, MPTS monolayer was first grown on Ag nanowires, and then tetraethylorthosilicate (TEOS) was further added to grow the silane shell with controllable thickness. Once again, the inter-particle distance was controlled by changing the relative concentration of the silicate precursors. Hybrid nanoarchitectures in the form of a more compact plasmonic/fluorescent system has been realized as metal-core@semiconductor-shell systems. A couple of studies has been reported where a continuous ultrathin Au-nanoshell has been used to grow around silica-encapsulated QDs [125, 142–145] (Fig. 13c, e).

In comparison to most solution based approaches, the substrate based fabrication of MNP-SNC self-assemblies offer more control. The substrate itself offers an additional degree of freedom to create various design of ordered nanoassemblies which could be created using various state of the art nanopatterning techniques. However, most often these nanopatterning top-down approaches could be rather time consuming and expensive and involve usage of specialized instruments and clean room nanofabrication facilities. Although this substrate based methods possess the capability to fabricate more uniform precise self-assembled structures, they generally involve the use of smaller quantities as compared to solution based techniques and are mostly reserved for single particle studies or synthesis of well-ordered nanoarrays. Two-dimensional binary superlattices using different components like MNPs and SNCs has been created using substrate based self-assembly method on comparatively large micron sized wafer or pre-patterned

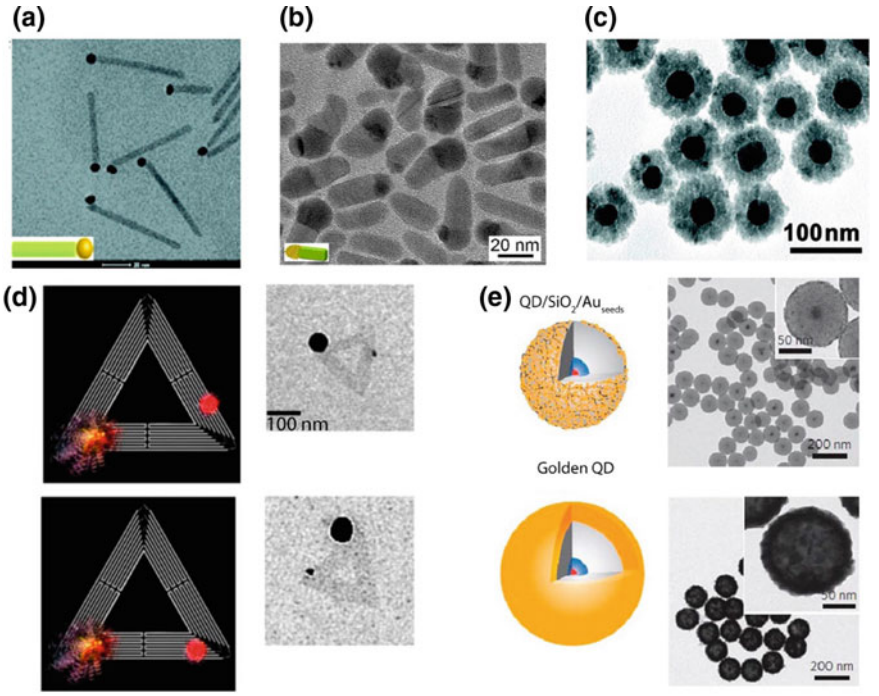

Fig. 13 TEM images of hybrid metal–semiconductor nanostructures. **a** Au-tipped CdS nanorods. **b** Heterogeneous Ag–CdSe nanorod. **c** Au@Cu_2O core@shell nanoparticles. **d** Schemes and corresponding TEM images of Au NP and a QD assembled onto a triangle DNA origami with controlled spacing. **e** Schematic representation and corresponding TEM images of QD/silica/Au seeds and QD/silica/Au nanoshell, Reproduced with permission from Dey et al., 2016

substrates. Several factors are involved while fabricating these nanodimensional superlattices like the solvent evaporation rate, physical properties of the solvent, functionality and steric factors from ligands, interactive forces between the substrate and the nanoparticles like VanderWaals force, electrostatic repulsion/attraction and interfacial cohesive/adhesive forces between the substrate and particles. Constructing such well-ordered nanoarrays require optimal conditions of these aforementioned variables. Using the so-called *Nanosphere Lithography*, it is also possible to use template material such as polystyrene-polyvinyl pyridine micro- or nanosphere beads to form well-ordered polygonal shaped monolayers of nanoarrays made out of MNPs or SNCs. Hybrids of these materials can be created using the *Layer-by-layer (LBL)* method of self-assembly. As the name itself suggest, two or more disparate materials can be successively deposited as layers one on top of other. Nanoparticles can be either immobilized or linked to each other on top of the pre-treated substrate by relying on the simple adsorption or chemistry of conjugation. Many of these coupling techniques has been discussed earlier to link plasmonic and semiconducting nanocrystals onto the substrate by means of

ligand-induced self-assembly, DNA hybridization, covalent bonding via EDC, EDC-NHS coupling, electrostatic attraction or even utilizing dielectric silica shells. Effective binding or immobilization of various NPs require optimal manipulation of surface chemistry and sometimes excess loading or incubation concentration of using different linkers like 4-aminothiphenol, thiol, carboxylate and so on. Often the thickness of the spacer layer depends of the specific type of molecules being used for linkage. One should be aware of the fact that depending on the size difference and relative concentration (or particle density) between the MNPs and SNCs, it can result in random arrangement of hybrid conjugates with different cross-linking sites or variation in binding sites. Until now, numerous experiments have been carried out several groups on studying the LBL deposition of MNPs and QDs. Almost all of these experiments employed spin casting as the most widely mode of deposition of nanoparticles on the substrate from its colloidal dispersion in certain solvents. The most straightforward way involved sequential deposition followed by subsequent drying. Until now, configurations of noble metal based plasmonic nanostructures in the form of Au nanospheres, Au nanorods, Ag nanocubes, Ag nanoprisms and so on has been deposited in combination with QDs as two separate layers one on top of other in order to study the plasmon-exciton interaction between them in these large-scale hetero-nanoassemblies [146–149] (Fig. 14). Most often, these LBL deposition between MNPs and QDs involve addition of an extra spacer layer (silica, polymer like PMMA, PDDA, PSS etc.) so as to avoid direct photoluminescence quenching of QDs arising from various non-radiative charge transfer phenomena like FRET (Fluorescence Resonance Energy Transfer), Dexter energy transfer, exciton-exciton energy transfer, self-quenching etc.

As reported earlier in few studies, silica spacers can be either grown on individual NPs in the solution or deposited as a separate layer between the sequential deposition steps. Sometimes, *electron beam lithography (EBL)* has been further employed in conjunction with LBL to fabricate well-ordered nanoarrays with specific dimensions and morphology. This allows precise patterning of NPs in specific arrangement. However, lithographically patterned matrices or arrays of NPs are often time consuming in addition to possessing grain boundaries that could potentially act as plasmon damping sites (for MNPs) leading to weaker near-field interactions or non-radiative trap states (for SNCs) reducing their performance capabilities. In addition to photolithography, there are other techniques that have been also developed based on scanning probe microscopy like AFM for precise placement of QDs in close proximity to MNPs and individual manipulation of MNP-QD hybrids.

The thrust behind developing all these different methodologies for fabrication of metal-semiconductor hybrid NPs lies in the fact that a synergistic and judicious combination of MNPs and QDs into a single coupled hybrid system lead to interesting and often new form of optical interactions between plasmons and excitons. As a result of this plasmon-exciton coupling, it results in either increase or decrease of photoluminescence QY, PL emission intensity and lifetime, variation in Purcell factor, change in PL intermittency (blinking) behavior, modification of exciton/biexciton quantum yield and single/multi-photon emitting capabilities of

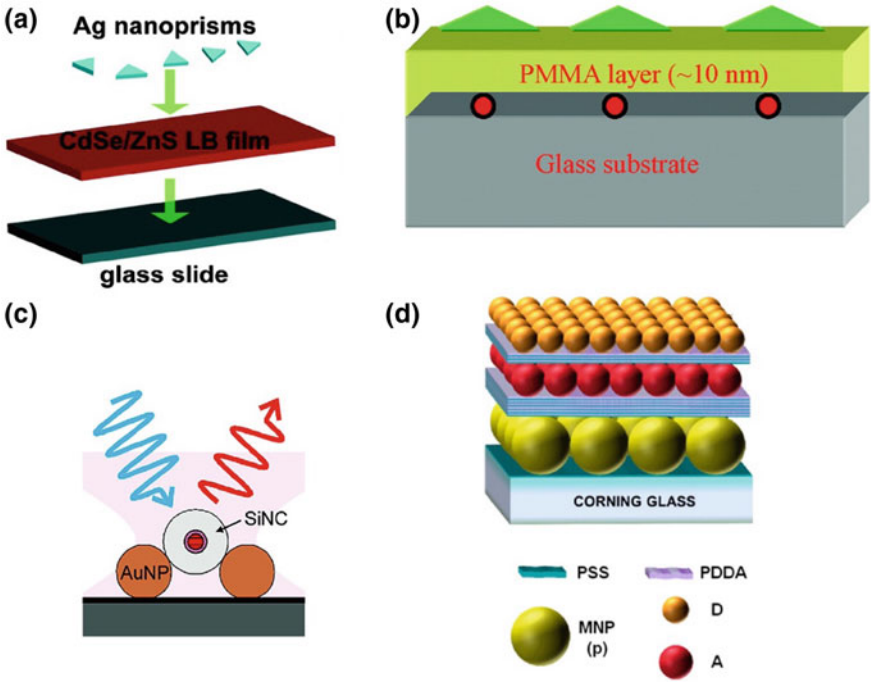

Fig. 14 **a** A schematic illustration of the substrate structure. A monolayer of quantum dots is made by Langmuir−Blodgett deposition. Ag nanoprisms are placed on top by drop casting., Reproduced with permission from Munechika et al., 2010. **b** Substrate sample configuration of Ag nanoprisms coupled CdSe/Zns QDs, Reproduced with permission from Yuan et al., 2009. **c** Sample sketch of silica coated CdSe multishell QDs on top of thin layer of Au NPs, Reproduced with permission from Ma et al., 2010. **d** Schematic showing the layered architecture (prepared via layer-by-layer deposition) of donor Au NPs with the acceptor QDs on top of it with intermediate deposition of polymeric PDDA to control the distance/spacing between the layers, Reproduced with permission from Ozel et al., 2013

single QDs. A combination of various processes are often responsible for this resultant modification of photoluminescence property of QDs like increase in excitation rate of QD, increase in effective absorption cross-section of QDs due to enhancement in plasmon-based local electric field, energy transfer from QD to MNP and subsequent change in radiative and non-radiative decay rates. Figure 15 shows modification of photon emission behavior of single QDs when coupled to various forms of plasmonic metal nanostructures as derived from photo correlation spectroscopic measurements [150–154].

On the other hand, for MNPs, this kind of local coupling effects can lead to modification in scattering properties affecting the primary plasmon peak frequency or depending on the degree of coupling occurrence of Fano resonances and Rabi splitting (Fig. 16) phenomena has been also observed. While designing such hybrid nanosystems, one should take into account different factors that might influence the

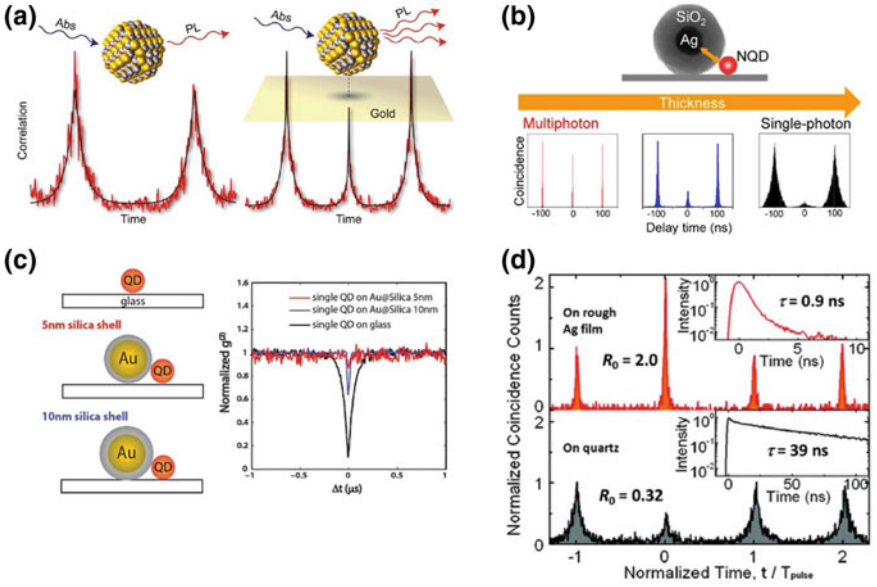

Fig. 15 **a** Photon correlation curves showing enhancement in multiphoton emission from single QDs on Au substrate as compared to bare glass, Reproduced with permission from LeBlanc et al., 2013. **b** Photon correlation curves showing degree of enhancement in multiphoton emission of single QDs in presence of plasmonic silica coated Ag NPs (multiphoton emission capability is investigated as a function of silica shell thickness), Reproduced with permission from Naiki et al., 2017. **c** Photon antibunching measurements under continuous wave excitation on single QDs coupled to variable thickness of silica coated Au NPs, Reproduced with permission from Dey et al., 2015. **d** Photon correlation measurements showing a significant change from photon antibunching to a completely bunching behavior from single QD adsorbed onto plasmonic rough Ag film substrate, Reproduced with permission from Park et al., 2013

plasmon-exciton coupling processes like particle's size, shape, composition, spectral overlap, inter-particle distance, spatial orientation etc. [155, 156].

So far, with the development of new synthetic methodologies in combination with theoretical modeling software (like FDTD, molecular dynamics, DDA, DFT, ab-initio and semi-empirical simulations) and time-resolved optical spectroscopic techniques, plasmonic manipulation of exciton/multiexciton emission of QDs have been successful and optimized in the form of various designs of MNP-QD hybrids. However, further effort is still required to better understand what regulate the mechanisms of plasmon-exciton coupling, how new charge/energy recombination pathways are created and what are the structure-property relationships concerning these hybrid hetero nanostructures.

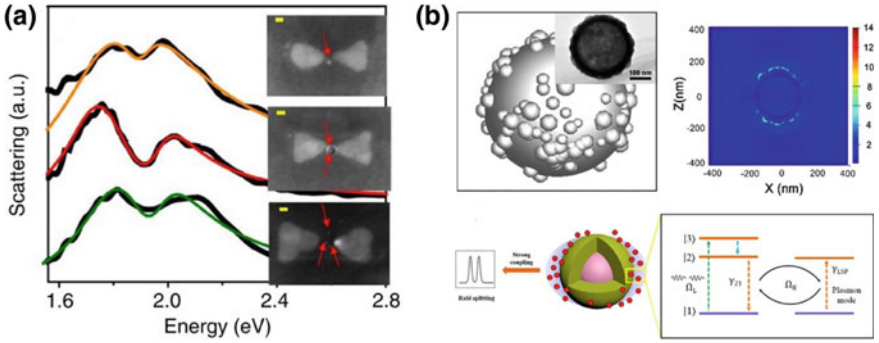

Fig. 16 **a** Scattering spectra of Au NP bowties with (from top to bottom) one, two and three QDs in the gap, respectively. All spectra show a transparency dip due to Rabi splitting as a result of strong plasmon-exciton coupling between the excitons in QDs and plasmons in Au bowties, Reproduced with permission from Santosh et el., 2016. **b** Schematic diagram of a rough SiO_2@Ag nanoshell with Ag NPs. The inset is the TEM image of a single Ag nanoshell, (right) Electric field distribution for a rough SiO_2@Ag nanoshell obtained by means of FDTD (Finite Domain Time Difference) simulation, (bottom) Schematic representation of collective strong coupling of many QDs with the radiative dipole mode of an Ag nanoshell, (bottom right) shows the energy diagram and optical transitions in the hybrid system, and the Rabi oscillation Ω_R describes the transfer of an excitation between the LSP mode of and the QDs emitters at Rabi frequency, Reproduced with permission from Zhou et al., 2016

4 Structural, Electrical and Optical Characterization Techniques

With the advent of modern electronics and hardware equipment, several characterization techniques have been developed so far in order to investigate the grain size, elemental composition, crystal structure and lattice parameters, magnetic properties, phase information and a variety of other physical properties of nanoparticles. With many more different kinds of nanomaterials that are being synthesized every day, it is imperative to develop more precise analytical characterization tools that would allow us to characterize the materials and get reliable information of their properties from all the way bulk to their nano- forms. Based on the different capabilities and limitations of each technique/s and the sort of information it can provide, they are chosen to study the samples. Classification of different techniques are usually based on the theory and concept the technique rely on and the kind of physical properties (structural, electrical, optical, magnetic etc.) they are destined for. Here, some of the structural (SEM, TEM, AFM, XRD); electrical (XPS, SPV, EBIC, EI, DLTS), optical (UV-Vis, PL, TA, TRPL, FTIR, Rayleigh and Raman Scattering, DLS)—the full names of the individual techniques will be provided later on in the text as they will be discussed in further details. Several of these methods are frequently used for characterization of materials involved in optoelectronic and photovoltaic devices.

5 Structural Methods

A *scanning electron microscope (SEM)* uses an electron gun to impinge highly energetic electron beam directed on the sample surface. The typical arrangement of essential components on this microscope based technique consists of an assembly of electro-optical vacuum chambers to which emits electron from a heated filament under some accelerating voltage in a constant beam down the column. The electron beam accelerates as they pass through a series of electromagnetic lens and interacts with the sample focused on a tight spot at the end of the column. Thus, smaller the spot size, the higher is the resolution. As the primary electron beam interacts with the sample, the material emits secondary, backscattered, x-ray and transmitted electrons (Fig. 17a shows the general outline of device components in a typical SEM). The SEM has a good spatial resolution and its depth of field is about 300 times than that of light microscope. The typical working distance using this technique wherein the height of the sample is kept between 10 and 25 mm. The materials that are characterized usually need to be prepared on certain conductive substrates like silicon wafer, Si/SiO_2, ITO etc. Conventional SEM can provide us with high resolution imaging of surfaces of various materials with different modes

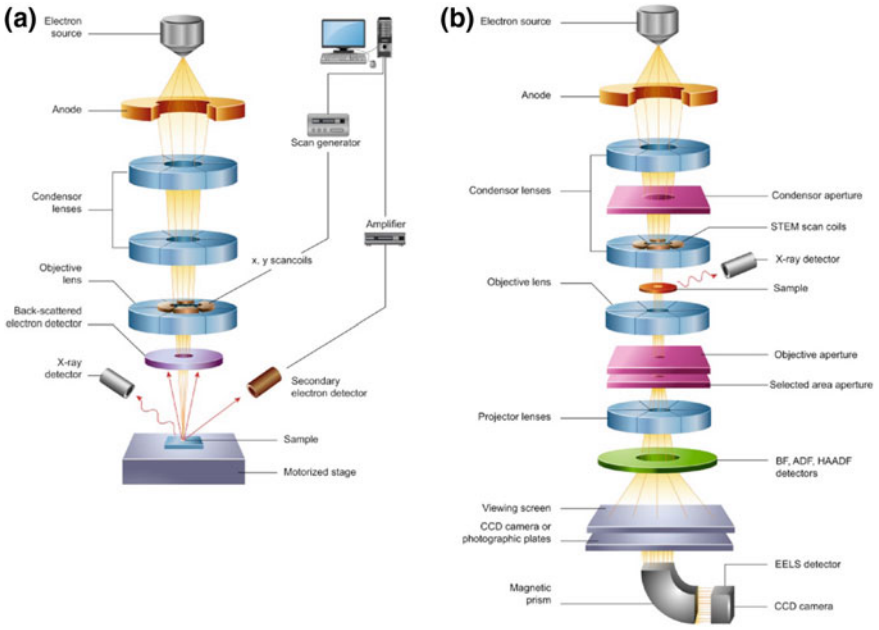

Fig. 17 Schematic illustrations show the various instrument components of **a** Scanning Electron Microscope (SEM) and **b** Transmission Electron Microscope (TEM) with their respective detector systems like secondary electron (SE), backscattered electron (BSE), X-ray, high angle annular diffraction (HAADF), Reproduced with permission from Inkson et al., 2016

of detection using certain kind of specific detectors: In-Lens, Secondary Electron (SE), Electron Back Scattering detector (EBSD) or E-T(Everhart-Thornley) to derive further topographical information about the materials [157].

Transmission Electron Microscopy (TEM) is another microscope (Fig. 17b shows a typical transmission electron microscope with its device parts along with its detectors) based high resolution imaging technique with typically much higher working accelerating voltage (60–200 keV) directed on a thin layer of sample deposited on a carbon grid. Especially because of its high spatial resolution, TEM can resolve objects that are separated by even less than 0.2 nm. It is by far one of the most hands-on characterization technique particularly to the materials scientist who are working on nanostructured materials particularly MNPs and QDs among other various kind of materials and desire to acquire high resolution fine images along with crystalline structural information obtainable from diffraction data. Being such a versatile characterization tool, it not only produces enhanced morphological and structural information of the nanomaterials, but it is also capable of other analytical information such as electronic structure (in *electron-energy loss spectroscopy, EELS)* and chemical composition (*energy dispersive X-ray spectroscopy, EDAX*) of the nanomaterials. *High-resolution TEM (HRTEM)* imaging combines the transmitted and scattered electron signal and forms image using phase contrast method. This method of phase contrast imaging mode by far provides the highest resolution of internal structure detectable down to single arrays of atoms in crystalline nanostructures. HRTEM in its Selected Area Electron Diffraction (SAED) mode can distinguish between amorphous, single and polycrystalline materials and offers opportunity to even further identify structural defects of the materials under investigation [157].

In Scanning Transmission EM (STEM) mode, the electron beam is focused on to a fine spot and the sample is raster scanned; this method of continuous scanning of the beam across the sample makes the STEM method more appropriate to implement Z-contrast annular dark field imaging and spectroscopic elemental mapping by energy-dispersive X-ray (EDX) or EELS spectroscopy. On the other hand, *high-angle annular dark field imaging (HAADF-STEM)* is a method of performing elemental mapping in the samples which help us visually analyze the individual elemental distribution in nanoparticles on the surfaces or interfaces by collecting the scattered electrons in with an annular dark-field detector and by acquiring Z-scan across the individual particles. This is a very informative tool useful particularly in doped and alloyed samples and often help us comprehend the growth mechanism process of colloidally synthesized NPs occurring via different mechanistic pathways like solid-state diffusion, Galvanic replacement, Kirkendall effect and so on.

Atomic Force Microscopy (AFM) is another scanning microscopy based technique which is capable of producing three-dimensional image of surfaces under certain magnification. The principle of this technique is based on the interaction between the AFM tip (probe) and the molecule on the substrate. The probe is a sharp tip usually coupled to the end of a cantilever made of silicon or silicon nitride. In order to study plasmon-exciton interaction, sometimes the AFM tip has been modified by attaching MNPs; subsequently due to this reason other techniques like

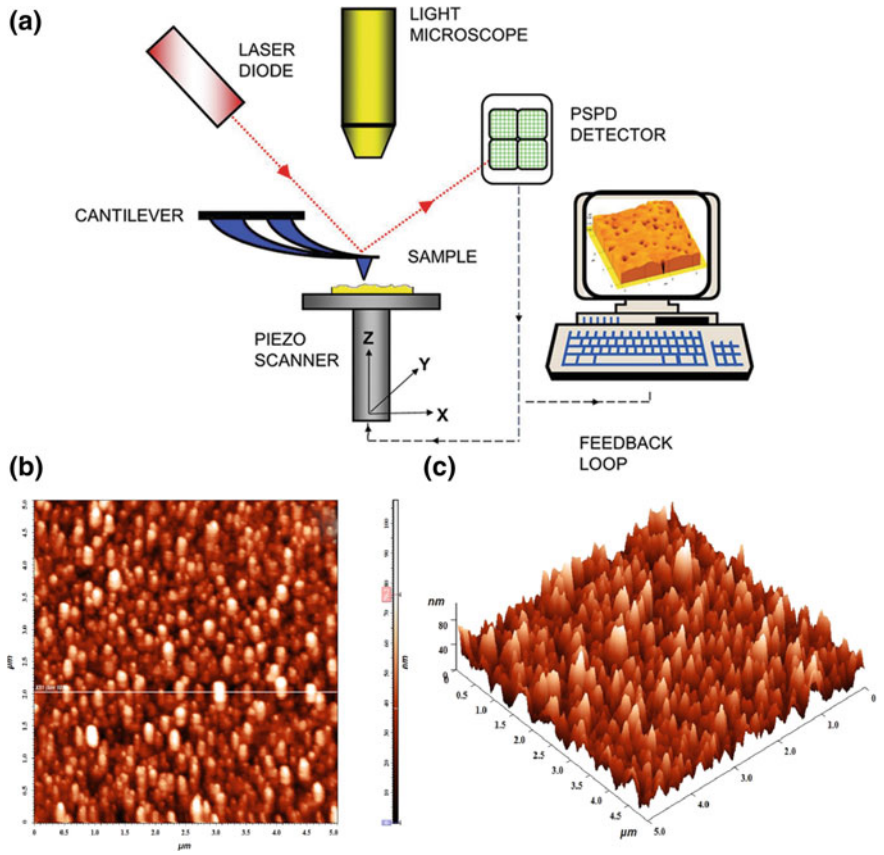

Fig. 18 **a** Schematic illustration of a typical Atomic Force Microscopy (AFM) setup. **b** A typical AFM image of Copper Zinc Tin Sulfide (CZTS) powder on quartz substrate, Reproduced with permission from Shyju et al., 2015

tip-enhanced Raman spectroscopy (TERS) has been developed which made possible to collect enhanced signals from the samples as a result of electric field enhancement from MNPs. AFM can scan the samples in different modes (contact, non-contact or intermediate tapping mode) depending on the degree of proximity between the probe and the sample. Vast topological information regarding the surfaces such as surface roughness, surface height, and grain boundaries in polycrystalline materials etc. can be derived using this technique. Figure 18a shows a typical instrumental configuration of a AFM microscope setup and Fig. 18b exhibit a typical AFM data plot generated which provides us with information like sample roughness, height and topographical features [157].

X-ray diffraction (XRD) is one of the most prevalently used structural characterization technique that provides detailed information on the crystalline structure, nature of the phase, grain size and lattice parameters. The composition

(stoichiometric ratio) of the elements in the particle can be deduced by comparing the position and intensity of the characteristic peaks with the reference patterns available in the database from International Center for Diffraction Data (ICDD) or Joint Committee on Powder Diffraction Standards (JCPDS). The lattice parameters are obtained from the Scherrer equation by observing the broadening of the most intense peak in the spectrum.

6 Electrical Measurement Tools

X-ray photoelectron spectroscopy (XPS) is a charge particle based chemical analysis tool (Fig. 19 shows the general outline of XPS technique and correlation of binding energy with kinetic energy of photoelectron, instrument work function and local electric potential) which is extremely sensitive to electrical potentials developed due to uncompensated electric charges [158]. Its underlying physical principle is based on the photoelectric effect. In addition to chemical composition and identity of elements along with their oxidation (valence states), electronic structure, binding energy of atoms, work function, change in chemical shift in response to local environment can be also determined. The surface depth sensitivity of this technique is between 10 and 15 nm which arises from the band-bending at the surface/vacuum interface. Depending on the mode of data collection, for example under photo-illumination conditions, once can even measure the photoconductivity

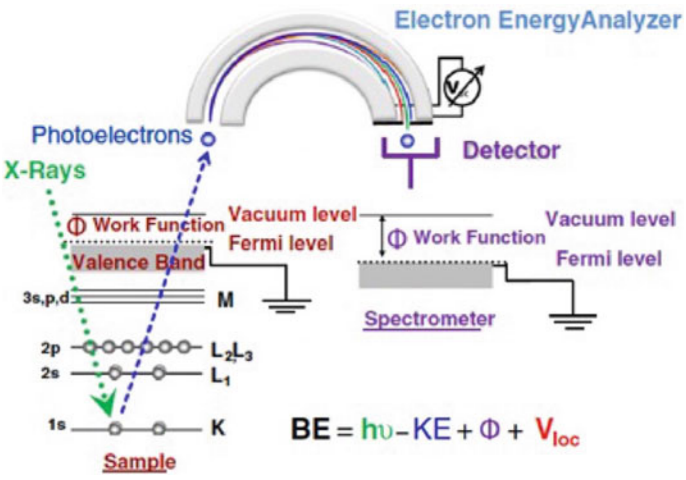

Fig. 19 Schematic diagram of the XPS technique and the equation correlating the binding energy (BE) with the kinetic energy (KE), work function (Φ) and local electric potential (V_{loc}) Note that the measured binding energy (B.E.) of a specific peak is influenced by the local electrical potential (V_{loc}) of the sample, in addition to its elemental nature and chemical state (chemical shift). Reproduced with permission from Sezen et al., 2013

and photo voltage shifts. This technique in general, can give us both qualitative and quantitative information related to nature of dopant, effect of substrate (p-/n-type) on interfacial charge accumulation & band bending, external bias (forward/reverse bias) polarity dependence on p- and n-domains of an operating p-n junction and even dynamics of electron and photoinduced charge accumulation in both bulk and thin films.

Surface Photovoltage (SPV or SPS) spectroscopy is a contactless method for measuring the change in electrochemical potential using a Kelvin probe in space-charge region of semiconductors under illumination of suitable wavelength (energy) and intensity. Figure 20 shows the outline of a typical SPV instrumental setup. It is often used to measure a wide range of material parameters and therefore deduce the quality of the samples determined from surface voltage, surface barrier height, surface charge density, minority carrier diffusion length, recombination lifetimes, doping density etc. Two major types of probes are used in SPV measurements: Kelvin probe, where the electrode vibrates vertically altering the capacitance between the probe and sample; and the Monroe probe where the electrode is fixed and a grounded shutter in front of the electrode is vibrated horizontally thereby modulating the probe to wafer capacitance. The contact potential difference (V_{CPD}) is measured using an AC current and determined from:

$$I = V_{CPD} \cdot \frac{dC}{dt}$$

where C is the capacitance between the probe and sample and CPD (difference between the work function of sample and probe) = $WF_{sample} - WF_{probe}$.

Another major application of SPV is to measure the minority carrier diffusion length and lifetimes thereby providing information regarding the low defect densities. It is a preferred characterization technique to determine diffusion lengths since it is a steady-state, non-destructive, contactless with no complex sample

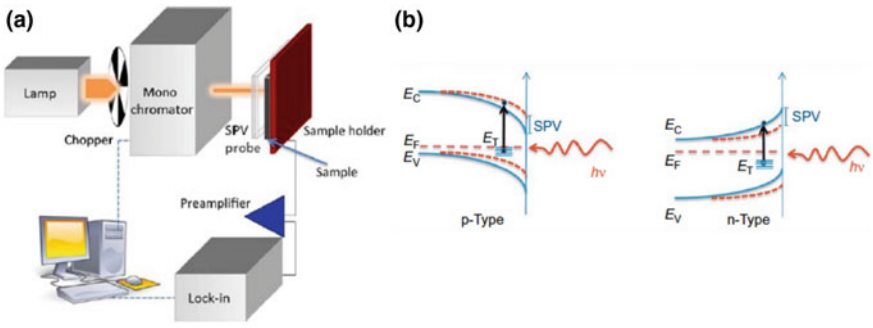

Fig. 20 **a** Schematic illustration of a Surface Photovoltage (SPV) instrumental setup. **b** Band diagram of a p-type (left) and n-type (right) semiconductor close to the surface under non-equlibrium/ above bandgap illumination condition. Band edges (E_C, E_V) and Fermi energy (E_F) are indicated in the diagram. Reproduced with permission from Cavalcoli et al., 2015

preparation requirements and the instruments are commercially available. The wafer could be homogenous or in the form of p-n junction or metal-semiconductor junction. In dynamic SPV, the sample wafer is illuminated by a monochromatic light pulse with high intensity. Depending on the excitation pulse width and photon flux, it gives information of surface band-bending, (Fig. 20b) density of interface states, recombination behavior and majority carrier lifetime. Whereas, in static SPV, the sample is illuminated with monochromatic light of tunable wavelength so that the penetration depth of the impinging photons could be varied. This gives information of diffusion length of excess carriers in sample [159].

Electron-Beam Induced Current (EBIC) is a SEM- based microscopic technique for characterizing the electrical properties of semiconducting materials and devices, and study the sub-surface electronic and defect states. The electrical current is typically measured that flows through the sample when it exposed to an electron beam. The principle of operation of EBIC involves creating local electron-hole pairs and subsequently measuring the contribution of each of electron and hole components from the current signals (Fig. 21a shows the schematic illustration of a typical EBIC and CL experimental setup). As the electron beam is scanned across the sample, it forms an image of the response at each point. The signal difference can originate as a result of junctions with electric fields, variation in doping levels/impurities in the device, or from crystalline defect states or surface/interface dangling bonds yielding important information on minority carrier diffusion lengths, relaxation times and microscopic images of width of depletion regions. The incident electron beam generates a large number of e-h pairs within a small interaction volume (considered as a teardrop shape that is dependent on Z contrast, atomic weight of the material, it density and also accelerating voltage of incoming electron beam). These e–h pairs can undergo either radiative relaxation by emitting light (signals measured via *Cathodoluminescence*, CL method), or non-radiatively in the form of heat, or electrical current within the external measurement device circuit (signals measured via *EBIC*). For a standard EBIC measurement, the internal

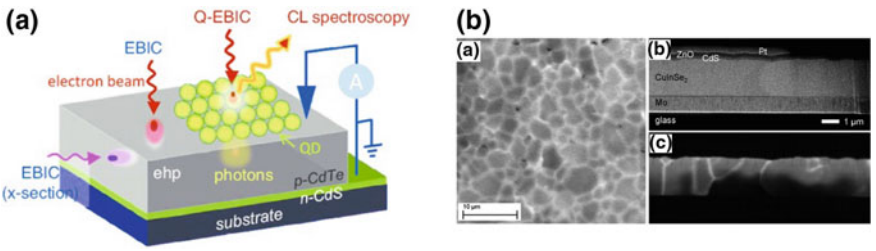

Fig. 21 **a** Schematic illustration of a typical EBIC and Cathodoluminescence (CL) experimental setup. **b** (**a**) EBIC image acquired at 10 keV on a Cu(In,Ga)Se_2/CdS/i-ZnO/ZnO:Al stack, lifted off the Mo/glass substrate; the Cu(In,Ga)Se_2 was in contact with Ag epoxy glue, leading to Ag diffusion into the Cu(In,Ga)Se_2 layer, assuming a decreased net-doping density in the absorber; grain boundaries exhibit enhanced EBIC signals as compared with the grain interiors. Reproduced with permission from Abou-Ras et al., 2019

electric field gradient associated with p-n junction causes charge separation and hence results in a net current flow. With a proper knowledge on carrier generation, drift, diffusion, recombination and collection, it is possible to estimate the factors that govern the EBIC signals. When characterizing the junctions, EBIC measurements can be performed in different specimen configurations both in planar or cross-sectional positions. The planar view configuration can be used to examine recombination centers such as dislocations, grain boundaries, homogeneity of junctions; whereas the cross-section studies can be used to locate and characterize the depletion regions, and measure diffusion lengths. With recent developments in electronics and optics, the detection levels and resolution of EBIC images have been pushed down to even investigate nano-electronic devices [159].

Impedance Spectroscopy (IS) is another powerful, non-destructive electrical characterization tool that can be implemented coupled with device illumination for in-situ monitoring of charge transport and recombination processes at different points of the solar cells. It has been frequently used to investigate device aging, performance loss mechanisms in response to external stress factors as well as how different protocols of fabrication affect the device performance. Usually, IS is a voltage perturbation method wherein a DC voltage potential establishes a steady-state condition and a small working AC potential is applied at different frequencies to monitor the change in impedance in addition to measuring recombination resistance and geometrical capacitance. In general, IS is applied to systems with electrical Ohmic contacts which involves measurement of AC electrical current I(ω) at a certain angular frequency ω under the application of an AC voltage, V(ω); then the impedance is $Z(\omega) = \frac{\widehat{V(\omega)}}{\widehat{I(\omega)}}$.

The impedance data are analyzed using equivalent circuit and capacitance-frequency models wherein the global response data of the sample is quantified from the resistive and capacitive contributions to the impedance spectrum over the full frequency range of measurement. Using these models, the transport and recombination processes are interpreted [160–162].

Deep-level Transient Spectroscopy (DLTS) is another efficient method in understanding the physics and engineering of photo-carrier generation, escape and collection processes in photovoltaic materials and characterizing electrically active deep-level defects/impurities in semiconductors. DLTS is a capacitance thermal scanning transient technique, usually operating at a high frequency (MHz) range. Utilizing the capacitance of a p-n junction or Schottky barrier, it monitors the changes in charge state of deep level traps/defects. It can distinguish between majority and minority carrier traps giving information on concentration, thermal stability, and energy and capture rates for both kind of traps. The transients provide the information regarding an impurity level in the depletion region by monitoring the capacitance transient originating from the initial to thermal equilibration state after a perturbation is applied to the system. DLTS has certain specific advantages over other previously mentioned techniques as it allows us for a complete characterization of a deep center and their correlation with the device properties.

In particular, it can measure effectively the capture cross-section and activation energy of deep level trap states in addition to just distinguishing between traps and recombination centers [160–162].

7 Optical Methods

Basic light-matter interactions are primarily governed by three different processes: absorption, scattering and transmission. The first two processes result in an attenuation of incident light intensity after passing through matter. And the total loss of these two processes is defined as extinction as $\gamma_{ext} = \gamma_{abs} + \gamma_{scatt}$.

UV-Visible (UV-Vis) spectroscopy is a relatively facile and straightforward low-cost optical characterization tool that is frequently used to study these optical parameters of nanomaterials. It measures the intensity of light reflected (transmitted) from a sample in comparison to the intensity of light reflected (transmitted) from the reference material (could be the blank solvent in which the actual sample is dispersed in, or air, or glass if measuring the samples in the form of solid thin films). MNPs in particular have optical properties (localized surface plasmon, LSP discussed earlier), these localized surface plasmon resonance, LSPR peak position and peak width are highly sensitive to size, shape, concentration, agglomeration state (polydispersity index), local dielectric environment or refractive index of the surrounding medium. This makes UV-Vis spectroscopy an important handy tool to rapidly identify and characterize the type and quality of materials as well as evaluate the stability of nanoparticles in different solvents. These LSPR bands could appear anywhere in the electromagnetic spectrum in UV, Visible to even near or far-IR regions. As for the QDs are concerned, the UV-Vis spectroscopy has proven to be an equally important tool to identify the quality and homogeneity of the samples since these colloidal semiconducting NCs often show their characteristic excitonic peaks arising from the different discrete electronic transitions/ energy levels in these so called “atom-like” quantum confined systems.

Photoluminescence Spectroscopy (PL) is another commonly used technique to study the photoluminescence emission behavior of optically active fluorophores such as metal nanoclusters, quantum dots, organic dye molecules and fluorescent proteins, polymers etc. It monitors the light emitted from atoms or molecules that have absorbed photons and results in re-emission of photons by releasing excess energy. Excited states both in single atoms or molecules can undergo optically-allowed transitions following certain sets of selection rules of transitions and give out the electromagnetic radiation in the form of light emission. Depending on the nature and relative timescales of emission from the excited states, PL can be broadly divided into fluorescence and phosphorescence.

Both the above techniques (UV-Vis absorption or PL spectroscopy) as discussed above can be performed under both steady-state and time-resolved conditions. Conventional and easy to perform steady-state measurements provide information of light-matter interaction primarily to and from/ with the ground states; whereas

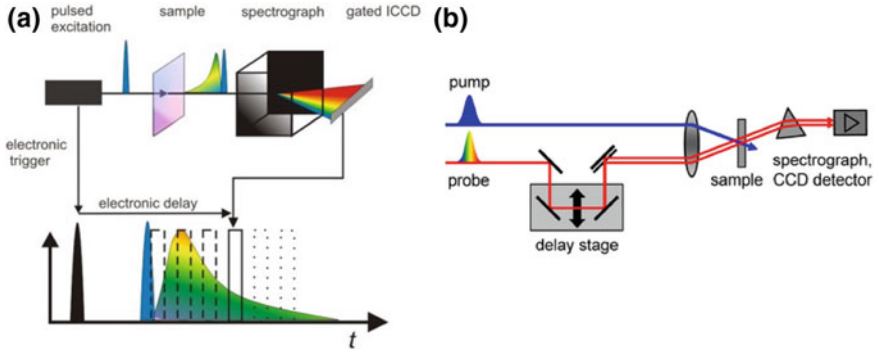

Fig. 22 Schematic illustration of experimental setups of **a** Time-resolved Photoluminescence spectroscopy (TRPL) and **b** pump-probe ultrafast transient absorption spectroscopy (TA). *Source* https://www.mpip-mainz.mpg.de/65134/Time_Resolved_Photoluminescence_Spectroscopy, https://www.temps.phc.uni-kiel.de/en/research/laboratories-and-instrumentation/fs-transient-absorption

time resolved spectroscopy gives us vivid information on interaction between different electronically higher order excited states occurring at different timescales (depending on the sensitivity of the technique itself or temporal resolution of the detectors) within the same or between different molecules.

Time-integrated or time-resolved photoluminescence spectroscopy (TRPL or TIPL) simply measures an integrated PL or temporal evolution over a time much longer (this can be well modulated by varying the repetition rate of the incoming excitation pulse) than the normal intrinsic emission lifetime of the materials under study. TRPL can be performed using different methods such as time-correlated single photon counting (TCSPC), phase modulation or by using streak camera detection for high temporal resolution and light sensitivity. Figure 22a shows the experimental scheme of a typical state of the art time-resolved PL setup.

Transient Absorption (TA) spectroscopy, (Fig. 22b shows a typical pump-probe spectroscopic setup) on the other hand measures the light absorption at the transient excited states, the temporal resolution of which could vary from few sub-picoseconds (ps) to even few hundreds to femtoseconds (fs). In order to monitor the transient absorption process at very fast timescales, two beams are used, namely the pump and the probe. The pump beam is usually strong and chirped short laser pulse to generate a population of the excited states; whereas the probe beam maybe continuous wave (CW) white light beam or pulsed which is sent through the sample to probe the perturbation caused by the initial pump beam on the sample. This could be monitored by sending the probe beam at some delayed times and also at other wavelengths with respect to the pump beam. This method gives us valuable information on different excited states and on various physical processes occurring at different timescales such as ground state bleaching, photoinduced absorption and stimulated emission.

Infrared (IR) spectroscopy is another essential and a straightforward characterization technique that is often used to elucidate the structure of matter at a molecular

scale. Information regarding the chemical composition, bonding arrangement, functional groups (or chemical identification of surface ligands) can be obtained from the characteristic fingerprint vibrational frequencies that appear in the spectrum. The Fourier-Transform IR (FTIR) obtain the spectrum by Fourier transformation of the signal in frequency domain that permits us to identify the chemical components or group of atoms that absorb IR at particular frequencies. In addition to chemical identification, this technique can be also used to measure tacticity, crystallinity and molecular strain of different polymers (macromolecules).

Raman Spectroscopy is a well-known optical tool, named after the eminent Indian scientist Dr. C.V. Raman who first observed this inelastic scattering phenomenon. This method is being used to detect vibrations at the molecular level which provides information on the chemical identification and physical forms of the materials. Samples in the form of solid, liquid, vapor or in the form of particles (powder) or surface layers can be studied using this method (Fig. 23a shows a typical Raman spectroscopic setup). Raman scattering might have certain disadvantages including sample degradation or fluorescence since most often signals collected from the sample are weak and thus higher laser excitation powers are used to study the particles. However this problem has been substantially reduced with modern and improved Raman spectroscopic methods like surface-enhanced or tip-enhanced Raman (SERS or TERS) which are being currently used for chemical imaging of surfaces at the nanometer scale.

Dynamic Light Scattering (DLS) is a widely employed optical technique (Fig. 23b) to estimate the size of colloidal NPs in suspensions that are typically in the nano- to sub-micron ranges. The NPs dispersed in a colloidal solution are in some continuous form of random Brownian motion. This method measures light scattering as a function of time which combined with the Stokes-Einstein assumption (Stokes-Einstein equation with Diffusion coefficient terms) in order to

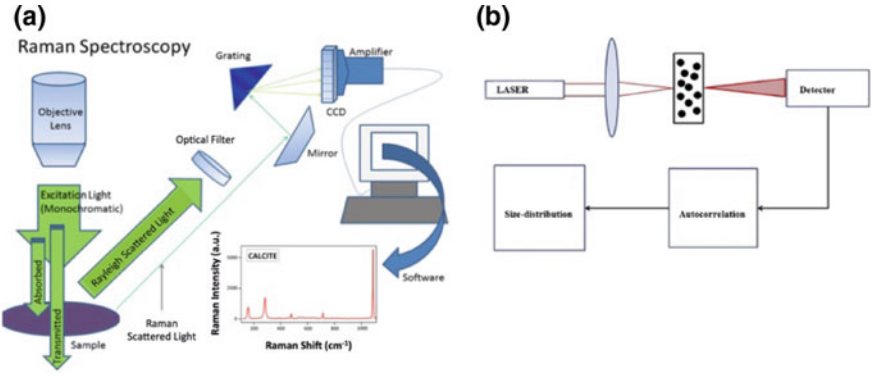

Fig. 23 Schematic illustration of instrumental setups of **a** Raman spectroscopy and **b** Dynamic Light Scattering. *Source* https://doi.org/10.13140/rg.2.1.3818.0322 MSc Thesis: Raman Spectroscopy Applied to Enhanced Oil Recovery Research, J. Magn. Magn. Mater. 427 (2017) 19e24

calculate the hydrodynamic diameter. Basically, it gives us a size distribution profile based on temporal fluctuations that are analyzed by means of intensity or photon auto-correlation function.

8 Operational Mechanism and Design Principles in Plasmon Enhanced Photovoltaics

The photovoltaic community has been actively studying the light-matter interaction in plasmonic metallic nanostructures in order to understand the plasmon enhancement mechanisms and as well as strive to improve and tune the spectral range of photon absorption (collection) and photon-to-electrical energy conversion efficiency. Surface plasmon, as we introduced earlier are collective oscillations of free electrons in metallic materials which when interact with the electromagnetic light creates a coherent optical response at certain frequency matching condition to generate what is known as the Surface Plasmon Resonance. Plasmonic enhancement could be achieved by judicious design and fabrication of MNPs incorporating within the energy based optoelectronic and photovoltaic devices as well as working through different mechanisms such as far-field scattering, near-field coupling, and charge or resonant energy transfer. Figure 24a shows the diagrammatic representation of various plausible plasmon induced mechanisms typically encountered in all plasmon mediated photovoltaics. It was by Atwater and Polman, who earlier outlined three different approaches that MNPs can be employed to enhance the light absorption properties of solar cells [163–165] (Fig. 24c). In the following paragraphs, different architectures of plasmonic nanoparticles and their role in enhancement mechanisms in photovoltaic devices will be discussed in details.

Firstly, plasmonic nanostructures or nanoarrays can be incorporated as sub-wavelength scattering centers for efficient coupling and trapping of the incoming radiation into the active absorbing layer (dyes, polymers, quantum dots and recently perovskites as individually identified as the different generations of solar cells). Usually within a thin active layer, the light absorption is insufficient, thus in order to improve the light absorption efficiency, plasmonic MNPs introduced as sub-wavelength scattering sites in different geometries and orientations would help increase the angular speed and travelling distance of generated excitons (e-h pairs) in the active layer. The vast array of assembled MNPs would also result in multiple scattering of exciton that will lead to an effective increase in optical path length and absorption and as well as enhancing the probability of charge collection efficiency. Depending on the dimension of NPs, the scattering direction could be manipulated, for e.g. smaller NPs result in forward scattering whereas larger NPs result in backward scattering (reflection) of the incident light. MNPs when placed between the interfaces of dielectric layers, the light gets preferentially scattered into the high index substrate. Since light scattering and the absorption losses in MNPs is highly sensitive to the material composition, size and shape, one needs to be extra

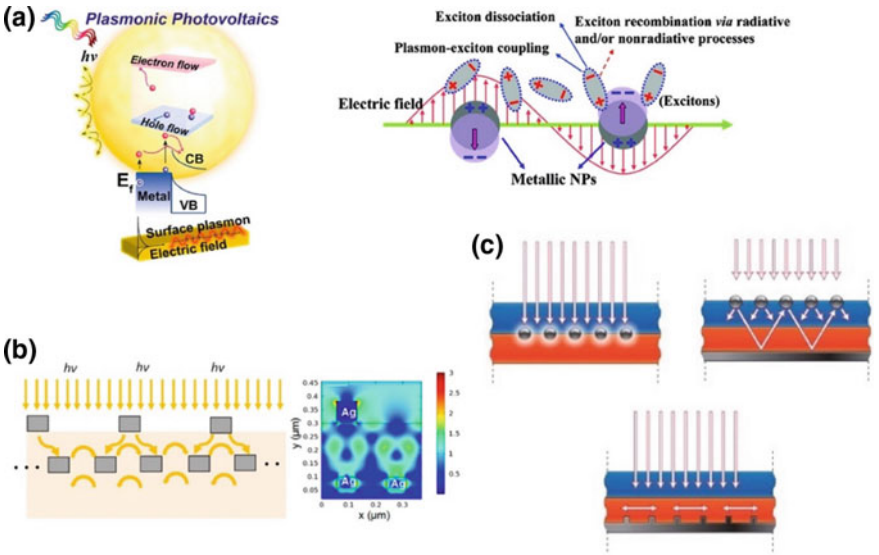

Fig. 24 **a** Schematic illustration show various mechanisms and effects related to plasmon mediated photovoltaics. Reproduced with permission from Jang et al., 2016; Wu et al., 2011. **b** Light trapping effect between the plasmonic nanostructures and simulated electric field profile (FDTD simulation) for scattering. Reproduced with permission from Lin et al., 2013. **c** Plausible light trapping geometries for thin film solar cells. Light trapping by scattering from metal nanoparticles at the surface of the solar cell. (left) Light is preferentially scattered and trapped into the semiconductor thin film by multiple and high-angle scattering, causing an increase in the effective optical path length in the cell. (right)Light trapping by the excitation of localized surface plasmons in metal nanoparticles embedded in the semiconductor. The excited particles' near-field causes the creation of electron–hole pairs in the semiconductor. (bottom) Light trapping by the excitation of surface plasmon polaritons at the metal/semiconductor interface. A corrugated metal back surface couples light to surface plasmon polariton or photonic modes that propagate in the plane of the semiconductor layer. Reproduced with permission from Atwater et al., 2010

careful while trading off the percentage contribution of scattering versus the percentage of absorption loss when selecting the size and shape of metallic nanoparticles. Ideally, we want to make sure that the plasmonic MNPs absorb little light (reduced parasitic absorption loss) and scatter more light (increased light-trapping via far-field scattering).

Secondly, the near-field coupling effect which results in strongly confined electric field near MNPs can be further exploited to increase the light absorption efficiency in solar cells. In this approach, the MNPs act as sub-wavelength nanoantennae that couple the electromagnetic light into their near-field. However, for relatively larger NPs, contributions from both scattering and near-field coupling effects play a dual role in enhancing the light absorption process. While comparing specific geometries of MNPs, it has been observed both experimentally and theoretically that for similar MNPs with identical volume, the field enhancement vary largely with different shapes in the order pyramidal > cube > cylinder > sphere

(the anisotropic structural effect plays quite a significant role in the extent of plasmonic evanescent field and degree of local electric field enhancement). Additionally, with an appropriate phase matching condition, the EM light could be also coupled with plasmons to generate surface plasmon polariton (SPP) modes at the interface between metal and semiconductor. Efficient excitation of SPP modes can be achieved by incorporating different 2D- or 3D- designs such as grooves, periodic gratings, holes, islands etc. Figure 25a, c, d show different configurations and designs involving metal NPs incorporated within the device. Since the propagation lengths of these SPP modes are quite large extending to even few hundreds of μm, it can contribute to further increase the absorption efficiency of solar cells. The concentrated near-field effect extends into both metal and dielectric layers where the photovoltaic enhancement takes place.

And finally, it is also possible to effectively utilize and harvest the plasmon induced hot charge carriers (hot electrons) to usable form of electricity by energy conversion. Hot carriers are generated by inducing electron excitation above the Fermi energy level either via intraband or interband transitions. The hot carriers with excess energy usually possess very short (ultrafast: of the order of few hundred femtosecond, 10^{-15} s to few picosecond, 10^{-12} s) lifetime resulting in rapid decay and dissipation of energy in the form of heat (Joule heating). However, if these metal nanostructures are located in near proximity or in direct contact to the active semiconducting layer, these hot electrons with sufficient energy and momentum via dephasing of plasmons can non-radiatively transfer or inject themselves into conduction band edge of the active layer thus yielding a usable photocurrent. Figure 25b, e show the general outline of plasmon induced hot carrier transfer mechanism from metal NP to nearby semiconductors. Plasmonically excited electrons with energy higher than the Schottky barrier establish an internal electric field which results in upward or downward band-bending depending on whether the semiconducting layer is n- or p-type that results in electron transport from the metal into the bulk of the active layer; however there is always a competition between the overall charge extraction and thermal relaxation as a consequence of these hot carriers generation [166–170].

The improvement and interpretation of enhancement mechanisms in photovoltaic performance by MNPs could be quite complicated where other energy transfer effects are often involved in addition to light trapping and harvesting. Coupling between plasmon in MNPs and excitons in the active semiconducting layer largely influence the charge transfer processes and facilitating exciton dissociation/ annihilation by modifying the dynamical properties of excited states and carrier relaxation/dissociation pathways of hot carriers. Plasmonic Resonant Energy Transfer (PRET) which is an analogous to Forster Resonance Energy Transfer (FRET) is yet another plausible mechanism that involves a form of non-radiative energy transfer between a coupled dipole-dipole fluorescent donor and acceptor within a certain distance. In PRET, the MNPs act as a donor wherein it transfers energy via charge carriers (electrons or holes) to the active semiconducting layer. This mode of energy transfer is a little different from that of the near-field effect in the sense that this mechanism follows the similar requirements of FRET (spectral

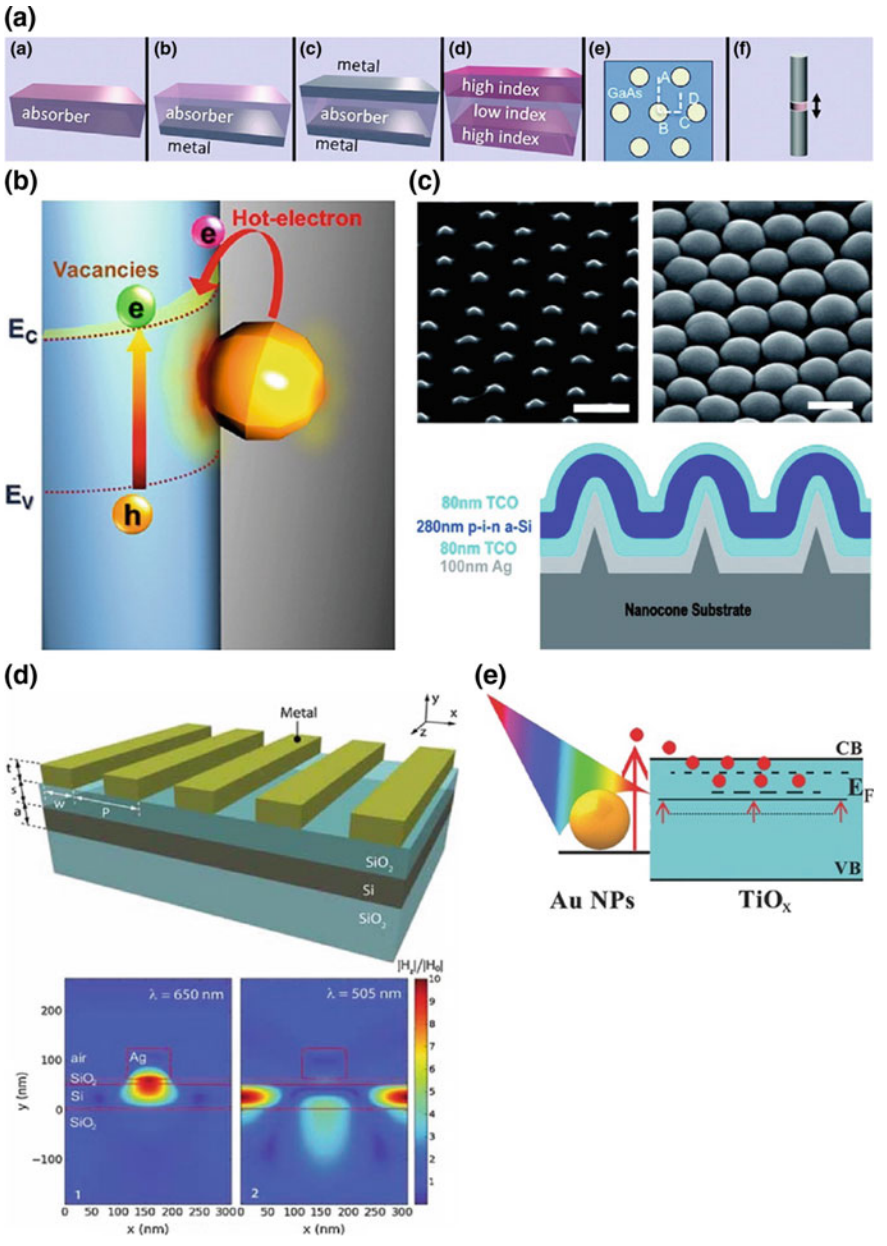
(a)
(a)
absorber
(b)
absorber
metal
(c)
metal
absorber
metal
(d)
high index
low index
high index
(e)
GaAs
A
D
B
C
(f)
(b)
Hot-electron
e
Vacancies
e
E_C
E_V
h
(c)
80nm TCO
280nm p-i-n a-Si
80nm TCO
100nm Ag
Nanocone Substrate
(d)
Metal
y
x
z
t
s
a
w
p
SiO_2
Si
SiO_2
$|H_y|/|H_0|$
λ = 650 nm
λ = 505 nm
air
Ag
SiO_2
Si
SiO_2
y (nm)
x (nm)
x (nm)
1
2
(e)
CB
E_F
VB
Au NPs
TiO_x

◂**Fig. 25** **a** Schematics for new solar cell designs with an elevated local density of optical states (LDOS) for the absorbers based on metal-absorber-metal or high-low-high index materials. Reproduced with permission from Callahan et al., 2012. **b** Cartoon showing the plasmon induced effect via hot electron transfer mechanism from metal NPs to the semiconducting photoactive layer in solar cell. Reproduced with permission from Chen et al., 2012. **c** Nanodome a-Si:H solar cell structure. SEM images taken at 45° on nanocone quartz substrate (top) and a-Si:H nanodome solar cells after deposition of multilayers of materials on nanocones (right). Scale bar 500 nm. Schematic showing the cross-sectional structure of nanodome solar cells (bottom). Reproduced with permission from Zhu et al., 2010. **d** Noble metal nanostructure designs utilizing high near-field effects surrounding the plasmonic nanostructures and coupling to waveguide modes with realization of broadband absorption enhancement. Reproduced with permission from Pala et al., 2009. **e** A unique sandwiched structure of TiO_x/Au-NPs/TiO_x that has been used to improve the charge transport properties of a TiO_x film via plasmonic-mediated hot carrier injection at the metal-semiconductor Schottky junction. Reproduced with permission from Yuan et al., 2015

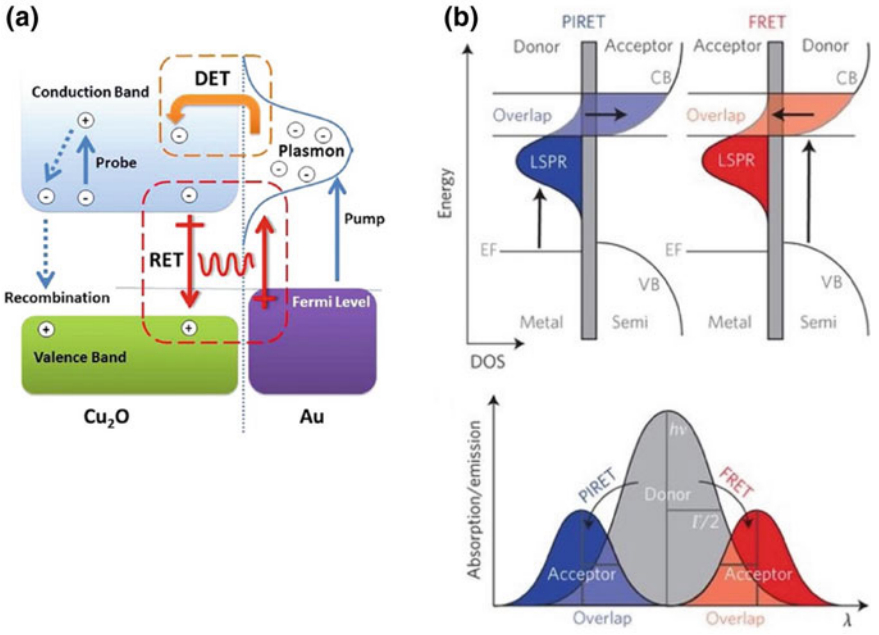

Fig. 26 **a** Plasmonic resonant energy transfer and charge separation mechanisms in hybrid metal NP-semiconductor photovoltaics. Metal@semiconductor structures can increase charge separation by direct electron transfer (DET) of hot electrons contained in LSPR to the semiconductor, local electromagnetic field enhancement (LEMF) of the semiconductor charge separation process, or by resonant energy transfer (RET) from the LSPR dipole to the electron hole pair in the semiconductor shell. Reproduced with permission from Cushing et al., 2012. **b** Complementary energy transfer mechanisms via Plasmon Induced Resonance Energy Transfer (PIRET) and Forster Resonant Energy Transfer (FRET) in Au@ SiO_2–Cu_2O hybrid systems. Parameters such as spectral overlap and dipole-dipole interaction depend on whether the semiconductor is excited by PIRET or quenched by FRET. Reproduced with permission from Li et al., 2015

overlap, distance between the particles <10 nm). Figure 26 show the outline of various plasmon induced resonant energy transfer mechanisms often encountered in plasmon mediated photovoltaic devices [171, 172].

Before the recent research surge with newly encountered perovskite solar cells, the early 3rd generation of photovoltaic devices were based on dye-sensitized active layer which have gained a significant interest due to their relatively low production cost as compared to traditional indirect band-gap Si solar cells combined with their high power conversion efficiency. Later on, plasmonic nanostructures were further incorporated into these dye-sensitized solar cells (DSSCs) to maximize the charge generation and efficient extraction processes. Figure 27 show incorporation of different plasmonic metal NPs within the DSSC which boosted the overall performance and efficiency of the devices. To date, plasmon-enabled DSSCs with a balanced broadband panchromatic light response yielded a highest efficiency of about 11%, a ~30% improvement in compared to the reference device. In 2000, it was Wen and co-workers who implemented Ag-island films in ruthenium based dye-sensitized photoelectrochemical cells and observed an increment in photoresponse in the visible region [173]. Hupp et al investigated the distance dependent optical response by adjusting the distance between the photosensitizer and plasmonic particles and correlated the connection between plasmon enhanced electromagnetic field and the enhanced extinction response of the dye sensitizer [173]. Ihara et al introduced modified Ag nanoparticles with block copolymers to increase

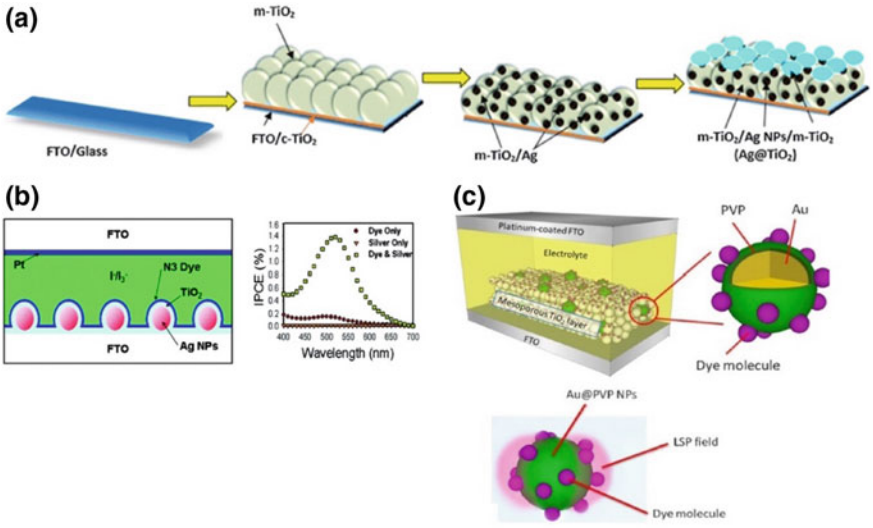

Fig. 27 **a** Schematic of plasmonic photoanode preparation process based on Ag NPs on mesoporous TiO_2. Reproduced with permission from Isah et al., 2016. **b** Configuration of solar cell containing Ag NPs and dye. Reproduced with permission from Standridge et al., 2009. **c** Configuration of core-shell Au@PVP nanoparticles (NPs) into dye-sensitized solar cells. Reproduced with permission from Xu et al., 2012

the stability of electrolyte [174]. Later, it was Liu et al who prepared plasmonic core/shell/metal organic Au/PVP NPs and embedded them within the TiO_2 photoanode [175].

These modified well coated NPs not only exhibited enhanced stability from recombination, or photolytic degradation or electrolyte corrosion but also possessed the ability to adsorb onto the dyes. It was Kamat and co-workers who reported that the photovoltaic performance could be influenced in at least two major ways: plasmonic and electronic charging effects (Fig. 28a). The increased excitation of the photosensitizer (dye) and subsequent increment in photocurrent could be attributed to enhanced EM field from the plasmonic NPs embedded within the device [175]. Hagglund et al demonstrated an enhanced charge carrier generation using photoconductivity measurements when performed on TiO_2 sensitized by a combination of dye molecules and arrays of elliptical Au nanodisks [175] (Fig. 28b). In 2009, Chen et al have implemented vertically aligned ZnO nanorod arrays coated with Au NPs as Schottky barrier solar cells and observed an enhancement in optical absorption in visible range due to the effect of surface plasmon resonance with an increment in PCE (power conversion efficiency) from 0.7% to 1.2% [176]. In 2010, McGehee and coworkers have used 2D arrays of Ag nanodomes as plasmonic back reflectors using nanoimprint lithography [177].

They observed an enhanced absorption through excitation of plasmonic modes and increased external quantum efficiency close to 15% due to light scattering effects in the long wavelength range 600–900 nm. In addition, there are several studies dedicated to numerous designs of plasmonic nanostructures such as $Au@SiO_2$, $Ag@TiO_2$, $Au@Ag_2S$, $Au@TiO_2$ hollow submicropheres and so on

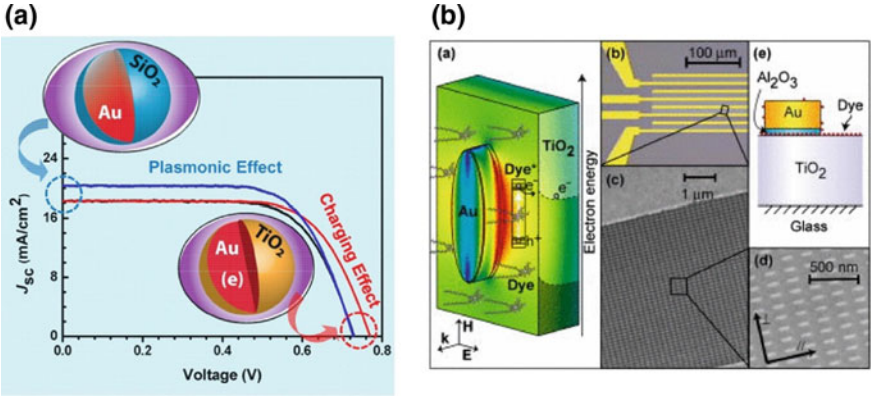

Fig. 28 **a** Charging effect ($Au@TiO_2$) versus plasmonic effect ($Au@SiO_2$) of metal core–oxide shell particles in dye-sensitized solar cells. Reproduced with permission from Choi et al., 2012. **b** Schematic shows enhanced charge carrier generation in dye sensitized solar cells by nanoparticle plasmons. The field amplifies excitation of dye molecules Dye* adsorbed on the semiconductor TiO_2 substrate, leading to enhanced electron transfer rate to the TiO_2 conduction band. The SEM images are close-ups of an array of elliptical Au disks, and the schematic picture shows the sample arrangement from the side. Reproduced with permission from Hagglund et al., 2008

which has observed the synergetic effect of enhanced light absorption and accelerated energy transfer in addition to plasmon induced charge excitation and separation [163, 178–181]. As a consequence of all these combined effects, an improvement in PCE parameters (short circuit current density: J_{SC}, open circuit voltage: V_{OC}) has been observed. The light harvesting capability in DSSCs was further demonstrated by incorporating dielectric silica coated Ag, Au nanoparticles with various interesting morphologies ranging from nanostars, nanorods, nanocubes, nanoprisms and taking advantage of their additional anisotropic plasmonic effect on the dye sensitizers (Fig. 29a, b). For example, Bardhan and coworkers observed an enhanced PCE of 7.8% from the reference 5.8% when silica coated (Au@SiO_2) nanocubes are embedded within the photoanodes of DSSCs [182] (Fig. 29c). Similarly, a panchromatic response in light harvesting capability of the

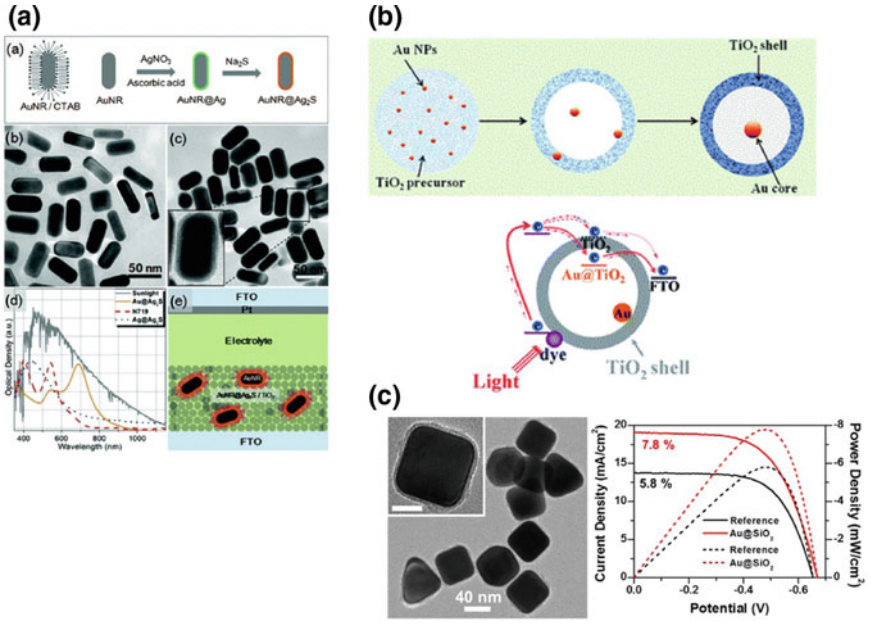

Fig. 29 **a** Schematic illustration of a Au nanorod stabilized by hexadecyltrimethylammonium bromide (CTAB) and a two-step chemical process towards AuNR@Ag_2S (a) (CTAB is not drawn in the synthesis scheme for clarity); TEM images of as-synthesized Au nanorods (b) and AuNR@Ag_2S with Ag_2S thickness of 2 nm (c); solar irradiance spectrum, absorption of AuNR@Ag_2S (2 nm in shell thickness), N719 dye solution in acetonitrile and t-butanol and Ag_2S-encapsulated Ag nanoparticles, AgNP@Ag_2S (d) and a 2D device configuration of the plasmon-enhanced DSSCs, in which dye molecules were not included for clarity (e). SEM images of the TiO_2/AuNR@Ag_2S anode film. Reproduced with permission from Chang et al., 2012. **b** Illustrations of (top) formation process of Au@TiO_2 hollow submicrospheres and (bottom) the charge separation process in the DSSCs with the photoanode of Au@TiO_2 hollow submicrospheres. Reproduced with permission from Du et al., 2012. **c** Enhancement in efficiency of dye sensitized solar cells when silica-coated nanocubes (Au@SiO_2 nanocubes) embedded in the photoanodes. Reproduced with permission from Zarick et al., 2014

DSSC was observed when $Au@SiO_2$ triangular nanoprisms were incorporated within the device resulting in a 15% increase of PCE from 3.9% to 4.4%. In another study by Elbohy et al., when Au nanostars are incorporated into photoanodes, the PCE of the solar cells were increased by ≈20% from 7.1% to almost 8.4% along with an improvement in the incident photon-to-current conversion efficiency (IPCE) and the spectral response was broadened in the region between 380 and 1000 nm [183]. Complex architectures involving bimetallic $Au/Ag/SiO_2$ and alloyed plasmonic nanostructures were also used for improved light trapping and subsequent enhancement in light harvesting capability resulting in increment of 26–30% of PCE with additional enhancement in charge carrier generation and rapid charge transfer to electrodes.

In addition to the above studies, recently solar cells with plasmonic sensitizers were also demonstrated in order to study the plasmon induced charge separation, which is believed to be an essential process for photocurrent generation. Su et al conducted a study on surface plasmon resonance of layer-by-layer Au NPs induced photoelectric current generation in plasmon sensitized solar cells and showed that by depositing multiple layers of Au NPs on surface of solar cells increases the amount of light scattering on its surface, thereby boosting the absorption and improving the device efficiency [184]. Finally, in addition to just merely incorporating plasmonic nanostructures of various forms and morphologies into the photoelectrochemical cells, MNPs has been also used to modify the electrodes (specifically the photoanodes) with different morphologies such as nanowires, nanotubes, sphere, hollow sphere and core-shell types. These metal nanoparticles modified photoanodes offer efficient photon collection as well as exhibit plasmon-enhanced light absorption [185–187].

Not just in DSSCs, plasmonic NPs and effect of surface plasmon resonance has been also observed in organic photovoltaic devices (OPVs). The principal consideration in designing plasmon enhanced OPVs is by trading off between two primary goals: minimizing the active layer or cell thickness down to the carrier diffusion length but at the same time to design cells with sufficient thickness to provide necessary degree of absorption by taking advantage of the enhanced electric field via utilizing the SPR effect. An increase of up to 24% was observed when a blend of Au nanospheres and nanorods were introduced into the hole-transport layer (HTL) [188]. Later on, Ginger, Chen and Jen's groups has independently conducted in-depth study on the multi-scattering effect from the LSPRs of Ag prisms and observed PCE values to increase from 6.55% to 9.02% [189–192]. Most of the studies have interpreted the improvement in device performance is due to enhanced optical absorption via near-field enhancement and light scattering effect resulting from the plasmonic nanostructures. However, these plasmonic NPs can also alter the electrical properties by promoting photocarrier mobility to the generated charge carriers and also the photoconductivity based on their metallic characteristics; largely depending on the morphology and location of these nanoparticles within the device. Recently, the Choy group investigated the mechanism of plasmonic effect in OPVs by embedding Au nanospheres within HTL; instead of enhancement in optical absorption, the IPCE was increased that

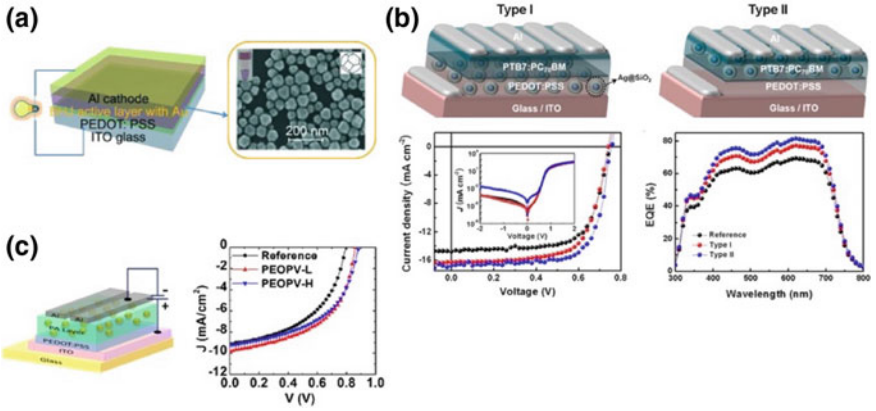

Fig. 30 **a** Addition of truncated octahedral Au nanoparticles (ca. 70 nm diameter) to bulk heterojunction (BHJ) photovoltaic cells fabricated from a variety of donor polymers and $PC_{70}BM$ as acceptor gives a boost in the power conversion efficiency (PCE). Reproduced with permission from Wang et al., 2011. **b** High performance polymer solar cells as a function of different positions of silica coated Ag NPs between the active and hole transport layers. Reproduced with permission from Choi et al., 2013. **c** Schematic device structure used to fabricate Organic Photovoltaics (OPVs), (right) PV characteristic curve of reference (PCDBT:PC70BMPCDBT:PC70BM) device doped with Au NPs. Reproduced with permission from Tyagi et al., 2016

contributed to the final device performance [193]. In another study by the same group, when a Ag metal grating was integrated onto the top electrode, the SPR effect led to a broadening of light absorption resulting in an increase in PCE and EQE values [194]. Besides investigation of scattering effect of Au or Ag NPs in active layers (Fig. 30a, c), Park and Heeger groups further implemented UPS and XPS to study the electron transfer mechanism in OPVs [195, 196]. The MNPs act as some sort of electron transport barrier and instead acted as hole transporting layer thereby efficient hole extraction was possible in these device configurations. Mathews and Sum groups further utilized Au nanowires in plasmonic OPVs, wherein the thickness of HTL was controlled to allow the evanescent field to extend to photoactive layer [197]. Due to the high aspect ratio and anisotropic properties, the metal nanorods and nanowires like system provided a platform to further investigate the polarization dependent effect on photocurrent and PCE. It was by Kim et al. [195] who later investigated the importance of plasmonic NPs location within the OPV devices and reported that a device with $Ag@SiO_2$ situated between the HTL and active layer showed a higher efficiency than th device with the nanostructures located between the bottom electrode and HTL (Fig. 30b). The coupling effect was observed to be much stronger between the Ag NPs and active layer when they are in close contact with the maximum PCE value of 8.92%, an improvement in $\sim$19% over the Ag NP free device.

Lately, with such a huge research interest globally in the field of perovskites based solar cells (PSCs), some of the recently developed approaches in efficient

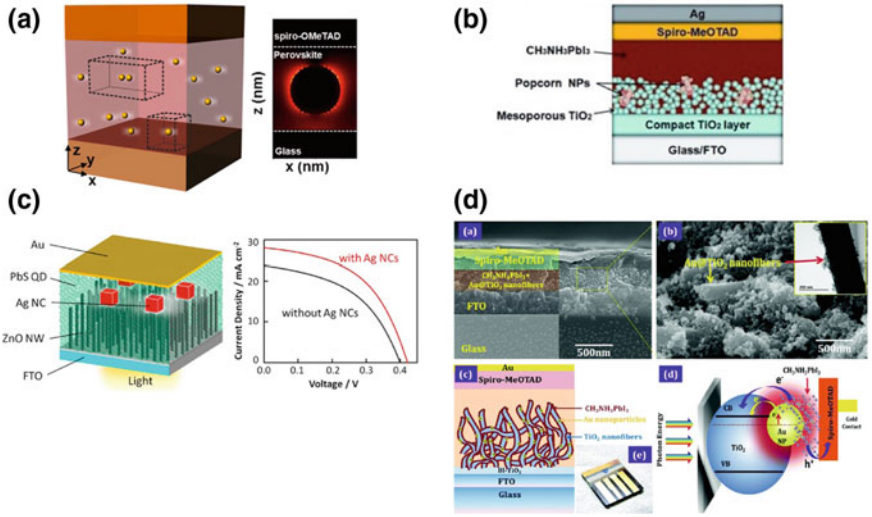

Fig. 31 **a** Schematics of a unit cell with dimensions $L_x \times L_y \times L_z$, of a glass–perovskite–SpiroOMeTAD system with plasmonic Au NPs embedded within the perovskite films show an absorption enhancement. Reproduced with permission from Palacios et al., 2015. **b** Schematic shows Plasmonic-enhanced perovskite solar cells using Au–Ag alloy popcorn nanoparticles. Reproduced with permission from Lu et al., 2015. **c** Schematic of a PbS QD/ZnO NW solar cell with embedded Ag NCs results in an improvement in PCE in BHJs Reproduced with permission from Kawawaki et al., 2015. **d** In situ processed gold nanoparticle-embedded TiO_2 nanofibers enabling plasmonic perovskite solar cells to exceed 14% conversion efficiency. Reproduced with permission from Mali et al., 2016

optical management have given efforts in exploiting the plasmonic effects in these classes of photovoltaic devices. PSCs are generally constructed based on an n-i-p and p-i-n architecture with the intrinsic active layer (organic/ inorganic lead halide based perovskites) embedded between the ETL and HTL. With an aim for a better optical (photon) management and achieving a higher performance device with improved device parameters (J_{SC},V_{OC}, FF), it might be an interesting strategy to employ plasmonic NPs and exploit the plasmonic effects especially in semi-transparent solar cells. The improvement in optical absorption due to Au NPs within the PSC have been theoretically demonstrated by Carretero-Palacios et al. [198] wherein the plasmonic near-field enhancement and scattering effects were correlated as a function of NP size using FDTD (Finite Domain Time Difference) simulations (Fig. 31a).

In a recent study, electrospinning has been employed to fabricate in-situ Au-embedded TiO_2 nanofibers for plasmon-enhanced generation in PSCs [199]. The photovoltaic performance was enhanced in Au@TiO_2 nanofiber based devices with a maximum photocurrent density of 21.63 mA cm^{-2} and PCE of 14.92%. In another report, Au-Ag alloy popcorn-shaped NPs [200] were employed in PSCs which lead to an increased performance resulting in an improvement in broadband

light absorption and efficient charge-transfer (Fig. 31b). Other attempts to improve the performance of plasmon mediated solar cells included Ag nanocubes embedded in a QD/ZnO nanowire [201] based bulk-heterojunction solar cell wherein, the location and stoichiometric amount of Ag nanocubes were controlled to enhance the photocurrent, particularly in the near-IR region (Fig. 31c). Implementation of metal NPs in other kind of CIGS solar cells has effectively improved the carrier transportation across the p-n junction by enhancing the absorption and carrier generation wherein the PCE has increased from 8.31% to 10.36% [202].

Having discussed the already explored numerous designs and architectures of plasmonic metal nanostructures being incorporated within the device active layer, embedded within the ETL or HTL or even used to modify the electrodes; there are still some inherent critical issues that is worth discussing here while rationally designing and fabricating plasmon mediated photovoltaics. Although with the capability of concentrating and trapping light through various mechanisms, there are several limitations when employing plasmonic NPs in the devices such as their physicochemical instability, charge recombination, narrowband absorption, plasmon radiative and non-radiative losses etc. that often hamper the long term performance of the as fabricated devices. In this final section, these currently existing problems will be comprehensively discussed and several points that need to be addressed.

First, the chemical and electrical stability must need to be guaranteed in these plasmon mediated photovoltaic devices. In order to do so, incorporation of various passivating layers such as silica, titania, and organic polymers on the surface of plasmonic nanostructures is an essential strategy to minimize any degradation or loss of plasmonic activity. Often these protective layers could simply resist against corrosion or prevent deterioration of charge separation and current collection capability of these metal NPs. In addition to this, they can also provide thermal and structural stability. However, when these additional protective layers are grown on the surface of plasmonic nanostructures, the crucial point to note is to take into consideration of other parameters like optimal thickness of the passivation layer that is required to maintain electrical or chemical stability, and inter-particle/ separation distance between the MNPs and the active photosensitizing layer and how it influence the electromagnetic field and plasmon-induced field enhancement factor.

Secondly, by now we already know that light harvesting efficiency can be improved by incorporating properly designed metal nanostructures into solar cells. Although taking into careful consideration of spectral overlap factor (between the SPR bands and the absorption spectrum of the photoactive material) and the efficiency of resonant energy transfer, it is equally important to tune the spectral position of the LSPR band (through proper size and shape control of the MNPs) in order to achieve a balanced light absorption. Tuning of LSPR band is not just because of the spectral overlap factor but also to extend the plasmonic response to a broader range by specifically improving the light absorption capability in the weakly absorbing regions of the solar spectrum. In this context, it is yet another feasible strategy to utilize the multiple plasmon modes (transverse, longitudinal) arising from anisotropic MNPs such as rods, nanowires, cubes, prisms etc.

In addition to just merely extending the absorption range all the way from UV-Vis to NIR from the multiple plasmon peaks, utilizing these kind of morphologies with sharp features like corners, edges additionally yield strong plasmonic field resulting in higher enhancement of electric fields, thereby boosting overall PCE of the devices.

Finally, let's discuss some of the future prospective approaches in the field of plasmon enhanced photovoltaics which could potentially open up not only exciting opportunities in all next generation hybrid photovoltaics with possibly new interesting features and capabilities, but at the same time will also allow us to further explore fundamental interaction mechanisms between the plasmon and exciton, therefore guiding us to rationally fabricate high performance plasmon based photovoltaic and optoelectronic devices. By far, most works until now have primarily focused on noble metals like Ag, Au, Cu which no doubt have contributed a significant growth in the field of plasmonic photovoltaics. However, recently there are many other alternative plasmonic materials such as Aluminum (Al), Aluminum Zinc Oxide (AZO), Gallium Zinc Oxide (GZO), Zirconium nitride (ZrN), Hafnium nitride (HfN) as well as non-noble metal based plasmonics like Graphene, alloys, Indium Tin oxide (ITO) etc. that have been recently proposed in addition to these conventional plasmonic NPs which could be potentially used in plasmon enhanced photovoltaics. Furthermore, dielectric NPs with sufficiently high permittivity and

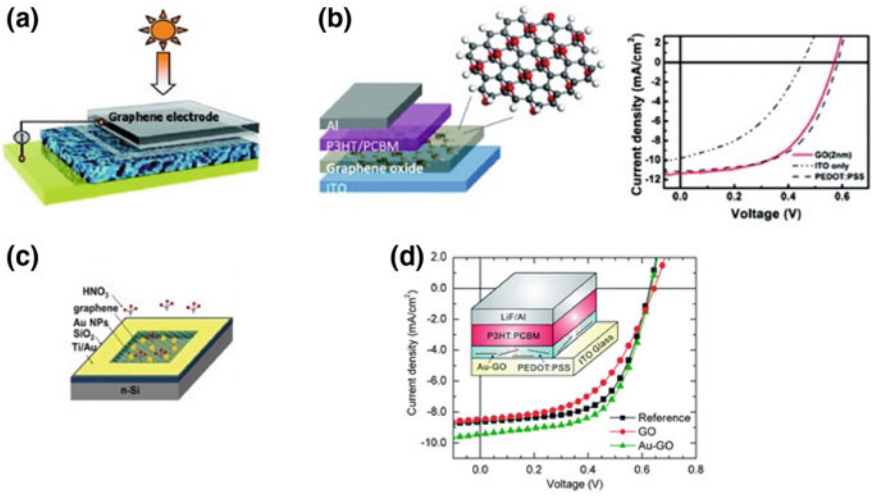

Fig. 32 **a** Illustration of dye-sensitized solar cell using graphene film as electrode, the four layers from bottom to top are Au, dye-sensitized heterojunction, compact TiO_2, and graphene film. Reproduced with permission from Wang et al., 2008. **b** Schematic of the photovoltaic device structure consisting of the following: ITO/GO (graphene oxide)/P3HT:PCBM/Al and PV characteristic curve with enhanced current density when GO being used as HTL. Reproduced with permission from Li et al., 2010. **c** Incorporation of Au-GOs into the anodic buffer layer (PEDOT:PSS) resulted in highly efficient plasmon enhanced solar cells. Reproduced with permission from Fan et al., 2012

low dissipation level can also result in certain degree of improvement in thin film semi-transparent solar cells. In order to achieve higher enhancement and increase PCE in these devices, the dielectric materials should have a low dissipation, low dispersion and high permittivity such as SiO_2, SiC, TiO_2 etc. Graphene plasmonics is a rapidly emerging field ever since it's experimental discovery and because of its immense potential in the field of electronics, photonics, telecommunication and optoelectronics. As such, the light-matter interaction in graphene has a promising prospect in the field of photovoltaics. The PCE of solar cells can be improved by exploiting dual coupling effect from metal as well as graphene plasmons. There are already few reports that are existing where graphene has been implemented as transparent electrodes, as well as component in HTL in OPV or even as interface modifiers in Si solar cells. So far, there has been several efforts in trying to utilize the synergetic effect by incorporating an ensemble/bulk graphene and metal nanostructures in photovoltaics. Figure 32 exhibit incorporation of different graphene, and graphene-oxide materials either in the form of electrodes or embedded within the active layer of the devices [203–206].

In addition to these examples, recently there has been a few reports where plasmon upconversion coupling effect has been implemented to produce photons with a higher energy through sequential absorption of two or more lower energy photons. Incorporating plasmonic nanoparticles within the cells as solar upconverters has been expected to enhance the performance. Lanthanide ion doped oxides whose emission wavelength overlap with the SPR frequency of MNPs will enable an increment in plasmon resonance energy transfer (PRET) process, thereby the resultant EM field could be strengthened, subsequently showing certain degree of improvement in photoconversion efficiency [207].

9 Concluding Remarks (Outlook and Perspective)

In this chapter, a fundamental background on plasmonics and excitonics has been introduced concisely followed by an in-depth discussion on various top-down and bottom-up based fabrication methodologies of metal nanoparticles, semiconducting nanocrystals and metal-semiconductor hybrid nanoheterostructures. Furthermore, some of the most frequently used state of the art structural, electrical and optical characterization tools along with their corresponding working principles that are essential for materials design and device fabrication have been discussed. The latter half of the chapter uncovers some of the most advanced solution and substrate based design strategies for manufacturing hybrid plasmon based metal-semiconductor nanoassemblies which are being currently employed in the form of either electrodes or photosensitive (active) layer in most currently available photovoltaic and optoelectronic devices. Additionally, a comprehensive survey to various operational mechanisms (mode of plasmon-exciton interaction) that are often encountered between the metal NPs and the photoactive fluorophores (dye, quantum dots) when incorporated within the device has been laid out which would

give an overview to the readers who would be interested to rationally design and further explore plasmon mediated/ enhanced energy and storage devices and their operational mechanisms. Although, to enhance the performance of these devices, further research needs to be extensively continued in the following directions. By now, we have realized that plasmonic effect could be an interesting means to improve the solar cell functionality and improve the overall device performance by exploiting their fascinating optical properties derived from the mutual coexistence of electrons and photons upon interaction with electromagnetic light and when confined in nano-dimensional spaces. In this regard, recently there has been active interest to develop inexpensive methods and fabricate viable plasmon mediated hybrid photovoltaic devices using solution processed metal NPs and semiconducting nanocrystals and their self-assemblies and further tailor the patterning to optimally tune the plasmonic functionality when embedded within the devices. However, the degree of improvement in the efficiency gained as a result of active incorporation of these plasmonic metal nanostructures may vary widely and depend critically on several important parameters (dimension, morphology, material composition, processing conditions, photochemical stability, location within the devices etc.) that need to be further optimized every time by taking into consideration all these variables that typically affect the overall performance of the devices.

Finally, to summarize, it is worthwhile mentioning that it is still a challenge to establish a unified approach for designing plasmonic solar cells which would yield the best performance, especially with all the necessary elements of the cell that all researchers working in this area need to consider for building any target-oriented solar cell types. However, with many new alternative plasmonic materials (plasmonic upconverters, graphene and 2D materials) that are frequently emerging, thanks to the material synthetic chemists, it is quite beneficial for most solar cell device engineers to come up with more creative solutions of fabricating next generation hybrid plasmon mediated energy devices. Additionally, in order for successful device fabrication, it is imperative to have a clear theoretical understanding and background on mechanisms (near field effects and electromagnetic field enhancement affecting exciton emission decay dynamics) involving manipulation of exciton and multiexciton efficiency of active layers (quantum dots, dyes, semiconducting polymers) due to various plasmonic nanostructures to be incorporated in these devices. However, much effort is still required to better comprehend the mode of interactions in hybrid plasmonic/excitonic systems and what regulates the strength of plexcitonic interaction and consequences in affecting the optical behavior and in turn the overall performance of the devices. Development of new synthetic methods with advanced material (and device) characterization tools are the key to answer these fundamental questions. With such a thorough understanding of these physical interaction processes, it is surely expected that hybrid metal/semiconductor heterosystems will potentially be the primary materials to be incorporated in all next generation hybrid plasmon mediated photovoltaic and optoelectronic devices and thereby transforming the key areas of renewable energy technologies.

References

1. Leonhardt, U.: Invisibility cup. Nat. Photonics **1**, 207–208 (2007). https://doi.org/10.1038/nphoton.2007.38
2. Freestone, I., Meeks, N., Sax, M., Higgitt, C.: The Lycurgus cup—a Roman nanotechnology. Gold Bull. **40**, 270–277 (2007). https://doi.org/10.1007/BF03215599
3. Sciau, P., Mirguet, C., Roucau, C., et al.: Double nanoparticle layer in a 12th century lustreware decoration: accident or technological mastery? J. Nano Res. **8**, 133–139 (2009). https://doi.org/10.4028/www.scientific.net/JNanoR.8.133
4. Heiligtag, F.J., Niederberger, M.: The fascinating world of nanoparticle research. Mater. Today **16**, 262–271 (2013). https://doi.org/10.1016/j.mattod.2013.07.004
5. Jana, J., Ganguly, M., Pal, T.: Enlightening surface plasmon resonance effect of metal nanoparticles for practical spectroscopic application. RSC Adv. **6**, 86174–86211 (2016). https://doi.org/10.1039/C6RA14173K
6. Willets, K.A., Van Duyne, R.P.: Localized surface plasmon resonance spectroscopy and sensing. Annu. Rev. Phys. Chem. **58**, 267–297 (2007). https://doi.org/10.1146/annurev.physchem.58.032806.104607
7. Petryayeva, E., Krull, U.J.: Localized surface plasmon resonance: nanostructures, bioassays and biosensing—a review. Anal. Chim. Acta **706**, 8–24 (2011). https://doi.org/10.1016/j.aca.2011.08.020
8. Zhang, J.Z., Noguez, C.: Plasmonic optical properties and applications of metal nanostructures. Plasmonics **3**, 127–150 (2008). https://doi.org/10.1007/s11468-008-9066-y
9. Mie, G.: Beiträge zur Optik trüber Medien, speziell kolloidaler Metallösungen. Ann. Phys. **330**, 377–445 (1908). https://doi.org/10.1002/andp.19083300302
10. Gans, R.: Über die Form ultramikroskopischer Goldteilchen. Ann. Phys. **342**, 881–900 (1912). https://doi.org/10.1002/andp.19123420503
11. Gans, R.: Über die Form ultramikroskopischer Silberteilchen. Ann. Phys. **352**, 270–284 (1915). https://doi.org/10.1002/andp.19153521006
12. Odom, T.W., Schatz, G.C.: Introduction to plasmonics. Chem. Rev. **111**, 3667–3668 (2011). https://doi.org/10.1021/cr2001349
13. Johnson, P.B., Christy, R.W.: Optical constants of the noble metals. Phys. Rev. B **6**, 4370–4379 (1972). https://doi.org/10.1103/PhysRevB.6.4370
14. Litinskaya MBT-RM in MS and ME: Polaritons☆. Elsevier (2019)
15. Fukui, M., Okamoto, T., Haraguchi, M.: Chapter 3—linear and nonlinear optical response of concentric metallic nanoshells. In: Kawata, S., Masuhara HBT-HN (eds.) Nanoplasmonics, pp. 31–54. Elsevier (2006)
16. Wang, X., Deng, Y., Li, Q., et al.: Excitation and propagation of surface plasmon polaritons on a non-structured surface with a permittivity gradient. Light Sci. Appl. **5**, e16179–e16179 (2016). https://doi.org/10.1038/lsa.2016.179
17. Ashoori, R.C.: Electrons in artificial atoms. Nature **379**, 413–419 (1996). https://doi.org/10.1038/379413a0
18. Henini, M.: Quantum dot nanostructures. Mater. Today **5**, 48–53 (2002). https://doi.org/10.1016/S1369-7021(02)00639-9
19. Brus, L.E.: Electron–electron and electron-hole interactions in small semiconductor crystallites: the size dependence of the lowest excited electronic state. J. Chem. Phys. **80**, 4403–4409 (1984). https://doi.org/10.1063/1.447218
20. Brus, L.: Zero-dimensional "excitons" in semiconductor clusters. IEEE J. Quant. Electron. **22**, 1909–1914 (1986). https://doi.org/10.1109/JQE.1986.1073184
21. Bawendi, M.G., Carroll, P.J., Wilson, W.L., Brus, L.E.: Luminescence properties of CdSe quantum crystallites: resonance between interior and surface localized states. J. Chem. Phys. **96**, 946–954 (1992). https://doi.org/10.1063/1.462114
22. Brus, L.: Quantum crystallites and nonlinear optics. Appl. Phys. A **53**, 465–474 (1991). https://doi.org/10.1007/BF00331535

23. Brus, L.: Electronic wave functions in semiconductor clusters: experiment and theory. J. Phys. Chem. **90**, 2555–2560 (1986). https://doi.org/10.1021/j100403a003
24. Bagga, A., Chattopadhyay, P.K., Ghosh, S.: Stokes shift in quantum dots: origin of dark exciton. In: 2007 International Workshop on Physics of Semiconductor Devices. pp. 876–879 (2007)
25. Wannier, G.H.: The structure of electronic excitation levels in insulating crystals. Phys. Rev. **52**, 191–197 (1937). https://doi.org/10.1103/PhysRev.52.191
26. Frenkel, J.: On the transformation of light into heat in solids. I. Phys. Rev. **37**, 17–44 (1931). https://doi.org/10.1103/PhysRev.37.17
27. Knoester, J.: Agranovich, V.M.: (2003) Frenkel and charge-transfer excitons in organic solids. In: Electronic Excitations in Organic Nanostructures, pp. 1–96. Academic Press
28. Mandal, S., Selvakannan, P.R., Pasricha, R., Sastry, M.: Keggin Ions as UV-switchable reducing agents in the synthesis of Au Core−Ag shell nanoparticles. J. Am. Chem. Soc. **125**, 8440–8441 (2003). https://doi.org/10.1021/ja034972t
29. Taton, T.A., Mirkin, C.A., Letsinger, R.L.: Scanometric DNA array detection with nanoparticle probes. Science (80-) **289**, 1757–1760 (2000). https://doi.org/10.1126/science.289.5485.1757
30. Kamat, P.V.: Photophysical, photochemical and photocatalytic aspects of metal nanoparticles. J. Phys. Chem. B **106**, 7729–7744 (2002). https://doi.org/10.1021/jp0209289
31. Elghanian, R., Storhoff, J.J., Mucic, R.C., et al.: Selective colorimetric detection of polynucleotides based on the distance-dependent optical properties of gold nanoparticles. Science (80-) **277**, 1078–1081 (1997). https://doi.org/10.1126/science.277.5329.1078
32. Link, S., Burda, C., Nikoobakht, B., El-Sayed, M.A.: How long does it take to melt a gold nanorod?: a femtosecond pump–probe absorption spectroscopic study. Chem. Phys. Lett. **315**, 12–18 (1999). https://doi.org/10.1016/S0009-2614(99)01214-2
33. Ahmadi, T.S., Wang, Z.L., Green, T.C., et al.: Shape-controlled synthesis of colloidal platinum nanoparticles. Science (80-) **272**, 1924–1925 (1996). https://doi.org/10.1126/science.272.5270.1924
34. Chen, H.M., Liu, R.-S.: Architecture of metallic nanostructures: synthesis strategy and specific applications. J. Phys. Chem. C **115**, 3513–3527 (2011). https://doi.org/10.1021/jp108403r
35. Jeevanandam, J., Barhoum, A., Chan, Y.S., et al.: Review on nanoparticles and nanostructured materials: history, sources, toxicity and regulations. Beilstein J. Nanotechnol. **9**, 1050–1074 (2018). https://doi.org/10.3762/bjnano.9.98
36. Hunt, E.M., Hampikian, J.M.: Ion implantation-induced nanoscale particle formation in Al_2O_3 and SiO_2 via reduction. Acta Mater. **47**, 1497–1511 (1999). https://doi.org/10.1016/S1359-6454(99)00028-2
37. Hunt, E.M., Hampikian, J.M.: Implantation parameters affecting aluminum nano-particle formation in alumina. J. Mater. Sci. **36**, 1963–1973 (2001). https://doi.org/10.1023/A:1017562311310
38. McHargue, C.J., Ren, S.X., Hunn, J.D.: Nanometer-size dispersions of iron in sapphire prepared by ion implantation and annealing. Mater. Sci. Eng. A **253**, 1–7 (1998). https://doi.org/10.1016/S0921-5093(98)00722-9
39. Sharma, S.K., Pujari, P.K.: Embedded Si nanoclusters in α-alumina synthesized by ion implantation: an investigation using depth dependent Doppler broadening spectroscopy. J. Alloys Compd. **715**, 247–253 (2017). https://doi.org/10.1016/j.jallcom.2017.04.285
40. Sigmund, P.: Mechanisms and theory of physical sputtering by particle impact. Nucl. Instrum. Methods Phys. Res. Sect. B Beam Interact Mater. Atoms **27**, 1–20 (1987). https://doi.org/10.1016/0168-583X(87)90004-8
41. Thompson, M.W.: II. The energy spectrum of ejected atoms during the high energy sputtering of gold. Philos. Mag. A J. Theor. Exp. Appl. Phys. **18**, 377–414 (1968). https://doi.org/10.1080/14786436808227358

42. Rashid, J., Barakat, M.A., Salah, N., Habib, S.S.: ZnO-nanoparticles thin films synthesized by RF sputtering for photocatalytic degradation of 2-chlorophenol in synthetic wastewater. J. Ind. Eng. Chem. **23**, 134–139 (2015). https://doi.org/10.1016/j.jiec.2014.08.006
43. Fumitaka, Mafuné, Kohno, J., Takeda, Y., et al.: Formation and size control of silver nanoparticles by laser ablation in aqueous solution. J. Phys. Chem. B **104**, 9111–9117 (2000). https://doi.org/10.1021/jp001336y
44. Kudryashov, I.S., Samokhvalov, A.A., Nastulyavichus, A.A., et al.: Nanosecond-laser generation of nanoparticles in liquids: from ablation through bubble dynamics to nanoparticle yield. Materials **12** (2019)
45. Ganjali, M., Vahdatkhah, P., Marashi, S.M.B.: Synthesis of Ni nanoparticles by pulsed laser ablation method in liquid phase. Proc. Mater. Sci. **11**, 359–363 (2015). https://doi.org/10.1016/j.mspro.2015.11.127
46. Matsubara, M., Yamaki, T., Itoh, H., et al.: Preparation of TiO_2 nanoparticles by pulsed laser ablation: ambient pressure dependence of crystallization. Jpn. J. Appl. Phys. **42**, L479–L481 (2003). https://doi.org/10.1143/jjap.42.l479
47. Tsai, S.C., Song, Y.L., Tsai, C.S., et al.: Ultrasonic spray pyrolysis for nanoparticles synthesis. J. Mater. Sci. **39**, 3647–3657 (2004). https://doi.org/10.1023/B:JMSC.0000030718.76690.11
48. Gavrilović, T.V., Jovanović, D.J., Dramićanin, M.D.: Chapter 2—synthesis of multifunctional inorganic materials: from micrometer to nanometer dimensions. In: Bhanvase, B.A., Pawade, V.B., Dhoble, S.J., et al. (eds.) Micro and Nano Technologies, pp 55–81. Elsevier (2018)
49. Gröhn, A.J., Pratsinis, S.E., Sánchez-Ferrer, A., et al.: Scale-up of nanoparticle synthesis by flame spray pyrolysis: the high-temperature particle residence time. Ind. Eng. Chem. Res. **53**, 10734–10742 (2014). https://doi.org/10.1021/ie501709s
50. Sunkari, S., Gangapuram, B.R., Dadigala, R., et al.: Microwave-irradiated green synthesis of gold nanoparticles for catalytic and anti-bacterial activity. J. Anal. Sci. Technol. **8**, 13 (2017). https://doi.org/10.1186/s40543-017-0121-1
51. Milkin, S.S., Starodubov, A.V., Herman, S.V., et al.: On the interaction of electromagnetic microwave radiation with emulsion containing magnetic nanoparticles. In: 2014 24th International Crimean Conference Microwave & Telecommunication Technology, pp. 968–969 (2014)
52. Sander, M.S., Gao, H.: aligned arrays of nanotubes and segmented nanotubes on substrates fabricated by electrodeposition onto nanorods. J. Am. Chem. Soc. **127**, 12158–12159 (2005). https://doi.org/10.1021/ja0522231
53. Maillard, M., Giorgio, S., Pileni, M.-P.: Silver nanodisks. Adv. Mater. **14**, 1084–1086 (2002). https://doi.org/10.1002/1521-4095(20020805)14:15%3c1084:AID-ADMA1084%3e3.0.CO;2-L
54. Toneguzzo, P., Viau, G., Acher, O., et al.: CoNi and FeCoNi fine particles prepared by the polyol process: physico-chemical characterization and dynamic magnetic properties. J. Mater. Sci. **35**, 3767–3784 (2000). https://doi.org/10.1023/A:1004864927169
55. Yener, D.O., Sindel, J., Randall, C.A., Adair, J.H.: Synthesis of nanosized silver platelets in octylamine-water bilayer systems. Langmuir **18**, 8692–8699 (2002). https://doi.org/10.1021/la011229a
56. Murphy, C.J., Sau, T.K., Gole, A.M., et al.: Anisotropic metal nanoparticles: synthesis, assembly, and optical applications. J. Phys. Chem. B **109**, 13857–13870 (2005). https://doi.org/10.1021/jp0516846
57. Huang, L.M., Wang, H.T., Wang, Z.B., et al.: Nanowire arrays electrodeposited from liquid crystalline phases. Adv. Mater. **14**, 61–64 (2002). https://doi.org/10.1002/1521-4095(20020104)14:1%3c61:AID-ADMA61%3e3.0.CO;2-Y
58. Whitney, T.M., Searson, P.C., Jiang, J.S., Chien, C.L.: Fabrication and magnetic properties of arrays of metallic nanowires. Science (80-) **261**, 1316–1319 (1993). https://doi.org/10.1126/science.261.5126.1316

59. Murphy, C.J., Gole, A.M., Hunyadi, S.E., Orendorff, C.J.: One-dimensional colloidal gold and silver nanostructures. Inorg. Chem. **45**, 7544–7554 (2006). https://doi.org/10.1021/ic0519382
60. Nicewarner-Peña, S.R., Freeman, R.G., Reiss, B.D., et al.: Submicrometer metallic barcodes. Science (80-) **294**, 137–141 (2001). https://doi.org/10.1126/science.294.5540.137
61. Wiley, B., Sun, Y., Mayers, B., Xia, Y.: Shape-controlled synthesis of metal nanostructures: the case of silver. Chem.—Eur. J. **11**, 454–463 (2005). https://doi.org/10.1002/chem.200400927
62. Sun, Y., Xia, Y.: Large-scale synthesis of uniform silver nanowires through a soft, self-seeding, polyol process. Adv. Mater. **14**, 833–837 (2002). https://doi.org/10.1002/1521-4095(20020605)14:11%3c833:AID-ADMA833%3e3.0.CO;2-K
63. Sun, Y., Xia, Y.: Multiple-walled nanotubes made of metals. Adv. Mater. **16**, 264–268 (2004). https://doi.org/10.1002/adma.200305780
64. Lee, J.S., Suh, J.S.: Uniform field emission from aligned carbon nanotubes prepared by CO disproportionation. J. Appl. Phys. **92**, 7519–7522 (2002). https://doi.org/10.1063/1.1525063
65. Sun, Y., Xia, Y.: Triangular nanoplates of silver: synthesis, characterization, and use as sacrificial templates for generating triangular nanorings of gold. Adv. Mater. **15**, 695–699 (2003). https://doi.org/10.1002/adma.200304652
66. Sun, Y., Xia, Y.: Mechanistic Study on the replacement reaction between silver nanostructures and chloroauric acid in aqueous medium. J. Am. Chem. Soc. **126**, 3892–3901 (2004). https://doi.org/10.1021/ja039734c
67. Sun, Y., Xia, Y.: Shape-controlled synthesis of gold and silver nanoparticles. Science (80-) **298**, 2176–2179 (2002). https://doi.org/10.1126/science.1077229
68. Sun, Y., Xia, Y.: Alloying and dealloying processes involved in the preparation of metal nanoshells through a galvanic replacement reaction. Nano Lett. **3**, 1569–1572 (2003). https://doi.org/10.1021/nl034765r
69. Sun, Y., Mayers, B., Xia, Y.: Metal nanostructures with hollow interiors. Adv. Mater. **15**, 641–646 (2003). https://doi.org/10.1002/adma.200301639
70. Sun, Y., Mayers, B.T., Xia, Y.: Template-engaged replacement reaction: a one-step approach to the large-scale synthesis of metal nanostructures with hollow interiors. Nano Lett. **2**, 481–485 (2002). https://doi.org/10.1021/nl025531v
71. Frens, G.: Controlled nucleation for the regulation of the particle size in monodisperse gold suspensions. Nat. Phys. Sci. **241**, 20–22 (1973). https://doi.org/10.1038/physci241020a0
72. Pong, B.-K., Elim, H.I., Chong, J.-X., et al.: New insights on the nanoparticle growth mechanism in the citrate reduction of Gold(III) salt: formation of the Au nanowire intermediate and its nonlinear optical properties. J. Phys. Chem. C **111**, 6281–6287 (2007). https://doi.org/10.1021/jp068666o
73. Kimling, J., Maier, M., Okenve, B., et al.: Turkevich method for gold nanoparticle synthesis revisited. J. Phys. Chem. B **110**, 15700–15707 (2006). https://doi.org/10.1021/jp061667w
74. Frens, G.: Particle size and sol stability in metal colloids. Kolloid-Zeitschrift und Zeitschrift für Polym **250**, 736–741 (1972). https://doi.org/10.1007/BF01498565
75. Turkevich, J., Stevenson, P.C., Hillier, J.: A study of the nucleation and growth processes in the synthesis of colloidal gold. Discuss. Faraday Soc. **11**, 55–75 (1951). https://doi.org/10.1039/DF9511100055
76. Larm, N.E., Essner, J.B., Pokpas, K., et al.: Room-temperature Turkevich method: formation of gold nanoparticles at the speed of mixing using cyclic oxocarbon reducing agents. J. Phys. Chem. C **122**, 5105–5118 (2018). https://doi.org/10.1021/acs.jpcc.7b10536
77. Sajanlal, P.R., Sreeprasad, T.S., Samal, A.K., Pradeep, T.: Anisotropic nanomaterials: structure, growth, assembly, and functions. Nano Rev. **2**, 5883 (2011). https://doi.org/10.3402/nano.v2i0.5883
78. Wiley, B., Sun, Y., Xia, Y.: Synthesis of Silver nanostructures with controlled shapes and properties. Acc. Chem. Res. **40**, 1067–1076 (2007). https://doi.org/10.1021/ar7000974

79. Phiri, M.M., Mulder, D.W., Vorster, B.C.: Seedless gold nanostars with seed-like advantages for biosensing applications. R. Soc. Open Sci. **6**, 181971 (2019). https://doi.org/10.1098/rsos.181971
80. Liu, B., Zeng, H.C.: Fabrication of ZnO "Dandelions" via a modified Kirkendall process. J. Am. Chem. Soc. **126**, 16744–16746 (2004). https://doi.org/10.1021/ja044825a
81. Yang, H.G., Zeng, H.C.: Preparation of hollow anatase TiO_2 nanospheres via Ostwald ripening. J. Phys. Chem. B **108**, 3492–3495 (2004). https://doi.org/10.1021/jp0377782
82. Yin, Y., Rioux, R.M., Erdonmez, C.K., et al.: Formation of hollow nanocrystals through the nanoscale Kirkendall effect. Science (80-) **304**, 711–714 (2004). https://doi.org/10.1126/science.1096566
83. Chang, Y., Lye, M.L., Zeng, H.C.: Large-scale synthesis of high-quality ultralong copper nanowires. Langmuir **21**, 3746–3748 (2005). https://doi.org/10.1021/la050220w
84. Zeng, H.C.: Synthetic architecture of interior space for inorganic nanostructures. J. Mater. Chem. **16**, 649–662 (2006). https://doi.org/10.1039/B511296F
85. Brust, M., Fink, J., Bethell, D., et al.: Synthesis and reactions of functionalised gold nanoparticles. J. Chem. Soc. Chem. Commun., 1655–1656 (1995). https://doi.org/10.1039/C39950001655
86. da Silva, A.G.M., Rodrigues, T.S., Haigh, S.J., Camargo, P.H.C.: Galvanic replacement reaction: recent developments for engineering metal nanostructures towards catalytic applications. Chem. Commun. **53**, 7135–7148 (2017). https://doi.org/10.1039/C7CC02352A
87. Bansal, V., O'Mullane, A.P., Bhargava, S.K.: Galvanic replacement mediated synthesis of hollow Pt nanocatalysts: significance of residual Ag for the H2 evolution reaction. Electrochem. Commun. **11**, 1639–1642 (2009). https://doi.org/10.1016/j.elecom.2009.06.018
88. Chen, H.M., Liu, R.-S., Lo, M.-Y., et al.: Hollow platinum spheres with nano-channels: synthesis and enhanced catalysis for oxygen reduction. J. Phys. Chem. C **112**, 7522–7526 (2008). https://doi.org/10.1021/jp8017698
89. Liu, X., Wang, D., Li, Y.: Synthesis and catalytic properties of bimetallic nanomaterials with various architectures. Nano Today **7**, 448–466 (2012). https://doi.org/10.1016/j.nantod.2012.08.003
90. Teng, X., Wang, Q., Liu, P., et al.: Formation of Pd/Au nanostructures from pd nanowires via galvanic replacement reaction. J. Am. Chem. Soc. **130**, 1093–1101 (2008). https://doi.org/10.1021/ja077303e
91. Cobley, C.M., Xia, Y.: Engineering the properties of metal nanostructures via galvanic replacement reactions. Mater. Sci. Eng. R. Rep. **70**, 44–62 (2010). https://doi.org/10.1016/j.mser.2010.06.002
92. Talapin, D.V., Lee, J.-S., Kovalenko, M.V., Shevchenko, E.V.: Prospects of colloidal nanocrystals for electronic and optoelectronic applications. Chem. Rev. **110**, 389–458 (2010). https://doi.org/10.1021/cr900137k
93. Somers, R.C., Bawendi, M.G., Nocera, D.G.: CdSe nanocrystal based chem-/bio- sensors. Chem. Soc. Rev. **36**, 579–591 (2007). https://doi.org/10.1039/B517613C
94. Peng, X., Chen, J., Misewich, J.A., Wong, S.S.: Carbon nanotube–nanocrystal heterostructures. Chem. Soc. Rev. **38**, 1076–1098 (2009). https://doi.org/10.1039/B811424M
95. Rogach, A.L., Klar, T.A., Lupton, J.M., et al.: Energy transfer with semiconductor nanocrystals. J. Mater. Chem. **19**, 1208–1221 (2009). https://doi.org/10.1039/B812884G
96. Frey, N.A., Peng, S., Cheng, K., Sun, S.: Magnetic nanoparticles: synthesis, functionalization, and applications in bioimaging and magnetic energy storage. Chem. Soc. Rev. **38**, 2532–2542 (2009). https://doi.org/10.1039/B815548H
97. de Mello, Donegá C., Liljeroth, P., Vanmaekelbergh, D.: physicochemical evaluation of the hot-injection method, a synthesis route for monodisperse nanocrystals. Small **1**, 1152–1162 (2005). https://doi.org/10.1002/smll.200500239
98. Nie, Z., Petukhova, A., Kumacheva, E.: Properties and emerging applications of self-assembled structures made from inorganic nanoparticles. Nat. Nanotechnol. **5**, 15–25 (2010). https://doi.org/10.1038/nnano.2009.453

99. Hillhouse, H.W., Beard, M.C.: Solar cells from colloidal nanocrystals: fundamentals, materials, devices, and economics. Curr. Opin. Colloid Interface Sci. **14**, 245–259 (2009). https://doi.org/10.1016/j.cocis.2009.05.002
100. Konstantatos, G., Sargent, E.H.: Nanostructured materials for photon detection. Nat. Nanotechnol. **5**, 391–400 (2010). https://doi.org/10.1038/nnano.2010.78
101. van Sark, W.G.J.H.M., Barnham, K.W.J., Slooff, L.H., et al.: Luminescent solar concentrators—a review of recent results. Opt. Express **16**, 21773–21792 (2008). https://doi.org/10.1364/OE.16.021773
102. Holder, E., Tessler, N., Rogach, A.L.: Hybrid nanocomposite materials with organic and inorganic components for opto-electronic devices. J. Mater. Chem. **18**, 1064–1078 (2008). https://doi.org/10.1039/B712176H
103. Wood, V., Panzer, M.J., Caruge, J.-M., et al.: Air-stable operation of transparent, colloidal quantum dot based LEDs with a unipolar device architecture. Nano Lett. **10**, 24–29 (2010). https://doi.org/10.1021/nl902425g
104. Michalet, X., Pinaud, F.F., Bentolila, L.A., et al.: Quantum dots for live cells, in vivo imaging, and diagnostics. Science (80-) **307**, 538–544 (2005). https://doi.org/10.1126/science.1104274
105. Robinson, R.D., Sadtler, B., Demchenko, D.O., et al.: Spontaneous superlattice formation in nanorods through partial cation exchange. Science (80-) **317**, 355–358 (2007). https://doi.org/10.1126/science.1142593
106. Milliron, D.J., Hughes, S.M., Cui, Y., et al.: Colloidal nanocrystal heterostructures with linear and branched topology. Nature **430**, 190–195 (2004). https://doi.org/10.1038/nature02695
107. Mokari, T., Rothenberg, E., Popov, I., et al.: Selective growth of metal tips onto semiconductor quantum rods and tetrapods. Science (80-) **304**, 1787–1790 (2004). https://doi.org/10.1126/science.1097830
108. Talapin, D.V., Nelson, J.H., Shevchenko, E.V., et al.: Seeded growth of highly luminescent CdSe/CdS nanoheterostructures with rod and tetrapod morphologies. Nano Lett. **7**, 2951–2959 (2007). https://doi.org/10.1021/nl072003g
109. Steiner, D., Dorfs, D., Banin, U., et al.: Determination of band offsets in heterostructured colloidal nanorods using scanning tunneling spectroscopy. Nano Lett. **8**, 2954–2958 (2008). https://doi.org/10.1021/nl801848x
110. Reiss, P., Protière, M., Li, L.: Core/Shell semiconductor nanocrystals. Small **5**, 154–168 (2009). https://doi.org/10.1002/smll.200800841
111. Cozzoli, P.D., Pellegrino, T., Manna, L.: Synthesis, properties and perspectives of hybrid nanocrystal structures. Chem. Soc. Rev. **35**, 1195–1208 (2006). https://doi.org/10.1039/B517790C
112. Costi, R., Saunders, A.E., Banin, U.: Colloidal hybrid nanostructures: a new type of functional materials. Angew Chemie Int. Ed. **49**, 4878–4897 (2010). https://doi.org/10.1002/anie.200906010
113. Casavola, M., Buonsanti, R., Caputo, G., Cozzoli, P.D.: Colloidal strategies for preparing oxide-based hybrid nanocrystals. Eur. J. Inorg. Chem. **2008**, 837–854 (2008). https://doi.org/10.1002/ejic.200701047
114. de Mello Donegá, C.: Synthesis and properties of colloidal heteronanocrystals. Chem. Soc. Rev. **40**, 1512–1546 (2011). https://doi.org/10.1039/C0CS00055H
115. Koole, R., Luigjes, B., Tachiya, M., et al.: Differences in cross-link chemistry between rigid and flexible dithiol molecules revealed by optical studies of CdTe quantum dots. J. Phys. Chem. C **111**, 11208–11215 (2007). https://doi.org/10.1021/jp072407x
116. Kairdolf, B.A., Smith, A.M., Nie, S.: One-pot synthesis, encapsulation, and solubilization of size-tuned quantum dots with amphiphilic multidentate ligands. J. Am. Chem. Soc. **130**, 12866–12867 (2008). https://doi.org/10.1021/ja804755q
117. Yu, W.W., Wang, Y.A., Peng, X.: Formation and stability of size-, shape-, and structure-controlled CdTe nanocrystals: ligand effects on monomers and nanocrystals. Chem. Mater. **15**, 4300–4308 (2003). https://doi.org/10.1021/cm034729t

118. Qu, L., Peng, X.: Control of photoluminescence properties of CdSe nanocrystals in growth. J. Am. Chem. Soc. **124**, 2049–2055 (2002). https://doi.org/10.1021/ja017002j
119. Peng, Z.A., Peng, X.: Nearly monodisperse and shape-controlled CdSe nanocrystals via alternative routes: nucleation and growth. J. Am. Chem. Soc. **124**, 3343–3353 (2002). https://doi.org/10.1021/ja0173167
120. Peng, Z.A., Peng, X.: Mechanisms of the shape evolution of CdSe nanocrystals. J. Am. Chem. Soc. **123**, 1389–1395 (2001). https://doi.org/10.1021/ja0027766
121. Peng, Z.A., Peng, X.: Formation of high-quality CdTe, CdSe, and CdS nanocrystals using CdO as precursor. J. Am. Chem. Soc. **123**, 183–184 (2001). https://doi.org/10.1021/ja003633m
122. Peng, X., Wickham, J., Alivisatos, A.P.: Kinetics of II-VI and III-V colloidal semiconductor nanocrystal growth: "focusing" of size distributions. J. Am. Chem. Soc. **120**, 5343–5344 (1998). https://doi.org/10.1021/ja9805425
123. Peng, X., Manna, L., Yang, W., et al.: Shape control of CdSe nanocrystals. Nature **404**, 59–61 (2000). https://doi.org/10.1038/35003535
124. Singh, R.D., Shandilya, R., Bhargava, A., et al.: Quantum dot based nano-biosensors for detection of circulating cell free miRNAs in lung carcinogenesis: from biology to clinical translation. Front. Genet. **9**, 616 (2018). https://doi.org/10.3389/fgene.2018.00616
125. Menagen, G., Macdonald, J.E., Shemesh, Y., et al.: Au growth on semiconductor nanorods: photoinduced versus thermal growth mechanisms. J. Am. Chem. Soc. **131**, 17406–17411 (2009). https://doi.org/10.1021/ja9077733
126. Mokari, T., Sztrum, C.G., Salant, A., et al.: Formation of asymmetric one-sided metal-tipped semiconductor nanocrystal dots and rods. Nat. Mater. **4**, 855 (2005)
127. Shemesh, Y., Macdonald, J.E., Menagen, G., Banin, U.: Synthesis and photocatalytic properties of a family of CdS-PdX hybrid nanoparticles. Angew Chemie Int. Ed. **50**, 1185–1189 (2011). https://doi.org/10.1002/anie.201006407
128. Habas, S.E., Yang, P., Mokari, T.: Selective growth of metal and binary metal tips on CdS nanorods. J. Am. Chem. Soc. **130**, 3294–3295 (2008). https://doi.org/10.1021/ja800104w
129. Dukovic, G., Merkle, M.G., Nelson, J.H., et al.: Photodeposition of Pt on colloidal CdS and CdSe/CdS semiconductor nanostructures. Adv. Mater. **20**, 4306–4311 (2008). https://doi.org/10.1002/adma.200800384
130. Banin, U., Ben-Shahar, Y., Vinokurov, K.: Hybrid semiconductor-metal nanoparticles: from architecture to function. Chem. Mater. **26**, 97–110 (2014). https://doi.org/10.1021/cm402131n
131. Li, M., Cushing, S.K., Wang, Q., et al.: Size-dependent energy transfer between CdSe/ZnS quantum dots and gold nanoparticles. J. Phys. Chem. Lett. **2**, 2125–2129 (2011). https://doi.org/10.1021/jz201002g
132. Maneeprakorn, W., Malik, M.A., O'Brien, P.: Developing chemical strategies for the assembly of nanoparticles into mesoscopic objects. J. Am. Chem. Soc. **132**, 1780–1781 (2010). https://doi.org/10.1021/ja910022q
133. Chang, E., Miller, J.S., Sun, J., et al.: Protease-activated quantum dot probes. Biochem. Biophys. Res. Commun. **334**, 1317–1321 (2005). https://doi.org/10.1016/j.bbrc.2005.07.028
134. Aldeek, F., Ji, X., Mattoussi, H.: Quenching of quantum dot emission by fluorescent gold clusters: what it does and does not share with the Förster formalism. J. Phys. Chem. C **117**, 15429–15437 (2013). https://doi.org/10.1021/jp404952x
135. Roller, E.-M., Argyropoulos, C., Högele, A., et al.: Plasmon-exciton coupling using DNA templates. Nano Lett. **16**, 5962–5966 (2016). https://doi.org/10.1021/acs.nanolett.6b03015
136. Cohen-Hoshen, E., Bryant, G.W., Pinkas, I., et al.: Exciton-Plasmon interactions in quantum dot-gold nanoparticle structures. Nano Lett. **12**, 4260–4264 (2012). https://doi.org/10.1021/nl301917d
137. Schreiber, R., Do, J., Roller, E.-M., et al.: Hierarchical assembly of metal nanoparticles, quantum dots and organic dyes using DNA origami scaffolds. Nat. Nanotechnol. **9**, 74 (2013)

138. Ko, S.H., Du, K., Liddle, J.A.: Quantum-dot fluorescence lifetime engineering with DNA origami constructs. Angew Chemie Int. Ed. **52**, 1193–1197 (2013). https://doi.org/10.1002/anie.201206253
139. Shevchenko, E.V., Talapin, D.V., Kotov, N.A., et al.: Structural diversity in binary nanoparticle superlattices. Nature **439**, 55–59 (2006). https://doi.org/10.1038/nature04414
140. Lee, J., Hernandez, P., Lee, J., et al.: Exciton–plasmon interactions in molecular spring assemblies of nanowires and wavelength-based protein detection. Nat. Mater. **6**, 291–295 (2007). https://doi.org/10.1038/nmat1869
141. Lee, J., Govorov, A.O., Dulka, J., Kotov, N.A.: Bioconjugates of CdTe nanowires and Au nanoparticles: Plasmon−Exciton interactions, luminescence enhancement, and collective effects. Nano Lett. **4**, 2323–2330 (2004). https://doi.org/10.1021/nl048669h
142. Ji, B., Giovanelli, E., Habert, B., et al.: Non-blinking quantum dot with a plasmonic nanoshell resonator. Nat. Nanotechnol. **10**, 170–175 (2015). https://doi.org/10.1038/nnano.2014.298
143. Chen, S., Thota, S., Reggiano, G., Zhao, J.: Generalized seeded growth of Ag-based metal chalcogenide nanorods via controlled chalcogenization of the seeds. J. Mater. Chem. C **3**, 11842–11849 (2015). https://doi.org/10.1039/C5TC02904J
144. Samanta, A., Zhou, Y., Zou, S., et al.: Fluorescence quenching of quantum dots by gold nanoparticles: a potential long range spectroscopic ruler. Nano Lett. **14**, 5052–5057 (2014). https://doi.org/10.1021/nl501709s
145. Zhang, L., Blom, D.A., Wang, H.: Au–Cu2O core-shell nanoparticles: a hybrid metal-semiconductor heteronanostructure with geometrically tunable optical properties. Chem. Mater. **23**, 4587–4598 (2011). https://doi.org/10.1021/cm202078t
146. Ozel, T., Hernandez-Martinez, P.L., Mutlugun, E., et al.: Observation of selective plasmon-exciton coupling in nonradiative energy transfer: donor-selective versus acceptor-selective plexcitons. Nano Lett. **13**, 3065–3072 (2013). https://doi.org/10.1021/nl4009106
147. Chen, Y., Vela, J., Htoon, H., et al.: "Giant" multishell CdSe nanocrystal quantum dots with suppressed blinking. J. Am. Chem. Soc. **130**, 5026–5027 (2008). https://doi.org/10.1021/ja711379k
148. Ma, X., Tan, H., Kipp, T., Mews, A.: Fluorescence enhancement, blinking suppression, and gray states of individual semiconductor nanocrystals close to gold nanoparticles. Nano Lett. **10**, 4166–4174 (2010). https://doi.org/10.1021/nl102451c
149. Munechika, K., Chen, Y., Tillack, A.F., et al.: Spectral control of plasmonic emission enhancement from quantum dots near single silver nanoprisms. Nano Lett. **10**, 2598–2603 (2010). https://doi.org/10.1021/nl101281a
150. Naiki, H., Uedao, T., Wang, L., et al.: Multiphoton emission enhancement from a single colloidal quantum dot using SiO2-coated silver nanoparticles. ACS Omega **2**, 728–737 (2017). https://doi.org/10.1021/acsomega.6b00520
151. LeBlanc, S.J., McClanahan, M.R., Jones, M., Moyer, P.J.: Enhancement of multiphoton emission from single CdSe quantum dots coupled to gold films. Nano Lett. **13**, 1662–1669 (2013). https://doi.org/10.1021/nl400117h
152. Park, Y.-S., Ghosh, Y., Chen, Y., et al.: Super-Poissonian statistics of photon emission from single CdSe-CdS core-shell nanocrystals coupled to metal nanostructures. Phys. Rev. Lett. **110**, 117401 (2013). https://doi.org/10.1103/PhysRevLett.110.117401
153. Dey, S., Zhou, Y., Tian, X., et al.: An experimental and theoretical mechanistic study of biexciton quantum yield enhancement in single quantum dots near gold nanoparticles. Nanoscale **7** (2015). https://doi.org/10.1039/c5nr00274e
154. Wax, T.J., Dey, S., Chen, S., et al.: Excitation wavelength-dependent photoluminescence decay of hybrid gold/quantum dot nanostructures. ACS Omega **3** (2018). https://doi.org/10.1021/acsomega.8b01959
155. Zhou, N., Yuan, M., Gao, Y., et al.: Silver nanoshell plasmonically controlled emission of semiconductor quantum dots in the strong coupling regime. ACS Nano **10**, 4154–4163 (2016). https://doi.org/10.1021/acsnano.5b07400

156. Santhosh, K., Bitton, O., Chuntonov, L., Haran, G.: Vacuum Rabi splitting in a plasmonic cavity at the single quantum emitter limit. Nat. Commun. **7**, ncomms11823 (2016). https://doi.org/10.1038/ncomms11823
157. Inkson, B.J.: 2—Scanning electron microscopy (SEM) and transmission electron microscopy (TEM) for materials characterization. In: Hübschen, G., Altpeter, I., Tschuncky, R., Herrmann H-GBT-MCUNE (NDE) M. (eds.), pp. 17–43. Woodhead Publishing (2016)
158. Sezen, H., Suzer, S.: XPS for chemical- and charge-sensitive analyses. Thin Solid Films **534**, 1–11 (2013). https://doi.org/10.1016/j.tsf.2013.02.002
159. Cavalcoli, D., Fraboni, B., Cavallini, A.: Chapter Seven—Surface and defect states in semiconductors investigated by surface photovoltage. In: Romano, L., Privitera, V., Jagadish, S. (eds.) Defects in Semiconductors, pp. 251–278. Elsevier (2015)
160. Bisquert, J., Bertoluzzi, L., Mora-Sero, I., Garcia-Belmonte, G.: Theory of impedance and capacitance spectroscopy of solar cells with dielectric relaxation, drift-diffusion transport, and recombination. J. Phys. Chem. C **118**, 18983–18991 (2014). https://doi.org/10.1021/jp5062144
161. Braña, A.F., Forniés, E., López, N., García, B.J.: High efficiency Si solar cells characterization using impedance spectroscopy analysis. J. Phys: Conf. Ser. **647**, 12069 (2015). https://doi.org/10.1088/1742-6596/647/1/012069
162. Wang, Q., Moser, J.-E., Grätzel, M.: Electrochemical impedance spectroscopic analysis of dye-sensitized solar cells. J. Phys. Chem. B **109**, 14945–14953 (2005). https://doi.org/10.1021/jp052768h
163. Wu, J.-L., Chen, F.-C., Hsiao, Y.-S., et al.: Surface plasmonic effects of metallic nanoparticles on the performance of polymer bulk heterojunction solar cells. ACS Nano **5**, 959–967 (2011). https://doi.org/10.1021/nn102295p
164. Atwater, H.A., Polman, A.: Plasmonics for improved photovoltaic devices. Nat. Mater. **9**, 205–213 (2010). https://doi.org/10.1038/nmat2629
165. Jang, Y.H., Jang, Y.J., Kim, S., et al.: Plasmonic solar cells: from rational design to mechanism overview. Chem. Rev. **116**, 14982–15034 (2016). https://doi.org/10.1021/acs.chemrev.6b00302
166. Yuan, Z., Wu, Z., Bai, S., et al.: Hot-electron injection in a sandwiched TiOx–Au–TiOx structure for high-performance planar Perovskite solar cells. Adv. Energy Mater. **5**, 1500038 (2015). https://doi.org/10.1002/aenm.201500038
167. Zhu, J., Hsu, C.-M., Yu, Z., et al.: Nanodome solar cells with efficient light management and self-cleaning. Nano Lett. **10**, 1979–1984 (2010). https://doi.org/10.1021/nl9034237
168. Pala, R.A., White, J., Barnard, E., et al.: Design of plasmonic thin-film solar cells with broadband absorption enhancements. Adv. Mater. **21**, 3504–3509 (2009). https://doi.org/10.1002/adma.200900331
169. Callahan, D.M., Munday, J.N., Atwater, H.A.: Solar cell light trapping beyond the ray optic limit. Nano Lett. **12**, 214–218 (2012). https://doi.org/10.1021/nl203351k
170. Chen, H.M., Chen, C.K., Chen, C.-J., et al.: Plasmon inducing effects for enhanced photoelectrochemical water splitting: X-ray absorption approach to electronic structures. ACS Nano **6**, 7362–7372 (2012). https://doi.org/10.1021/nn3024877
171. Li, J., Cushing, S.K., Meng, F., et al.: Plasmon-induced resonance energy transfer for solar energy conversion. Nat. Photonics **9**, 601 (2015)
172. Cushing, S.K., Li, J., Meng, F., et al.: Photocatalytic activity enhanced by plasmonic resonant energy transfer from metal to semiconductor. J. Am. Chem. Soc. **134**, 15033–15041 (2012). https://doi.org/10.1021/ja305603t
173. Isah, K.U., Jolayemi, B.J., Ahmadu, U., et al.: Plasmonic effect of silver nanoparticles intercalated into mesoporous betalain-sensitized-TiO_2 film electrodes on photovoltaic performance of dye-sensitized solar cells. Mater. Renew. Sustain. Energy **5**, 10 (2016). https://doi.org/10.1007/s40243-016-0075-z
174. Ihara, M., Kanno, M., Inoue, S.: Photoabsorption-enhanced dye-sensitized solar cell by using localized surface plasmon of silver nanoparticles modified with polymer. Phys E

Low-dimensional Syst. Nanostruct. **42**, 2867–2871 (2010). https://doi.org/10.1016/j.physe.2010.04.001
175. Xu, Q., Liu, F., Meng, W., Huang, Y.: Plasmonic core-shell metal-organic nanoparticles enhanced dye-sensitized solar cells. Opt. Express **20**, A898–A907 (2012). https://doi.org/10.1364/OE.20.00A898
176. Chen, Z.H., Tang, Y.B., Liu, C.P., et al.: Vertically aligned ZnO nanorod arrays sentisized with gold nanoparticles for Schottky barrier photovoltaic cells. J. Phys. Chem. C **113**, 13433–13437 (2009). https://doi.org/10.1021/jp903153w
177. Ding, I.-K., Zhu, J., Cai, W., et al.: Plasmonic dye-sensitized solar cells. Adv. Energy Mater. **1**, 52–57 (2011). https://doi.org/10.1002/aenm.201000041
178. Li, Y., Wang, H., Feng, Q., et al.: Gold nanoparticles inlaid TiO_2 photoanodes: a superior candidate for high-efficiency dye-sensitized solar cells. Energy Environ. Sci. **6**, 2156–2165 (2013). https://doi.org/10.1039/C3EE23971C
179. Du, J., Qi, J., Wang, D., Tang, Z.: Facile synthesis of Au@TiO_2 core–shell hollow spheres for dye-sensitized solar cells with remarkably improved efficiency. Energy Environ. Sci. **5**, 6914–6918 (2012). https://doi.org/10.1039/C2EE21264A
180. Chang, S., Li, Q., Xiao, X., et al.: Enhancement of low energy sunlight harvesting in dye-sensitized solar cells using plasmonic gold nanorods. Energy Environ. Sci. **5**, 9444–9448 (2012). https://doi.org/10.1039/C2EE22657J
181. Brown, M.D., Suteewong, T., Kumar, R.S.S., et al.: Plasmonic dye-sensitized solar cells using core−shell metal−insulator nanoparticles. Nano Lett. **11**, 438–445 (2011). https://doi.org/10.1021/nl1031106
182. Zarick, H.F., Erwin, W.R., Boulesbaa, A., et al.: Improving light harvesting in dye-sensitized solar cells using hybrid bimetallic nanostructures. ACS Photonics **3**, 385–394 (2016). https://doi.org/10.1021/acsphotonics.5b00552
183. Elbohy, H., Kim, M.R., Dubey, A., et al.: Incorporation of plasmonic Au nanostars into photoanodes for high efficiency dye-sensitized solar cells. J. Mater. Chem. A **4**, 545–551 (2016). https://doi.org/10.1039/C5TA06425B
184. Su, Y.-H., Ke, Y.-F., Cai, S.-L., Yao, Q.-Y.: Surface plasmon resonance of layer-by-layer gold nanoparticles induced photoelectric current in environmentally-friendly plasmon-sensitized solar cell. Light Sci. Appl. **1**, e14–e14 (2012). https://doi.org/10.1038/lsa.2012.14
185. Wang, Q., Butburee, T., Wu, X., et al.: Enhanced performance of dye-sensitized solar cells by doping Au nanoparticles into photoanodes: a size effect study. J. Mater. Chem. A **1**, 13524–13531 (2013). https://doi.org/10.1039/C3TA12692G
186. Sahu, G., Gordon, S.W., Tarr, M.A.: Synthesis and application of core-shell Au–TiO_2 nanowire photoanode materials for dye sensitized solar cells. RSC Adv. **2**, 573–582 (2012). https://doi.org/10.1039/C1RA00762A
187. Ahn, S.H., Kim, D.J., Chi, W.S., Kim, J.H.: Plasmonic, interior-decorated, one-dimensional hierarchical nanotubes for high-efficiency, solid-state, dye-sensitized solar cells. J. Mater. Chem. A **3**, 10439–10447 (2015). https://doi.org/10.1039/C5TA00801H
188. Lee, K.-S., El-Sayed, M.A.: Dependence of the enhanced optical scattering efficiency relative to that of absorption for gold metal nanorods on aspect ratio, size, end-cap shape, and medium refractive index. J. Phys. Chem. B **109**, 20331–20338 (2005). https://doi.org/10.1021/jp054385p
189. Kulkarni, A.P., Noone, K.M., Munechika, K., et al.: Plasmon-enhanced charge carrier generation in organic photovoltaic films using silver nanoprisms. Nano Lett. **10**, 1501–1505 (2010). https://doi.org/10.1021/nl100615e
190. Salvador, M., MacLeod, B.A., Hess, A., et al.: Electron accumulation on metal nanoparticles in Plasmon-enhanced organic solar cells. ACS Nano **6**, 10024–10032 (2012). https://doi.org/10.1021/nn303725v
191. Yao, K., Salvador, M., Chueh, C.-C., et al.: A general route to enhance polymer solar cell performance using plasmonic nanoprisms. Adv. Energy Mater. **4**, 1400206 (2014). https://doi.org/10.1002/aenm.201400206

192. Yang, X., Chueh, C.-C., Li, C.-Z., et al.: High-efficiency polymer solar cells achieved by doping plasmonic metallic nanoparticles into dual charge selecting interfacial layers to enhance light trapping. Adv. Energy Mater. **3**, 666–673 (2013). https://doi.org/10.1002/aenm.201200726
193. Wang, C.C.D., Choy, W.C.H., Duan, C., et al.: Optical and electrical effects of gold nanoparticles in the active layer of polymer solar cells. J. Mater. Chem. **22**, 1206–1211 (2012). https://doi.org/10.1039/C1JM14150C
194. You, J., Li, X., Xie, F., et al.: Surface Plasmon and scattering-enhanced low-bandgap polymer solar cell by a metal grating back electrode. Adv. Energy Mater. **2**, 1203–1207 (2012). https://doi.org/10.1002/aenm.201200108
195. Choi, H., Lee, J.-P., Ko, S.-J., et al.: Multipositional Silica-coated silver nanoparticles for high-performance polymer solar cells. Nano Lett. **13**, 2204–2208 (2013). https://doi.org/10.1021/nl400730z
196. Wang, D.H., Kim, D.Y., Choi, K.W., et al.: Enhancement of donor-acceptor polymer bulk heterojunction solar cell power conversion efficiencies by addition of au nanoparticles. Angew Chemie Int. Ed. **50**, 5519–5523 (2011). https://doi.org/10.1002/anie.201101021
197. Oo, T.Z., Mathews, N., Xing, G., et al.: Ultrafine Gold nanowire networks as plasmonic antennae in organic photovoltaics. J. Phys. Chem. C **116**, 6453–6458 (2012). https://doi.org/10.1021/jp2099637
198. Carretero-Palacios, S., Calvo, M.E., Míguez, H.: Absorption enhancement in organic-inorganic Halide Perovskite films with embedded plasmonic gold nanoparticles. J. Phys. Chem. C **119**, 18635–18640 (2015). https://doi.org/10.1021/acs.jpcc.5b06473
199. Mali, S.S., Shim, C.S., Kim, H., et al.: In situ processed gold nanoparticle-embedded TiO_2 nanofibers enabling plasmonic perovskite solar cells to exceed 14% conversion efficiency. Nanoscale **8**, 2664–2677 (2016). https://doi.org/10.1039/C5NR07395B
200. Lu, Z., Pan, X., Ma, Y., et al.: Plasmonic-enhanced perovskite solar cells using alloy popcorn nanoparticles. RSC Adv. **5**, 11175–11179 (2015). https://doi.org/10.1039/C4RA16385K
201. Wang, H., Gonzalez-Pedro, V., Kubo, T., et al.: Enhanced carrier transport distance in colloidal PbS quantum-dot-based solar cells using ZnO nanowires. J. Phys. Chem. C **119**, 27265–27274 (2015). https://doi.org/10.1021/acs.jpcc.5b09152
202. Moroz, P., Liyanage, G., Kholmicheva, N.N., et al.: Infrared emitting PbS nanocrystal solids through matrix encapsulation. Chem. Mater. **26**, 4256–4264 (2014). https://doi.org/10.1021/cm501739h
203. Liu, X., Zhang, X.W., Meng, J.H., et al.: High efficiency Schottky junction solar cells by co-doping of graphene with gold nanoparticles and nitric acid. Appl. Phys. Lett. **106**, 233901 (2015). https://doi.org/10.1063/1.4922373
204. Li, S.-S., Tu, K.-H., Lin, C.-C., et al.: Solution-processable graphene oxide as an efficient hole transport layer in polymer solar cells. ACS Nano **4**, 3169–3174 (2010). https://doi.org/10.1021/nn100551j
205. Fan, G.-Q., Zhuo, Q.-Q., Zhu, J.-J., et al.: Plasmonic-enhanced polymer solar cells incorporating solution-processable Au nanoparticle-adhered graphene oxide. J. Mater. Chem. **22**, 15614–15619 (2012). https://doi.org/10.1039/C2JM31878D
206. Wang, X., Zhi, L., Müllen, K.: Transparent, conductive graphene electrodes for dye-sensitized solar cells. Nano Lett. **8**, 323–327 (2008). https://doi.org/10.1021/nl072838r
207. Goldschmidt, J.C., Fischer, S.: Upconversion for photovoltaics—a review of materials, devices and concepts for performance enhancement. Adv. Opt. Mater. **3**, 510–535 (2015). https://doi.org/10.1002/adom.201500024